Master's thesis

NTNU
Norwegian University of Science and Technology
Faculty of Engineering
Department of Mechanical and Industrial Engineering

Osema Cherif

Impressed current system for internal corrosion protection in monopiles for offshore windmills

Investigation of the calcareous deposits formation mechanism and behaviour in confined and partially open compartments

Master's thesis in Mechanical Engineering
Supervisor: Roy Johnsen
Co-supervisor: Sven Morten Hesjevik, Sidsel Skauby
June 2022

NTNU
Norwegian University of Science and Technology

Osema Cherif

Impressed current system for internal corrosion protection in monopiles for offshore windmills

Investigation of the calcareous deposits formation mechanism and behaviour in confined and partially open compartments

Master's thesis in Mechanical Engineering
Supervisor: Roy Johnsen
Co-supervisor: Sven Morten Hesjevik, Sidsel Skauby
June 2022

Norwegian University of Science and Technology
Faculty of Engineering
Department of Mechanical and Industrial Engineering

NTNU
Norwegian University of
Science and Technology

Acknowledgements

I would like to express my genuine appreciation to professor Roy Johnsen who has been my faculty supervisor during this thesis. You have contributed greatly with encouragement, motivation and knowledge during the process of completing this work.

A sincere acknowledgment is also to be given to Cristian Torres for providing an excellent working environment at the laboratory and for his guidance during this thesis.

Finally, I would also like to thank Sven Morten Hesjevik and Sidsel Skauby for providing excellent insight on the work and for all the very beneficial conversations we have had.

Osama Cherif

June 10, 2022 | Trondheim, Norway

Abstract

Impressed current cathodic protection (ICCP) is a highly effective corrosion protection system for submerged structures. When polarising the steel to its immune state by applying a protective current, the interfacial pH increases as a result leading to the precipitation of calcareous deposit on the steel surface. The calcareous deposits acts then as a protective coating as it is a good barrier against oxygen diffusion on the steel surface. Thus, lowering the current demand. However, when it comes to confined spaces, the application of ICCP leads to the production of chlorine which decreases the pH as there is no water renewal.

The reduction of pH creates then new challenges as the interfacial pH is decreased and the precipitation of the calcareous deposit is hindered. The calcareous deposits depends on various factors such as the applied potential, current density, pH, seawater chemistry, flow rate etc. The following factors have been investigated through literature to build an understanding of how they may affect the calcareous deposits such that they can be adjusted to build an effective calcareous deposit layer for a sustainable cathodic protection system. Hence, a literature review combined with testing were conducted to answer the following problem.

During this MSc project, three ICCP systems were simulated. The first two systems were ICCP system in simulated confined environment of grinded and precorroded samples. The third and last ICCP system was conducted on both precorroded and grinded samples in a simulated partially open environment with a weekly water exchange of 10% every 1-2 weeks. The steel samples were polarised to -1050 mV vs. Ag|AgCl for 12 weeks at room temperature. The current density after 12 weeks of continuous polarisation of the precorroded and grinded samples was measured to be 170 $\frac{mA}{m^2}$ and 190 $\frac{mA}{m^2}$, respectively. Meanwhile, the final current density in the water renewal system was found to be 290 $\frac{mA}{m^2}$.

Furthermore, the quality of the calcareous deposit was investigated through SEM and EDS analyses. It was found that the precorroded samples had a calcareous deposit made of magnesium hydroxide and large amounts of calcium carbonate. Meanwhile, the grinded samples was made of primarily magnesium hydroxide with some calcium carbonate. Hence, the precorroded samples had a better calcareous deposit quality. The suppression of the formation of the calcium carbonate on the grinded samples was hindered by the low pH, as the duration of the acidification lasted twice as long for these samples compared to the precorroded samples. Hence, the magnesium hydroxide is the favorable mineral under low pH and the calcium carbonate is the favorable mineral at more neutral pH.

The acidification behaviour observed in the three experiment varied but ultimately followed the same trend. Acidification was observed in all three experiments, however, the duration of acidification seemed to increase with the increase of the volume to area ratio. Hence, a hypothesis was proposed to explain the behaviour of the pH with respect to the measured current density and the counter electrode potential. It was hypothesised that the initial cause of acidification was indeed the CER. However, this mechanism changed as the cause of acidification was believed to be induced by the formation of magnesium hydroxide. And that the neutralisation of pH is a result to the stoppage of the formation of this mineral. The following hypothesis was supported by investigating the CER potential limit which was measured to lay between approximately 1160-1200 mV vs. Ag|AgCl.

After approximately 6 weeks of continuous polarisation, one grinded and one precorroded samples were disconnected from the CP system to freely corrode for 1 week. Thereafter, they were connected back to the system to measure the repolarisation current density. This was done under neutral pH. Similar experiment was done but at low pH. A precorroded sample was continuously polarised for 1 week before disconnecting it from the CP system to freely corrode for 6 days before repolarising the sample. The repolarisation current density exhibited a similar behavior to the one observed under neutral pH. And the main difference in the repolarisation under low and neutral pH was the duration before the curve converged back to the curve of the continuously polarised samples.

Contents

List of Figures

List of Tables

Nomenclature

ST	Structural Steel
OWT	Offshore Wind Turbines
CP	Cathodic Protection
CER	Chlorine Evolution Reaction
OER	Oxygen Evolution Reaction
ORR	Oxygen Reduction Reaction
MIC	Microbially Induced Corrosion
OCP	Open Circuit Potential
HE	Hydrogen Embrittlement
HISC	Hydrogen Induced Stress Cracking
ICCP	Impressed Current Cathodic Protection
GACP	Galvanic Anode Cathodic Protection
SACP	Sacrificial Anode Cathodic Protection
SEM	Scanning Electron Microscopy
EDS	Energy dispersive X-ray Spectroscopy
Ag|AgCl	Silver-Silver Chloride Reference
RHE	Reversible Hydrogen Electrode Reference
OCl^-	Hypochlorite ions
HCl	Hydrochloric Acid
$HOCl$	Hypochlorous Acid
Ca^{2+}	Calcium ions
Mg^{2+}	Magnesium ions

$CaCO_3$	Calcium Carbonate, Aragonite, Calcite
$Mg(OH)_2$	Magnesium Hydroxide, Brucite
OH^-	Hydroxide anions
H^+	Hydrogen anions
Ca/Mg	Protectiveness Index
Cl_2	Chlorine
Cl^-	Chloride
T	Temperature
a	Chemical activity of a substance
η	Overpotential
$i_{corrosion}$	Corrosion Current Density
$E_{corrosion}$	Corrosion Potential

Chapter 1

Introduction

Energy production from offshore wind turbines is a highly growing market due to the high wind speeds and availability of space making them highly efficient. In marine atmosphere and seawater, metallic materials are projected to corrosion. As the foundation (Monopile) of the wind turbine is made of carbon steel and filled with stagnant water, corrosion is to be expected and a cathodic protection system is needed to ensure the integrity of the structure. One of the recommended cathodic protection systems is the impressed current cathodic protection system (ICCP). However, there are a few uncertainties surrounding this solution. Thus, the purpose of this thesis is to clarify these uncertainties through a literature review and experimental work, and ideally finding a method for optimization of this CP technique.

1.1 Background

Offshore and floating wind turbines are currently the most developed renewable energy found at sea [1]. There is no doubt that renewable energy is on the way to take over the global energy needs. It was earlier defined by the European Union that 20% of the global quota should be sourced from renewable energy [2]. A number that was crushed as the renewable energy is responsible for 28% of the total energy consumption per Q1 of the year 2020 [3]. From which the wind energy provides approximately two thirds of the total renewable energy together with solar photovoltaic systems [3].

There are 4 main types of fixed wind turbine foundations, namely, gravity base, monopile, tripod and jacket foundations, all of which are installed in water depths

less than 50 m. The different foundations are displayed in Figure 1.1a. However, monopile foundations are the most popular representing 80.1% of the total offshore wind turbine structures in 2016 [4], as displayed in Figure 1.1b. One of the main challenges that the offshore wind turbine is facing is the high costs, in comparison to onshore wind. The foundations represent approximately 20-35% of the total costs of an offshore wind turbine making it the most expensive component [5]. Thus, it is crucial to optimize the design of the structures for better economic efficiency and structural integrity [6]. One of the biggest challenges the oil and gas industry has faced is corrosion, as it is the root cause of approximately 20-24% of the total failures [7]. Therefore, there is no doubt that enhancing the corrosion protection of the structures will provide longer service life in addition to safer operations and less costs in the long run.

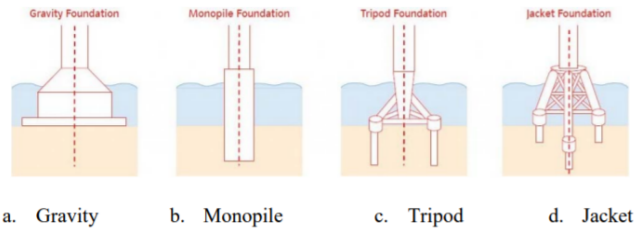

(a) Schematic diagram illustrating bottom-fixed offshore wind turbine foundations [8].

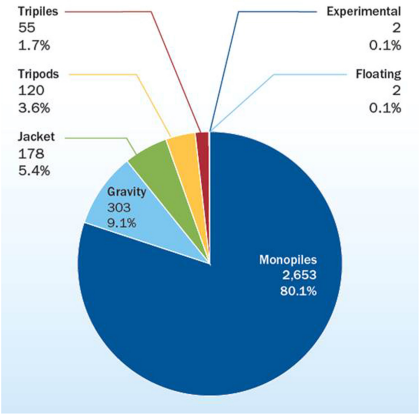

(b) Share of substructures types for online wind turbines end 2015 [4].

Figure 1.1: *Schematic diagram and pie distribution illustrating the type of offshore foundation and the share of the Monopile type structure of the total offshore wind turbines [4, 8].*

As previously mentioned, the monopile foundation is the most popular structure used for offshore wind. Figure 1.2 displays the components of the monopile and their respective zone in sea water environment. The structure consists of a large cylindrical tube (monopile) that is implanted into the seabed with the help of different techniques such as hammering or vibration. This part of the structure is categorized to be within the buried and submerged zones. Thereafter, a transition piece is used to connect the monopile with the tower. The transition piece is exposed to two environmental zones the submerged zone and the splash zone which is the most corrosive part of the entire structure. Finally, the last piece of the structure is the tower over which the turbine engine and the blades are installed. This part of the structure is characterized to being in the atmospheric zone.

The degree of corrosiveness of the different zones varies a lot as it can be seen in Figure 1.3a. According to the DNV-OS-J101 standard [11], the different zones are

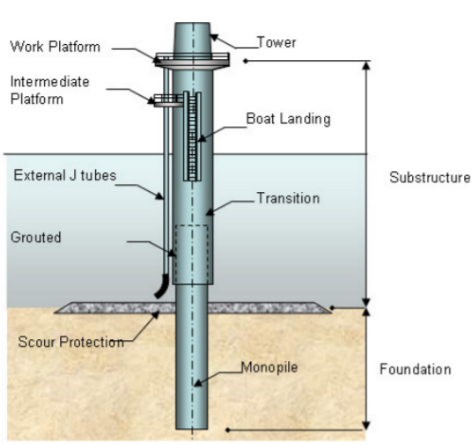

(a) Schematic representation of the components that constitutes a monopile [9].

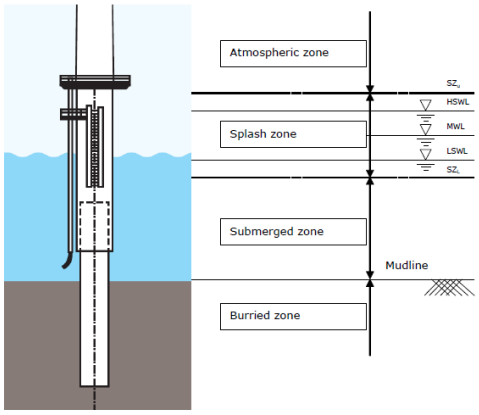

(b) Schematic representation of levels and zones in sea water environment as standardized by DNV GL [10].

Figure 1.2: *Schematic representations of the components of a monopile and the different zones in sea water [9, 10].*

characterised as follows:

- Atmospheric Zone;
  This zone represents the internal and external surfaces positioned over the splash zone. The corrosion rates are quite low as they are estimated to be around 0.1 mm/yr. This zone is usually protected with a coating and if the corrosion rates are lower, corrosion allowance might be an appropriate solution as well [11].
- Splash Zone:
  This zone is characterised by being intermittently exposed to sea water due to the presence of waves and tide. This leads to a highly corrosive environment where cathodic protection is not effective and the maintenance of the corrosion protection is not an option as it is extremely expensive. Thus, the most practical corrosion protection is by corrosion control and by applying a thick coating. The corrosion rates in this region range from 0.3-0.4 mm/yr externally and between 0.1-0.2 mm/yr internally. [10, 12].
- Submerged and Buried Zone:
  The submerged zone can be seen as the zone below the splash zone together with the buried zone. The submerged zone is characterized by having a corrosion rate of approximately 0.1 mm/yr internally and 0.1-0.2 mm/yr externally [11, 12]. It is usually Protected with a cathodic protection system together with a coating. The buried zone on the other hand is characterized by having a less severe corrosion as the corrosion rates are usually between 0.06-0.1 mm/yr and are normally protected by a cathodic protection system com-

bined with a coating if needed [12].

The different zones of the monopile structure are projected to different environments which leads to different corrosion rates. However, the forms of corrosion that appear in these regions varies a lot as it is displayed in Figure 1.3b. At the transition piece internally and externally, hydrogen may be presented if cathodic protection is not optimal which may lead to Hydrogen Induced Stress Cracking (HISC). Moreover, if there is Sulphate-Reducing Bacteria (SRB), H_2S may be produced leading to Sulfide Stress Cracking (SSC) and acidification. The inside of the monopile is filled with stagnant sea water and is usually characterized with uniform corrosion, and Microbially Induced Corrosion (MIC) and localised corrosion if the monopile foundation is leaking. The difference between the presence of the MIC internally will be discussed further in the theory. The grouted connection between the monopile and the transition piece, and the J-tube cable entry presents ingress of aerated seawater and oxygen which promotes higher corrosion rates internally. Other parts of the monopile may be subjected to poor protection caused by poor coating or insufficient cathodic protection. [13, 14]

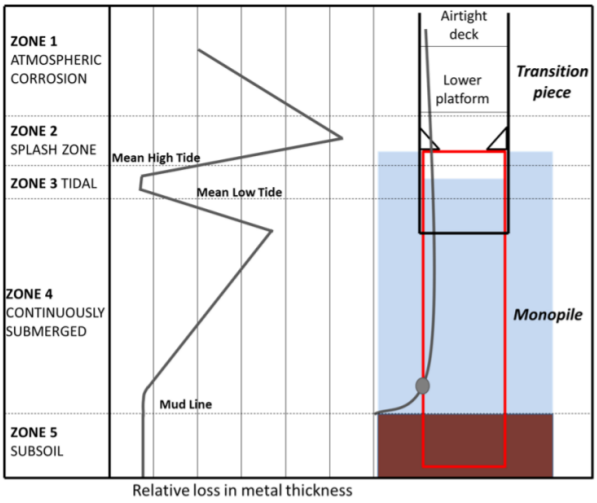

(a) Relative loss of metal thickness of unprotected steel on offshore wind turbine structure in seawater [13].

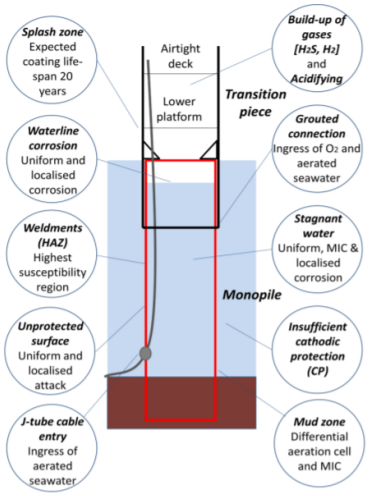

(b) Types of corrosion and its preferential locations in Offshore Wind Turbines [13].

Figure 1.3: *Relative corrosion rates and forms of corrosion in the offshore wind turbines [13].*

The closed/leaking system inside the monopile develops a unique environment in various monopile foundations. The special environment is quite unknown and therefore is very challenging when it comes to predicting the corrosion rate and mechanisms. Earlier it was assumed in the DNV-OS-J101 standard (2007) that the system is completely sealed and the only way for oxygen is due to maintenance routines and that the external cathodic protection is sufficient to protect

the monopile[11]. However, this was proven to be wrong as the inside was not air-tight, since the J-tube seals and grout connections fails in practice [15, 16]. Thus, modifications occurred in the recommendations as it is now recommended that a CP system is to be used inside the monopile as stated in DNV-OS-J101[17]. However, poorly designed cathodic protection installations leads to acidification of the seawater (pH dropped to 4-5), build up of gases and eventually the corrosion rate and anodes consumption accelerates [18]. The following occurred specifically under the use of aluminium anodes, on the other hand, zinc anodes could have been a good candidate but since the system is closed, toxicity hazards makes this solution undesirable. Finally, an impressed current cathodic protection system (ICCP) could be a great candidate to replace the last two solutions [19].

1.2 Problem description and motivation

Offshore wind turbines are designed to obtain a lifetime of 20 years which is equivalent to 10^9 cycles. Thus, the design of the structure is for fatigue which means that no minor corrosion is accepted as fatigue crack growths are extremely sensitive to this kind of defects and may lead to not reaching the designed lifetime [20]. As previously mentioned, the seawater inside the monopile leads to internal corrosion of the foundation, hence, a cathodic protection system is necessary to protect the structure. However, as the system is partially open, a unique environment is developed inside the monopile and various challenges arise when it comes to using the traditional cathodic protection systems. Practice has shown that aluminium based sacrificial anodes leads to acidification of the seawater as the anode corrodes. Zinc anodes on the other hand are highly toxic, combined with the fact that the system is closed and circulation of water is not optimal, the use of these anodes is not favorable. ICCP system could be a perfect candidate for the protection of the structure. However, this technique leads to the production of chlorine on the impressed current anode if the potential is more positive than the chlorine evolution potential which may lead to the pollution of the environment and acidification. Thus, various questions have to be answered concerning the limitations and challenges produced by this protection technique to properly evaluate its efficiency. One of the main limitations of this technique is that in case of a troubleshoot where the system is shut down, no protection would be available and as the water is acidic, there are concerns that the calcareous deposits would disintegrate from the surface and not provide sufficient protection during the time the system is not active. Thus, this report will focus on the behaviour of calcareous deposits under acidic environments and how the different factors such as pH, tem-

perature, calcium and magnesium concentrations, water circulation etc affect the formation of the protective calcareous layer.

1.3 Research questions and limitations

The following section includes the research questions studied in the specialization project, along with a summary of the most important findings. The following is crucial as the research question for this thesis will be based on these findings.

1.3.1 Previous Research Questions & Findings

During the specialization project, 5 important research questions were studied as shown below;

1. What is the current requirements on the steel surface in a closed environment?
2. Will calcareous deposit develop in acidic environment ?
3. How long will it take before the calcareous layer is developed ?
4. Will the generated chlorine affect pH, current requirement and the stability of the protection layer ?
5. Will the generated chlorine cause any additional environmental challenges inside the tower?

The main purpose of the previous work was to study the calcareous deposits behaviour in seawater and brackish water. The main findings during this work is displayed in Table 1.1. As it is shown, acidification occurred in both seawater and brackish water. The low pH seems to have affected the quality of the calcareous deposit, which was found to consist of Brucite (Low electrical resistivity). The final current density was found to be higher than the DNV GL specifications and the OCP was found to equal the normal OCP. Hence, the calcareous deposit was of low quality and didn't provide any significant protection when the CP is shut off. Furthermore, the calcareous deposit on the continuously polarized samples had very weak adhesion to the surface. On the other hand, the repolarized samples (after corroding freely for 1 week) had a very good adhesion to the surface. Moreover, the barrier properties of the repolarized samples seemed to be superior to the continuously polarized samples. It was then speculated that this behaviour could be due

to the formation of corrosion products below the calcareous deposit which in turn enhanced the barrier properties of the coating. Thus, two important aspects are to be studied; 1) A water renewal system to avoid acidification, and 2) Polarization of precorroded samples vs ideal conditioned samples.

Table 1.1: *Key findings from the specialization project [21].*

Electrolyte	Time [Days]	pH	Current Density [mA/m^2]	Microstructure	OCP	Repolarization Current Density [mA/m^2]
Seawater	0	7.95	2040	Brucite with a few aragonite islands	- 595 mV Ag|AgCl	340 after 1 week of repolarization
	9	4.5	750			
	28	7.5	400			
	42	6.7	340	NA		
Brackish Water	0	7.95	1200	Brucite	- 610 mV Ag|AgCl	190 after 1 week of repolarization 102 after 3 weeks of repolarization
	4	3.5	800			
	28	7.3	390			
	42	6.5	220	NA		
	69	NA	170	NA		

1.3.2 New Research Questions

This MSc project has 5 main research questions which will be used to direct the path of the MSc project and center the research. The questions are as follows:

1. What is the effect of water exchange on the pH, cathodic current density and the quality of the calcareous deposit?
2. What is the affect of the precorroded surface on the adhesion and the barrier qualities of the calcareous deposit?
3. What is the effect of acidification on the quality of the calcareous deposit ?
4. What is the difference between the Chlorine evolution reaction on the platinum anodes compared to the MMO anodes ?
5. How can the behaviour of pH during the CP be explained ?

1.3.3 Limitations

This report will primarily focus on the advancements and the work done within this field from relevant literature. As there are quite a few limitations such as time and the size of the project, the experimental work done during this work is limited

and the main purpose is to clarify which concerns are critical. For this project, the main focus will be on the behaviour of the calcareous deposits under acidic environment. Nevertheless, previous work done by Equinor will also be used to build a conclusion and hypothesis which will be the basis of future work.

1.4 Objectives of the Thesis

The first objective of this thesis is to study the effect of precorroded structures on calcareous deposition under the application of an ICCP system in confined environment and in a partially open system. This will be done by applying ICCP on precorroded and ground specimens in completely closed and partially open systems. The second objective will be to study the main difference in the Chlorine Evolution Reaction (CER) on the different inert anodes, namely, platinum (Control anode), MMO and Magnetite anodes. Finally, the last and final objective will be to create a parametric study from these results to find the optimal parameters (polarization potential, pH, anode type and water exchange rate) in case of the application of an ICCP system in a bare leaking monopile.

1.5 Outline of the thesis

This thesis consists of 7 chapters. In chapter 1, a brief introduction on offshore wind turbines and corrosion is given. The chapter ends with various research questions and limitations to specify the scope of the project and the work to be done. chapter 2 includes the theory behind the corrosion mechanisms and kinetics, in addition to studying the different cathodic protection techniques and the specifications needed to achieve adequate protection. Thereafter, the experimental approach and methodology will be presented in chapter 3. The results achieved from the experimental work and the relevant data from previous work done on this topic will be presented in chapter 4 in a proper manner. Thereafter, the results are discussed in chapter 5. Finally, the conclusion and the recommendation for future work are presented in chapter 6 and chapter 7, respectively.

Chapter 2

Theory and Literature Review

In the following chapter, the theoretical background needed related to this work will be defined and explained. This covers the cathodic protection methods (Sacrificial Anode Cathodic Protection and Impressed Current Cathodic Protection) and other factors induced by the following protection techniques, such as, hydrogen evolution, chlorine generation and calcareous deposition. In addition, to a comparison between the environments of a completely sealed and a leaking monopile foundation. Moreover, this chapter will include a literature review on the most recent research and advancement done on the topic of this work. In addition, the data provided from the experimental work will be analysed to properly estimate the behaviour of the system.

2.1 Cathodic Protection

Corrosion protection and control in marine environment can be achieved by different techniques, such as, coatings, cathodic protection, material selection, chemical inhibitors etc[22]. However, one of the most effective methods for corrosion protection is cathodic protection. The technique is simply based on supplying electrons to the protected metal from an external source. By doing so, the anodic reaction at the protected metal cannot produce electrons and the anodic reaction occurs at the external anodes where the electrons are supplied. Thus, the metal is protected. There are two main cathodic protection techniques that are commonly used in the industry, namely, sacrificial anode cathodic protection systems (SACP) and ICCP. [23]

As mentioned earlier, the cathodic protection system stops the anodic reaction from occurring at the metal surface. By doing so, the corrosion rate of the protected structure is controlled as the corrosion potential is reduced, bringing the metal to an immune state. The main difference between the two techniques is that the ICCP system uses an external power source with inert anodes. On the other hand, the SACP system uses the naturally occurring electrochemical potential difference between the sacrificial anodes and the metal to maintain protection.

Both methods are highly efficient, nevertheless, each of the two systems has their advantages and disadvantages. The ICCP system provides better protection than the traditional methods, as it is much more controlled and the design may be altered with changing conditions. Moreover, this system has very little effect on the environment and little carbon footprint. However, it has higher costs and has a relatively complex design and installation methods. Differently, the system cost much less to install and has a very simple design. It is however not environmentally friendly due to the large amounts of metal dissolved in water which makes it toxic and thus, not preferable. In addition, the large amounts of anodes needed is constituted with a large carbon footprint which goes against the strategy of various companies [22, 24]. The major criteria to consider when evaluating whether the ICCP system or the SACP is more appropriate, is the resistivity of the environment or terrain and the current requirements. As such, if the current requirement is less than 1000 mA and the the resistivity (ρ) of the system is lower then 3000 ohm·cm, the ICCP system is appropriate to use. The advantages and disadvantages of the two CP systems are displayed in Table 2.1[23].

Table 2.1: *Advantages and Disadvantages of the SACP and the ICCP [16, 23].*

ICCP	
Advantages	***Disadvantages***
Less number of anodes	Risk of over protection causing hydrogen induced stress cracking (HISC)
Installation costs is lower	Requires control reference electrodes which should work properly otherwise protection is lost
Lower unit cost of the current	Requires external power source and rectifiers
Long lifetime without retrofit needed if commissioned correctly	No protection is provided before the system is energized
Remotely controlled by an (ROV)	Generates more hydrogen than galvanic anodes
Freedom to adjust the required current if the corrosion rate increases	Known to need more maintenance
SACP	
Advantages	***Disadvantages***
No external power source is needed	Larger quantity of anodes is required
Protection is provided right away	Shorter lifetime than ICCP
No maintenance is needed	Larger drag force on the structure of the structure
Produces less hydrogen than ICC, thus no danger for HISC	Interference with anodes when placed together
No risk for overprotection	Unit cost of the current is higher
Easier to install	Only cost effective if the design is aimed for a short lifetime

2.1.1 Galvanic Anode Cathodic Protection -

The SACP technique uses the natural potential difference that exists between the metallic structure and the sacrificial metal in the same electrolyte to provide the driving potential. A schematic of this technique is displayed in Figure 2.1. As it is shown no external power source is required and the protective current is supplied directly from the anode. In practice these anodes are usually welded to the structure. The system also contains a reference electrode to measure the potentials against. However, the schematic does not include the reference electrode as it's assumed that it is installed. [25, 26, 27]

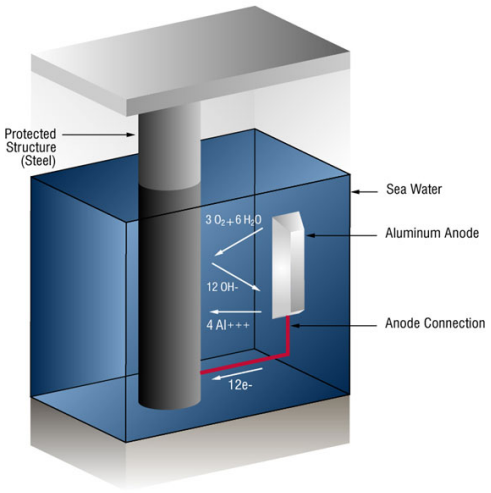

Figure 2.1: *Schematic of the system [27].*

2.1.1.1 Zinc, Magnesium & Aluminum Anodes

When it comes to the material of the sacrificial anodes, there are 3 main materials that are commonly used; Aluminum, Magnesium and Zinc. The open circuit potential difference of Magnesium is very negative which makes it problematic as a large number of anodes will be needed and hydrogen embrittlement is introduced. Meanwhile, the potential difference on the zinc and aluminium anodes is more positive which decreases the risk of hydrogen embrittlement. On the other hand, the open circuit potential of zinc is much lower and more positive than that of the magnesium. However, Zinc has been known to being toxic and induces pollution [28]. Similarly, the aluminium anodes are also bio-accumable but are less toxic [29]. Aluminium anodes are 2.5 times lighter than zinc making them cost effective. However, aluminium may become passive in sea water which leads to a potential shift closer to that of carbon steel. The preferred anodes for offshore structures are

aluminium zinc alloys as they are highly efficient, less toxic and contrary to the magnesium anodes, they are not consumed as fast. Therefore, premature consumption of the anodes is avoided if installed correctly. Although, aluminum anodes are efficient in open environment, they seem to be inefficient in closed environment as it was found that the evolution of aluminum ions in water leads to the acidification of the water and eventually self-consumption and increased corrosion rates. Hence, the aluminium anodes are not an option in closed environment. [18, 30, 31]

2.1.2 Impressed Current Cathodic Protection - ICCP

The ICCP system consists of an external power source, an impressed current anode, the electrolyte, a reference electrode and the structure to be protected. The power source induces positive current from the impressed current electrode through the corrosive solution and on to the protected structure[26, 27, 32]. Figure 2.2 displays this technique, but note that the reference electrode is not included in this schematic. One of the major challenges of this technique in closed environments are overvoltage and chlorine generation. The chlorine generated at the anode may lead to acidification of the water as the evolution of chlorine in seawater leads to the generation of hydrochlorous acid (HOCl). The drop of pH would also lead to higher corrosion rates and possibly increased current requirement. On the other hand, the calcareous deposits at the steel surface may be broken down leading again to an increase in the current requirement. The importance of the calcareous deposits will be further discussed in the next section.[23, 30]

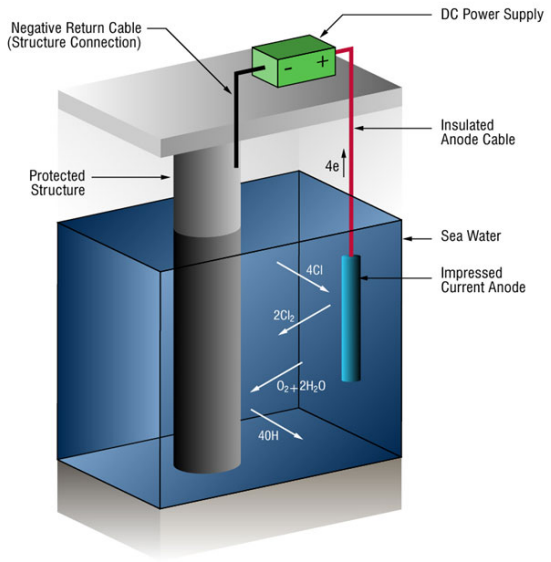

Figure 2.2: *Schematic of the ICCP system [27].*

2.2 Fully Sealed Vs Leaking Monopiles

2.2.1 Fully Sealed Monopiles

Offshore wind turbines monopiles were initially designed to be completely sealed. Hence, no water replenishment or renewal would occur. With this in mind, the DNV guidelines specified that no protection would be needed, provided that no new oxygen would enter the system. The reasoning to this assumption will be given in the next subsection.

Corrosion induced by Dissolved Oxygen

Although the system is completely sealed, the initial electrolyte in the monopile is saturated with oxygen. And as there is no protection, the steel will corrode by the dissolved oxygen. But how significant is this corrosion. The following can be calculated with some simple assumptions on the dimensions of the monopile. Assuming that the monopile foundation is 10 meters in diameter and contains a 24 meter high water column, and 6 meters between the surface of the water and the airtight deck. From this assumption, the volume of the water would be 1885 m^3 and the volume of the air is 471 m^3. We then make a conservative assumption that the concentration of oxygen in seawater is 10 mg/l. Hence, we would get 18.85 kg of oxygen in seawater. The second assumption would be that oxygen in the air column would be 99 kg assuming 21 % of oxygen in the air. Thus, the total oxygen mass would be 117.85 kg. From the chemical reaction between water and iron as displayed in Equation 2.1, we find that 1 kg*mole of oxygen dissolves 2 kg*mole of iron. From the previous assumption we get that 1 kg of oxygen dissolves 3.5 times of iron. Thus, a total of 412.5 kg of steel will be dissolved. Now, assuming that the thickness of the monopile walls are 70 mm, the volume of metal lost is 0.052 m^3 and the submerged surface is 753.6 m^2. We finally get that the lost thickness is 69 μm, which is approximately 0.1 % of the total thickness. Hence, the corrosion induced by the dissolved oxygen is significantly small and wouldn't affect the integrity of the structure. The calculations are displayed in more detail below. The following assumptions are highly conservative, and even so, the corrosion induced by the dissolved column is still not significant.

$$2Fe + 2H_2O + O_2 \rightarrow 2Fe(OH)_2 \tag{2.1}$$

$$
\begin{aligned}
&V_{Water} = \pi \cdot 5^2 \cdot 24 = 1885 \ [m^3] \\
&V_{Air} = \pi \cdot 5^2 \cdot 6 = 471 \ [m^3] \\
&M_{DO} -= 10 mg/l \cdot 1885 m^3 = 18.85 \ [kg] \\
&M_{Oxygen-Air} = 471 \cdot 0.21 = 99 \ [kg] \\
&M_{Total-Oxygen} = 18.85 + 99 = 117.85 \ [kg] \\
&Dissolution-Ratio = \frac{56 \cdot 2}{16 \cdot 2} = 3.5 \\
&A_{submerged-surface} = \pi \cdot 10 \cdot 24 = 753.6 \ [m^2] \\
&M_{Loss} = 117.85 \cdot 3.5 = 412.5 \ [kg] \\
&V_{Loss} = 412.5/7800 = 0.052 \ [m^3] \\
&Thickness-Loss = 0.052/753.6 = 69 \ [\mu m]
\end{aligned}
\tag{2.2}
$$

However, the previous calculations are extremely conservative compared to reality as one has neglected the fact that there are aerobic organisms inside the column. These organisms will consume the oxygen in the air, leading to anaerobic conditions with very little dissolved oxygen. Lee et al. [33] reported that under typical marine storage conditions, dioxygen in natural seawater exposed to fuel and carbon steel was reduced to < 0.1 mg/l within 2 days due to consumption by corrosion reactions and aerobic microbial respiration. Moreover, one should take onto consideration that the concentration of oxygen is lower in deeper water. Hence, much lower corrosion would be observed in the deeper parts of the monopile. With this in mind, it can be proved that the previous calculations are very conservative and in reality no corrosion will be observed, provided the system is completely sealed.

Microbially Induced Corrosion (MIC)

Theoretically speaking, the anaerobic conditions in the monopile combined with the natural sulfate content in seawater the activation of the metabolization of the SRB (Sulfate Reducing Bacteria) is possible. The SRB's activity will increase dramatically and extremely fast leading to a possible initiation of the MIC. However, in practice the reproduction rate of the SRB is very limited and can't be sustained for long as the volume is closed and there is only so much volume in the monopile.

Hence, the reproduction of the SRB's stops well before it becomes a risk as they are suppressed by the build-up of their metabolic byproducts and the fact that they would eventually run out of nutrients as the system is closed. In conclusion, MIC could initiate in a closed monopile, however, it would eventually cease and ultimately would not cause any significant damage.

2.2.2 Leaking Monopiles

In practice, it was found that the assumption of fully sealed monopile is not always valid, as there are very few monopiles that were completely sealed. This led to many problems as the monopiles had to be checked more often then usual which means that the air-tight deck would be opened much more often then anticipated. Furthermore, unexpected movements of the transition piece were observed leading to additional loads on the J-tube which lead to the failure of the J-tube seals. As a result, the damaged seals permitted the inflow of water leading to active corrosion.

As the assumption of a completely sealed system became invalid, the DNV guidelines and iso standards changed its specification to needing protection internally, either by CP or Corrosion allowance. Most of papers and researches have favoured the use of a CP system as it seemed to be the fastest and most practical solution for the current wind turbines that are in service. However, when talking about the application of a CP system, one can't neglect the production of hydrogen gas which comes with various hazards as stated in NS-EN 12499 (Internal cathodic protection of metallic structures-2003). Thus, the application of the CP in a sealed closed system requires the installation of a ventilation system in the head spaces. This becomes problematic as the desired air tight environment is not possible to achieve anymore.

Various attempts and studies were done on the application of a CP system in confined spaces. The application of CP with aluminium as sacrificial anodes led to acidification. On the other hand, zinc did not lead to the same amount of acidification, however, its use is not preferable by many companies. Finally, CP by impressed current seemed to be the next best thing. However, it came with its own challenges as well. Due to the large area difference, the potential on the inert anodes was very high leading to the production of chlorine and consequently acidification. This is studied in much more detail in section 2.7.

2.3 Calcareous deposition under Cathodic Protection

An extremely critical quality of the use of cathodic protection in seawater is the formation of a calcareous layer (magnesium and calcium containing compounds) on the steel surface [34]. The formed calcareous deposits reduce the rate of diffusion of dissolved oxygen to the steel surface which reduces the necessary current to provide a long and sufficient cathodic protection [35, 36, 37]. Various studies have investigated the dependency of the rate and quality of calcareous deposition on the chemical and physical variations of seawater. From which it was found that the protective layer depends on the applied potential, flow characteristics, current density, pH, temperature, surface finish and seawater chemical composition [38].

2.3.1 Formation of the Calcareous Deposit

The calcareous deposition starts with the formation of a thin uniform Mg rich inner layer ($Mg(OH)_2$), followed by a layer of aragonite and calcite ($CaCo_3$) [39, 40]. The formation of the ($Mg(OH)_2$) film is dependent on the increase of pH as a result of the corrosion reactions. After the the formation of the ($Mg(OH)_2$) the pH drops locally leading to the formation of the aragonite. The main reactions that occur during the corrosion of steel structures in seawater are iron oxidation, oxygen reduction and hydrogen evolution as shown in Equation 2.1 and Equation 2.3.

$$2H_2O + 2e^- \rightarrow H_2 + 2OH^- \tag{2.3}$$

The increase of the OH^- concentration on the steel surface leads to an increase in pH and eventually the precipitations of $Mg(OH)_2$ on the surface as shown in Equation 2.4.

$$Mg^{2+} + 2OH^- \rightarrow Mg(OH)_2 \downarrow \tag{2.4}$$

After the formation of the $Mg(OH)_2$ film, the pH drops locally as the hydroxides are used up to form aragonite. While on the electrode surface, the production of OH^- changes the inorganic carbon equilibrium and results in a buffering reaction which eventually leads to the precipitation of $CaCO_3$, as shown in Equation 2.5

and Equation 2.6.

$$OH^- + HCO_3^- \Longleftrightarrow H_2O + CO_3^{2-} \tag{2.5}$$

$$Ca^{2+} + CO_3^{2-} \rightarrow CaCo_3 \downarrow \tag{2.6}$$

From the aforementioned reactions it can be concluded that the concentrations of calcium and magnesium are critical for the calcareous deposits. Neville and Morizot [39] investigated this by testing the formation of the calcareous deposits under different electrolytes as displayed in Figure 2.3. From the results, it can be seen that the magnesium-free electrolyte led to very little surface coverage in the first few hours but covered approximately 70% of the surface by the third day. On the other hand, the calcium free electrolyte led to the coverage of approximately 50-60% of the surface after just the first hour and came to cover 90% of the surface after 3 days. Finally, the Ca+Mg electrolyte led to covering approximately 50% of the surface which is very similar to the calcium free electrolyte. By the third day approximately 100% of the surface was covered. the following observations fits very well with the theory of the calcareous depositions, as the mechanism is primarily driven by the Mg concentration in the beginning which can be seen from the similar behaviour between Ca-free seawater and the Ca+Mg seawater the first few hours. Thereafter, the build up of the calcareous layer is dominated by the formation of the Aragonite and Calcite ($CaCO_3$).

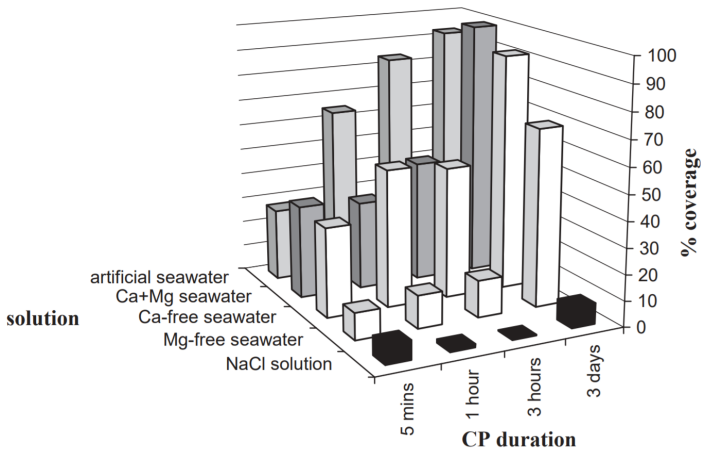

Figure 2.3: *Quantification of scale after various periods of CP and in different electrolytes determined by the electrochemical analysis [39].*

2.3.2 Factors Affecting the Build Up of the Calcareous Deposits

As previously mentioned, there are various factors that affect the formation of the calcareous deposits such as temperature, current density, surface pH, flow characteristics, surface conditions (corrosion products) and seawater chemical composition [34, 38, 41]. Thus, it is critical to be aware of how these parameters affect the calcareous deposits. As this makes it possible to highlight the key differences between the laboratory and the real conditions, which makes it easier to know what to expect in practice.

Applied Potential, Current Density and surface pH

The effect of the applied potential on the calcareous deposition and current density is displayed in Figure 2.4. It is clear that the calcareous deposition is faster with the increase of the applied potential. This effect comes from the change of the potential on the metal surface, as the cathodic current density increases with the increased potential leading to a higher concentration of OH^-. As the formation of the $Mg(OH)_2$ depends on the activity of OH^-, we obtain a higher calcareous deposition rate [40]. Barchiche et al. [41] showed also that the type of mineral varies with the applied potential. As he reported that at potentials lower than -1.345 V vs. Ag|AgCl, brucite was the only formed mineral, while at aragonite was formed at potentials between -0.945 and -1.145 V vs. Ag|AgCl. Differently, a blend between aragonite and brucite was formed at potentials between -1.145 V and -1.245 V vs. Ag|AgCl [41].

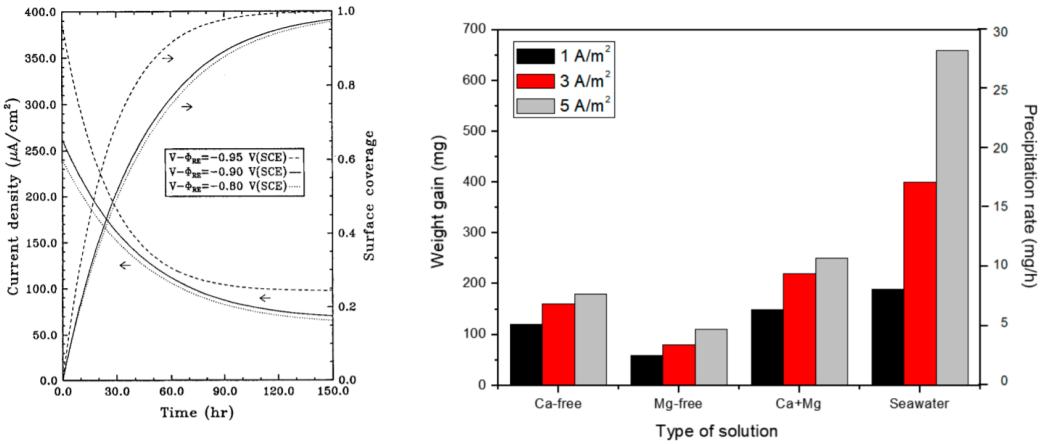

(a) Effect of applied potential on the change in current density and surface coverage with time [34].

(b) Variation of weight gain on calcareous deposit films in artificial seawater and natural seawater after 24 hours [40].

Figure 2.4: *Effect of the applied potential and current density on the formation rate of the calcareous layer [34, 40].*

Temperature and Precipitation pH

According to Ce and Paul [42], the minimum necessary pH for the precipitation of brucite ($Mg(OH)_2$) and aragonite/Calcite ($CaCO3$) decreases with the increase of temperature. This effect can be seen in Figure 2.5. As lower the calcareous precipitation pH means needing lower concentrations of OH^-. Thus, lower applied potential and current density is needed to form a similar amount of calcareous deposits on the metal surface at higher temperatures than at lower temperatures. This was also researched by Barchiche et al. [41] where it was found that the necessary current was halved after 7.5, 15 and 41 hours at 30 °C, 20°C and 10 °C, respectively [41]. Moreover, it was reported that at higher temperatures aragonite was found to be the dominating mineral, while calcite was the dominating minerals at lower temperatures [43].

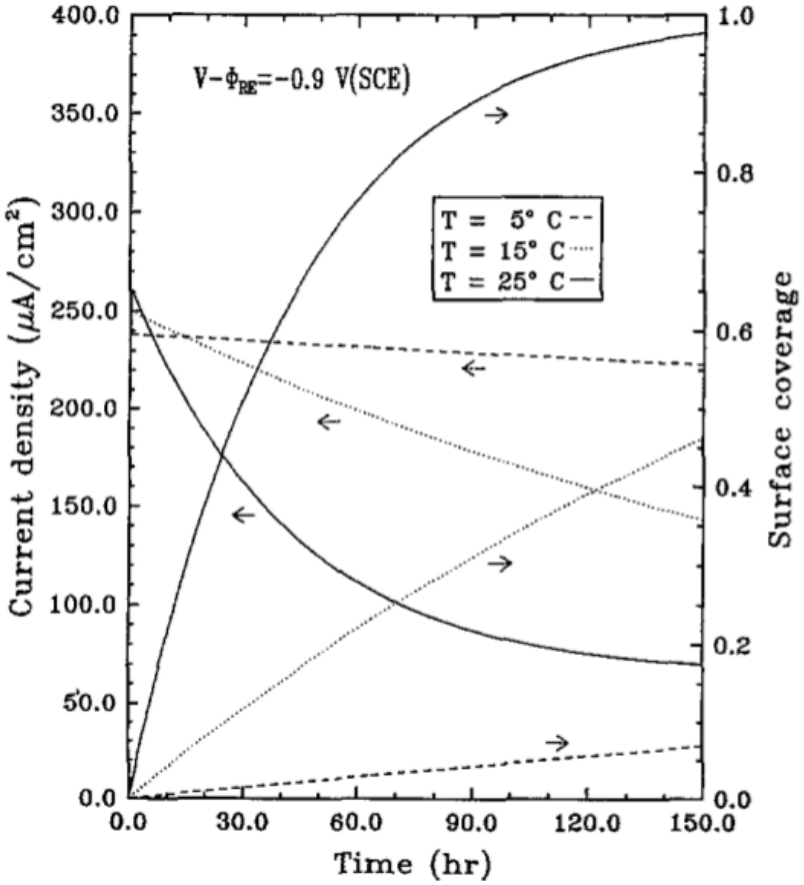

Figure 2.5: *Effect of temperature on the change in current density and surface coverage with time [34].*

Flow Rate and Seawater Composition

The stirring of the electrolyte controls the mass transport of O_2, Ca^{2+}, HCO_3 and Mg^{2+} at the electrode interface. Thus, the hydrodynamic conditions near the electrode strongly affect the calcareous deposit formation, both in terms of composition and kinetics [44, 45]. Hartt et al. [38] studied the effect of flow rate on the formation of the calcareous deposit. It was found that the film thickness of protective layer decreased with increased flow rate [44]. This is due to the increase of the required current and mass transfer with the increase of flow rate [46]. It was also found that the effect of flow rate on the thickness is much more significant for higher applied potentials [38]. Seawater composition was shown to be significant for the growth rate of aragonite and calcite, as the formation of two minerals were found to be inhibited due to increased concentrations of Mg^{2+}, PO_4^{3-}, HPO_4^{2-} and SO_4^{2-} [41, 43].

2.3.3 Quality of the Calcareous Deposits

2.3.3.1 Protectiveness Index-Ca/Mg Ratio

One of the most important parameters to be considered when evaluating the quality of the calcareous deposit is the Ca/Mg ratio (typically 5.2 mol/mol [41]), or else referred to as the protectiveness index [47]. The protectiveness ratio is a good indicator to evaluate how effective the calcareous deposit is, as the protection increases with the increase of this ratio. According to Li and Du [48], the low Ca/Mg ratio indicated a high concentration of the magnesium ions which occupied the place of calcium ions and prevents calcite and aragonite from precipitation on the surface. Thus, the calcareous deposits becomes less effective. This was also proven by Barchiche et al. [41]. This phenomena has been investigated by Deslouis et al. [49]. The results from this research is displayed in Figure 2.6. Deslouis et al. [49] investigated the reduction of current density with increased Mg^{2+} concentration as shown in Figure 2.6a. As it is displayed the time needed for the reduction of the current density increased with the increase of the magnesium concentration (where $[Mg^{2+}]_{ref}$=5.5 mol/l : Typical magnesium concentration in sea water) [49]. Figure 2.6b displays the reduction of the current density w.r.t the composition of the layer. It is clear that the protective layer that consists of brucite is much less effective in reducing the current density which supports the theory that the decreased presence of $CaCO_3$ leads to lower protection. Hence, the $[Mg^{2+}]$ and the Ca/Mg ratio should be monitored to be able to evaluate the effectivity and quality of the obtained calcareous deposits.

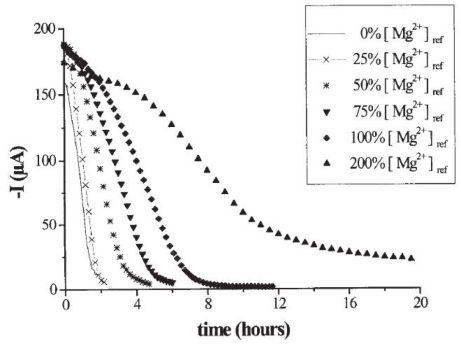

(a) Influence of Mg^{2+} concentration on calcareous deposits on steel in artificial seawater at -0.945V Ag|AgCl.

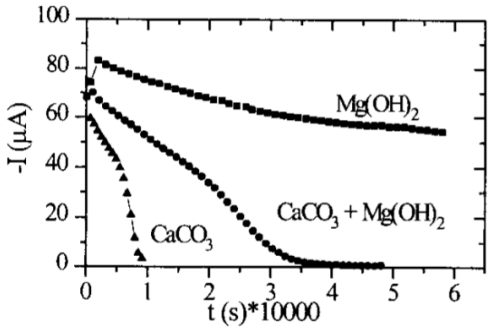

(b) Chronoperometric curves for $CaCO_3$, $Mg(OH)_2$ and Calcareous deposits ($CaCO_3$+$Mg(OH)_2$).

Figure 2.6: *Effect of the Mg^{2+} on the quality of the calcareous deposits [49].*

2.3.3.2 Microstructure of the Calcareous Deposits

As previously established, The calcareous deposits consists primarily of a thin brucite film and a thick $CaCO_3$ which is built up over this film. The $CaCO_3$ comes primarily in two forms, namely, aragonite and calcite [39, 49]. The $CaCO_3$ is the most important mineral as it has a much higher electrical insulating properties than $Mg(OH)_2$ [50]. This effect was discussed earlier and is illustrated in Figure 2.6b [49]. Deslouis et al. [51] studied the affect of the magnesium ions on the two forms of $CaCO_3$ and found that their growth rate is inhibited by these ions. However, it was also found that the aragonite is not further affected by these ions once it has formed. On the other hand, the calcite is affected even when it is formed [43]. Hence, under the presence of magnesium ions the aragonite would be the dominating mineral. This was proven by Möller [52] as he reported that in the presence of magnesium ions, aragonite was the only form found. While in the absence of magnesium, calcite was the only form of $CaCO_3$ found [52]. Furthermore, it was reported by Möller [52] that The aragonite crystals are more effective in covering the surface than the calcite crystals and are therefore more useful in preventing oxygen from reaching the steel surface. The microstuctures of calcite and aragonite are displayed in Figure 2.7a and Figure 2.7b, respectively. The calcite is characterized with having a rhombohedral shape, while aragonite has a flower like shape [52]. The third most common form of the calcareous deposit is magnesium-hydroxide or Brucite. This type of microstructure forms much smaller crystalls that have a needle-like shapes or shaped like thin threads. The microstructure of brucite is displayed in Figure 2.8.

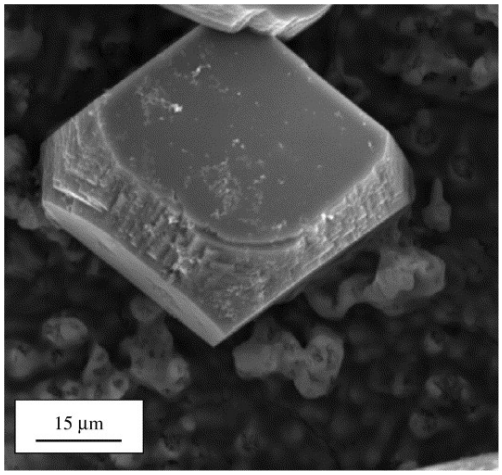

(a) High magnification SEM image showing the characteristic rhombohedral shape of a calcite precipitate.

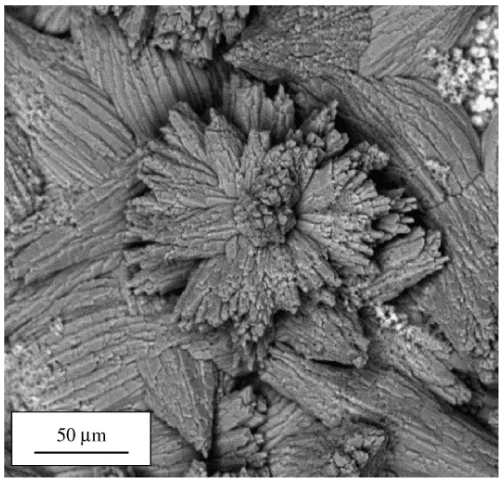

(b) SEM image showing aragonite deposits that formed during immersion for 21 days in Mg^{2+}

Figure 2.7: *Illustration of the different microstructures of $CaCO_3$ [52].*

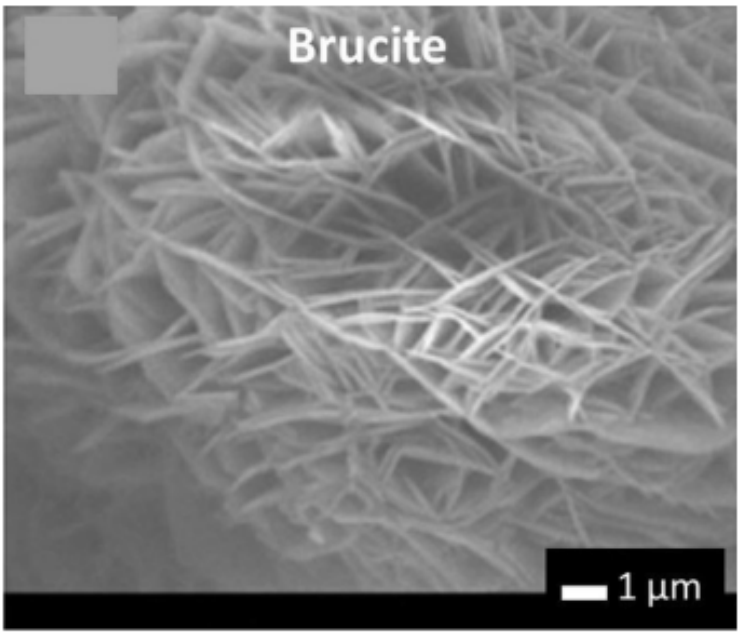

Figure 2.8: *Picture by scanning electron microscopy og $Mg(OH)_2$ brucite [53].*

2.4 Cathodic Protection of Precorroded Structures

The calcareous deposition occurs on various types of electrodes. However, the mechanism and morphology of the calcareous deposit is dependent on the surface conditions of the electrode as shown in various studies [44, 54, 55]. Barchiche [55] reported that the surface roughness has no affect on the kinetics and mechanisms of the formation of the calcareous deposits. However, the existence of an oxide layer on the surface led to a change in the deposit formation kinetics. As Barchiche [55] explained that a part of the cathodic current is taken by the oxide layer which leads to a modification of the reduction reaction on the steel surface.

Refait et al. [56, 57] studied the behavior of strongly rusted carbon steel under cathodic protection. Refait et al. [56] studied coupons which had been corroding freely for 6 years before being subjected to CP for 1 year. The CP system was found to be quite effective and the corrosion was reduced by an order of 10. Nevertheless, complete protection was not achieved. The surface inspections showed that the film formed on the surface was made of corrosion products with a calcareous deposit outer layer. Figure 2.9 displays the structure of the calcareous deposits and corrosion products formed. The following structure was explained by Yang [58]. As the pH increases under CP. Hence, if the potential is not low enough the steel will form iron oxide (magnetite) which is built below the calcareous deposit. The following mechanism was observed by Refait et al. [56] as magnetite and other corrosion products were detected below the calcareous deposits formed under CP.

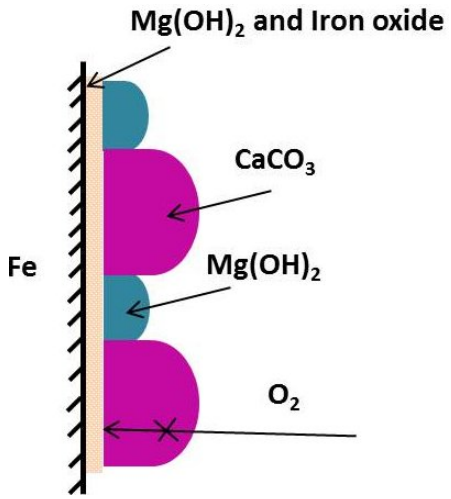

Figure 2.9: *Schematic of calcareous film on mild steel surface during cathodic protection in artificial sea water [58, 59].*

Refait et al. [57] studied three cases of CP systems in a tidal zone as follows; 1) Permanent cathodic protection for 7 years, 2) Delayed cathodic protection, 6 years without CP + 1 year with CP and 3) Interrupted cathodic protection, 6 years with CP + 15 months with no protection. Refait et al. [57] found that the permanently protected coupons experienced corrosion rates similar to atmospheric corrosion. Moreover, it was observed that the delayed CP system obtained an effective protection within a few days. In addition, It was found that part of the Fe(III) oxyhydroxides were reduced to magnetite as a result cathodic polarisation. For the last case, it seemed that the interruption of the cathodic protection system had similar corrosion rates to the permanently protected system, as the calcareous deposit on the surface may have provided enough protection to the steel such that corrosion is minor. Nevertheless, new corrosion products were found below the calcareous deposit. Thus, the steel did corrode when the protection was interrupted but with a lower rate as the calcareous layer provided some protection.

From the aforementioned research, it is likely to form corrosion products or iron oxides below the calcareous layer. This is highly crucial to understand as the electrical resistivity of the coating is different from pure calcareous deposits. Gartland et al. [54] studied this effect and it was reported that surfaces with rust beneath the calcareous layer have the lowest average current densities. Analytically, this could be explained by having two resistances in series, the first electrical resistance is from the magnetite (corrosion product) and the second electrical resistance is induced by the calcareous deposit. Liu et al. [60] also observed a very important mechanism. It was found that calcite is the form of calcareous deposits that forms under room temperature and under potentials between -945 mV to 1245 mV(Ag|AgCl). It was observed that the calcite crystals have large gaps between the individual precipitates where the rust were formed. Hence, enhanced barrier properties was obtained. In other words, the rust led to a denser protective layer and the needed current density decreased as a consequence.

2.5 Chlorine Evolution under ICCP

2.5.1 Formation of acidic products

Under ICCP, there are two reduction reactions that are competing. The first reaction is oxygen evolution reaction (OER) and chlorine evolution reaction (CER) as shown in Equation 2.8 and Equation 2.7. [61, 62]

$$\begin{aligned} &2Cl^- \rightarrow Cl_2 + 2e^- \\ &E^\circ_{Cl_2/Cl^-} = +1.161V \ vs \ (Ag|AgCl) \end{aligned} \tag{2.7}$$

$$\begin{aligned} &2H_2O \rightarrow O_2 + 4H^+ + 4e^- \\ &E^\circ_{O_2/H_2O} = (1.031 - 0.059 \cdot pH)V \ vs \ (Ag|AgCl) \end{aligned} \tag{2.8}$$

This is valid in the presence of chloride which is found in seawater. As the pH drops below a pH 8, the evolved chlorine reacts with water and leads to the production of hypochlorous acid (HOCl), hypochlorite ions (OCl^-) and chloride acid (HCl) [63, 64] which act as anti-fouling reagents [65]. The following reactions are displayed in Equation 2.9, Equation 2.10, Equation 2.11 and Equation 2.12.

$$Cl_2 + H_2O \longleftrightarrow HCl + HOCl \tag{2.9}$$

$$Cl_2 + H_2O \longleftrightarrow HOCl + H^+ + Cl^- \tag{2.10}$$

$$Cl_2 + OH^- \longleftrightarrow HOCl + Cl^- \tag{2.11}$$

$$HOCl \longleftrightarrow H^+ + OCl^- \tag{2.12}$$

The form at which the aqueous chloride species are present depends on the pH. At pH levels ($3 \geq$ pH ≤ 7.46), Equation 2.11 is the dominating reaction, and the the hypochlorous is the form of the aqueous chloride. However, a shift occurs as the pH increases ($pH \geq 7.46$), the present form becomes dominated by the hypochlorite ions. The aqueous chlorine form with respect to the change of pH is displayed in Figure 2.10. [64, 66, 67]

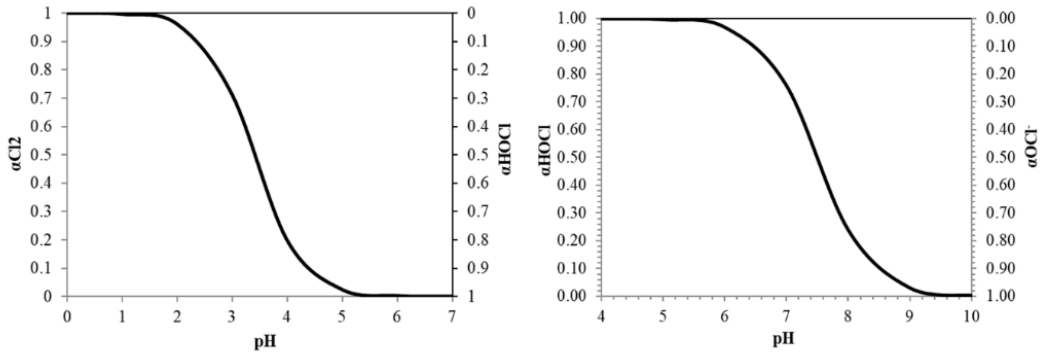

Figure 2.10: *Distribution of aqueous chlorine and hypochlorous acid in electrolyzed seawater at different pH levels [66].*

2.5.2 Selectivity and Competition Between the Anodic Evolution of Oxygen and Chlorine

As mentioned previously, the CER leads to acidification of the water in closed system due to the production of chlorine, Cl_2. Hence, it is of critical importance to understand which factors affects the CER and how it is related to the OER. Vos and Koper [68] studied the selectivity between chlorine evolution and oxygen evolution in aqueous media under low pH. Figure 2.11 displays the change of the CER and OER currents with the increase of potential.

It can be seen that after 1250 mV vs. Ag|AgCl the CER becomes more dominant as the current,i_{CER}, becomes much higher than the OER current, i_{OER}. Hence, at potentials higher than the CER potential, the anodic reaction becomes dominated by the CER. As the current density is directly related to the potential, it can be reasoned that the CER is more dominant at higher current densities. Similar trends were observed by Hine et al. [69], as it it was shown that the increase of current density caused the OER efficiency to decrease and the CER to increase. These ob-

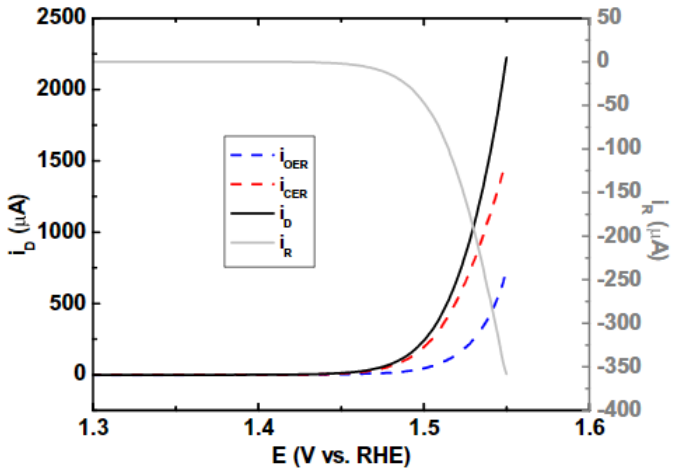

Figure 2.11: *Change of the CER and OER currents with the increase of potential [68], where i_D is the current measured on the steel disk, i_r is the current demand on the Pt Ring and RHE refers to the reversible hydrogen electrode.*

servations agree well with the theory as it was previously reported that the CER exchange current density is generally 4–7 orders of magnitude higher than OER because of the easier catalysis of a two-electron process (CER) vs the a four-electron process (OER)[70]. Hence, when the potential exceeds CER potential, the cathodic reaction will be highly dominated by the CER. Hine et al. also investigated the effect of NaCl concentrations (salinity) on the the efficiency of the reactions. From which he reported that the change of efficiencies is specially noticed in waters with low salinity, where waters with high salinity $[NaCl] \geq 3\%$ had maintained the same efficiencies as the current density increased. Vos and Koper [68] explored the effect of the chloride concentration,$[Cl^-]$, on the OER and CER efficiencies as shown in Figure 2.12. As it is displayed, the OER rate is not effected by the chloride concentration. However, the CER rate seems to be dependent on the chloride under higher potentials (potential $\geq$ 1200-1250 mV vs. Ag|AgCl). Hence, chloride concentrations will increase the efficiency of the CER. Therefore, the chlorine production in seawater will be aggressive.

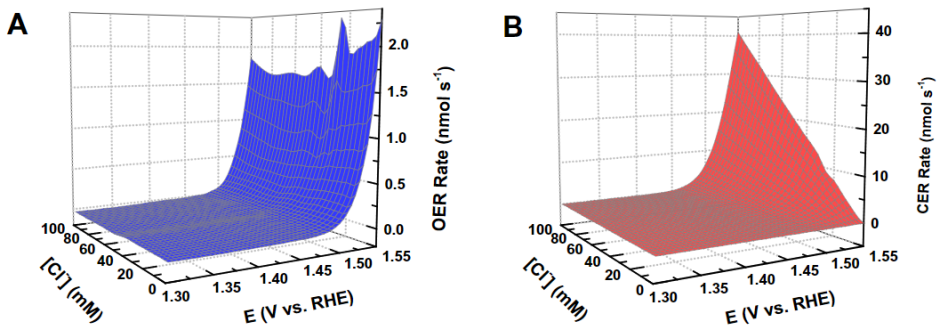

Figure 2.12: *Plots of the OER rates (A) and CER rates (B) as a function of Cl^- concentration and electrode potential [68].*

2.6 Testing Methods

There are various methods to characterise the calcareous deposits. However, during this report there are 2 main parameters that are to be studied. The first parameter is the calcareous formation under cathodic polarisation. On the other hand, the testing will occur in simulated confined spaces and in a partially open space. Thus, acidification can be expected. Therefore, it is crucial to study the behavior of calcareous deposits in an acidic environment. The cathodic polarisation will be done by using potentiostatic polarisation. This method is based on applying a constant potential (-1050 mV vs. Ag|AgCl), while measuring the corresponding current as a function of time. By doing so, one can observe the current requirement drop induced by the calcareous deposits. Thereafter, the calcareous deposits will be characterized by studying their chemical composition and microstructures. This is achieved by using Scanning Electron Microscope (SEM) to identify the present microstructures & topography, and Energy dispersive X-ray Spectroscopy (EDS) will be used to find the chemical composition of the calcareous deposits. Finally, the last test will be to dip the polarised specimens in the acidic seawater and observe the behaviour of the calcareous deposits in acidic environment. A summary of the tests to be performed during this report is displayed in Table 2.2. A precise explanation of the different test set-ups will be provided in chapter 3. [71, 72, 73]

Table 2.2: *Overview of the tests to be performed and their objective*

Test	Objective/Output
Potentiostatic polarisation	Evolution of the current requirement vs time of precorroded and non-corroded structures in closed and a partially open systems
Potentiodynamic polarisation curves	Effect of the calcareous deposit on the cathodic polarisation curve
Scanning Electron Microscope (SEM)	Calcareous deposit microstructure (Brucite, Calcite, Aragonite, Dolomite etc...)
Energy dispersive X-ray Spectroscopy (EDS)	Chemical composition of the calcareous deposits
Calcareous deposits in acidic solution	Degradation of the calcareous deposit in acidic environment

2.7 Literature Review and Recent Works

This section will include a summary of the relevant literature and case studies. In addition, this section will include the critical analysis of the research done around "*internal corrosion and use of cathodic protection in closed compartments*" to refine the topic and frame the research questions. Up to the year 2010, it was assumed that the monopile foundations were completely sealed. Hence, the approach of 'Nearly closed compartments' was used according to DNV-OS-J101 [17]. By way of explanation, this is to say that there is little to no interaction between the inside and the outside of the monopile foundation. Consequently, the O_2 is constant and will decrease with time. Thus, a very low corrosion rate is expected. On the other hand, the bacteria will stop growing as the nutrients are limited and the MIC will not be of danger. Hence, no corrosion protection is needed for the internal of the monopile. However, this was proved to be wrong as practical experience and inspection showed that these structures are not airtight and according to DNVGL-RP-0416 recommended practice [10], protection of the internal surfaces of the monopile should be applied by using either a coating system, corrosion allowance, a CP system, or a hybrid system.

Sacrificial Anodes CP

Due to economic and practical issues, cathodic protection with sacrificial anodes and impressed current systems were the corrosion protection methods to go for. Delwiche and Tavares et al. (2017) conducted a trial on the use of the aluminium anodes for internal protection. The study helped establish the current density requirements of CP system. However, an unexpected drop in pH (pH$\approx$ 4.5) was observed. Although no significant H_2 levels were measured, but the introduction of CP in monopiles has found that hydrogen sulphide gas can be evolved in the initial period [74]. This called for a deeper study to clarify the aforementioned observations. The acidification was mainly observed under the use of aluminium anodes in confined compartments. This occurs as a result of the reactions on the aluminium anode. The first part of the acidification process occurs by the production of the aluminium ions as shown in Equation 2.13.

$$Al \rightarrow Al^{3+} + 3e^{-} \tag{2.13}$$

Thereafter, the aluminium anodes reacts with the water and produces aluminium-hydroxides and hydrogen ions which eventually results in the decrease of pH as

demonstrated in Equation 2.14.

$$Al^{3+} + 3H_2O \rightarrow Al(OH)_3 + 3H^+ \tag{2.14}$$

Delwiche and Lydon et al. (2018) studied the water pH and gas evolution risks associated with the use of aluminium and zinc anodes for the internal protection. The trial was conducted in a monopile structure in the north sea. Delwiche and Lydon [75] reported that the CP with aluminum anodes led to a high reduction in pH (pH ≈5) within a few days. Furthermore, he observed that the application of CP with sacrificial anodes resulted in localized increases in acidity and production of H_2S, H_2 and CO_2. Delwiche and Lydon [75] discussed that the decrease in pH and observed behaviour could be a result to hydrolysis of the Al anodes corrosion products which produced the observed acidic conditions. Moreover, the application of CP system leads the to the production of the hydroxide ions which removed the buffering salts from the solution and contributes to the reduction in pH. Another important observation was the fact that the hydroxide ions formed at the buried steel surface, are trapped by the mud. Hence, it didn't contribute to buffering the solution. Delwiche and Lydon [75] concluded that in case of the use of aluminum anodes in confined spaces, hydrogen sulfide may be produced and a very low pH is to be expected. Thus, replenishment of the water is essential to avoid these risks. However, it is preferred that the zinc anodes are to be used over the aluminum anodes if the replenishment of the water is possible as the decrease in pH is less aggressive and lower circulation rate would be needed.

Maher and Swain et al. (2019) studied the possibility of using zinc anodes for CP of the internal surface of the monopile. Maher and Swain [76] tested the effectivity of the use of Zinc anodes in a sealed system and a system where the water is circulated to avoid acidification. It was reported that the sealed CP system led to acidification and was found to be covered with Zinc carbonate, $ZnCO_3$, chalking. Another important observation found was the lack of calcareous deposits on the surface. This could be a potential problem as the calcareous scale decrease the current needed. Thus, accelerated consumption of the zinc anodes could occur if the calcareous deposit is not effective. On the other hand, the open CP system was found to be very effective, as the pH was quite stable and a calcareous deposit had formed on the steel surface. Maher and Swain [76] also studied two cases where the steel was corroding with no protection under a confined system and a circulating system. From which it was reported that the dissolved oxygen concentration of the latter system was 4 times higher than the closed system, meaning a significantly higher corrosion rate should be expected.

Briskeby et al. (2015) investigated the efficiency of the use of zinc and aluminium sacrificial anodes for CP of internal surfaces. Similarly, it was found that the pH decreases dramatically under the use of the aluminum anodes (pH $\approx$ 4.3). Meanwhile, the zinc anodes experienced a much lower degree of acidification (pH $\approx$ 6.5). Briskeby et al. [77] reported that the acidification increased the current and current density needed for protection. The initial and mean current density requirements for the CP with aluminium anodes were found to be 170 and 120 mA/m^2 respectively. Delwiche and Tavares [74] reported similar values for the initial current density requirement (i = 150 mA/m^2). On the other hand, the zinc anodes only needed 120 and 30 mA/m^2 for the initial and mean current densities. Hence, the zinc base CP system was found to be much more effective than the aluminum anodes. The values for the low current densities are reasoned to be because of the better calcareous deposit formed. This is believed to be due to the lower degree of acidification that takes place under the use of zinc anodes. Delwiche and Tavares (2017), studied the required water replenishment rate to avoid acidification of the water. The J-tube seals were modified such that a 5% daily water circulation occurs. This rate did not lead to a complete avoidance of acidification of the water as the pH was around pH 6, nevertheless, this rate was considered to be satisfactory.

Impressed Current CP System

Another suggested solution was the use of impressed current cathodic protection for the inside of the monopile. Krebs et al. (2018) conducted a pilot study on the application of an ICCP system for internal protection. The system was installed and is currently operating successfully in 39 different wind turbines in the Baltic sea near Germany. The inert anodes were made of magnetite instead of the usual MMO anodes. Krebs [15] justified the following choice by the fact that the magnetite anodes have a lower oxygen overvoltage but a lower chlorine production efficiency. The reasoning was based on the anodes surface microstructure, as the magnetite anodes is a ferrite materials which have a lower oxygen overvoltage and a higher oxygen efficiency than the usual MMO anode. Hence, lower amount of chlorine will be generated and the water exchange through the imperfect seals will be sufficient to maintain the pH at an ambient level. Krebs [15] reported that the specific current density demand needed for protection was as small as 15mA/m^2. However, the structures were polarised to -800 mV vs. Ag|AgCl which is the reason for the low current density required. Another possible reason for the low current density is that the calcareous deposit formed under CP is very effective. And as there is no large flow speeds, the calcareous deposit probably also has very good adhesion to the surface. For approximately a year, no chlorine gas nor hydrogen gas has been

detected and the pH values were found to be around pH 7. Hence, no excessive acidification. However, the report didn't include any specific numbers on the water replenishment rate.

Hesjevik et al. (2017) studied the application of an ICCP system in confined spaces more closely. The testing showed that the acidification occurred for both seawater and diluted seawater. The acidification occurred quite fast as the pH stabilized around pH 4 after only 3 days. Thus, continuous replenishment of the water is necessary to maintain a neutral pH. The following was reported to have occurred because of the high potential at the counter electrode which was found to be much higher than the chlorine evolution reaction (CER) potential. The chlorine then reacted with the water and produced Hypochlorous acids, $HOCl$. The free chloride generated in the water was measured to be above 5 ppm, meaning that Microbially Induced Corrosion is less likely to occur. Hesjevik [78] discussed also the needed current density for repolarisation at low pH (pH3-4) and reported that the needed current density is 1-2 orders higher in magnitude than the mean current density. This again shows the importance of neutralizing the pH.

The ICCP system has been of great interest as they seem to be much more economically efficient than the SACP systems. However, ICCP systems tend to fail from time to time and continuous maintenance is needed to provide protection to the structure. However, this becomes even more challenging with the fact that the water becomes acidic. As the corrosion rate increases dramatically in case of ICCP malfunction. This will mean that the maintenance should be provided immediately, in case water replenishment is not an option.

Water renewal system to prevent water acidification

As mentioned earlier both the SACP and ICCP systems led to acidification. Hence, a water renewal system to maintain a neutral pH is required. Tran et al. (2019) reviewed the following problem and reported that the water renewal system should provide a minimal value of pH 6. When exchanging the water, there is 1 very important factor to be aware of which is the fact that the water that is in the buried zone will still be stagnant as shown in Figure 2.13a. Hence, to efficiently circulate the water and avoid zones where the water is not renewed, the water should be circulated to the bottom of the pile. Tran et al. [79] suggested the use of tidal water to drive this mechanism as shown in Figure 2.13b. During rising tide, the water level rises and the pile is filled with water by flowing through the cable seals. On the other hand, during falling tide the water level drops and the water is emptied of the monopile. To ensure that the water is circulating, the type of valves used are check

valves. In other words the water flows through 1 direction and the influx is not the same as the outflux. The valves are operated by the tidal force which generates enough power to open the valves and drive the system.

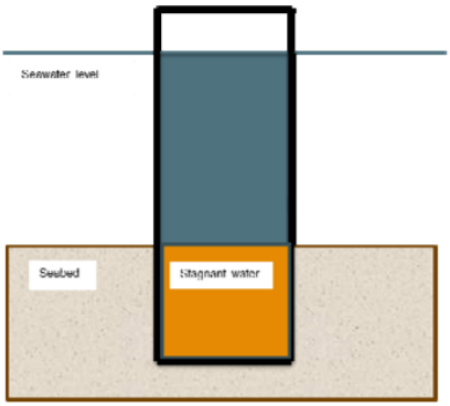

(a) Water in drilled pile.

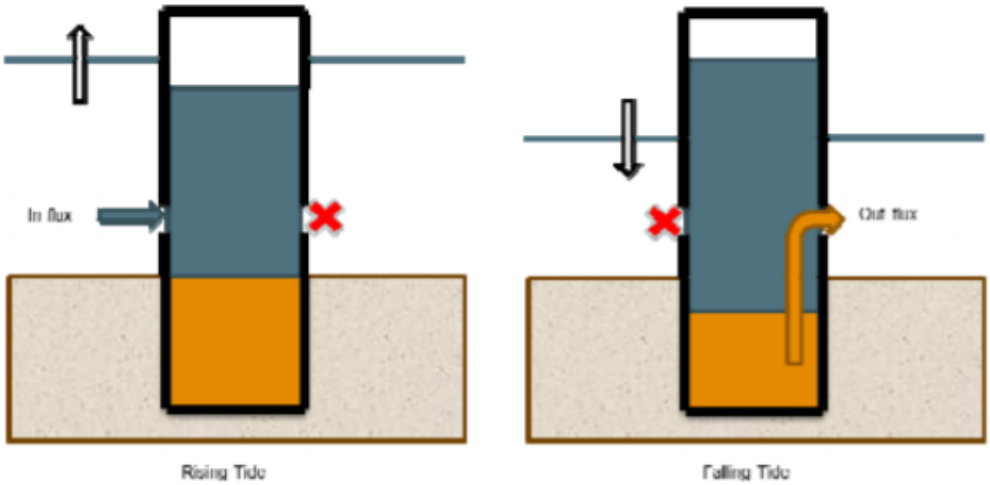

(b) Water renewal principles.

Figure 2.13: *Water renewal design basis [79].*

Chapter 3

Experimental Methodology

3.1 Test Setups

3.1.1 Cathodic Polarisation

Two different setups were used for the stagnant conditions and the partially open system. The testing in the stagnant system was done by placing the steel specimens and the Pt counter electrode (inert anode) in the same container and thereafter covering it with a plastic foil to avoid the evaporation of the test electrolyte. The steel specimens were 40 mm in diameter and 4 mm in thickness. For the partially open system, a similar set up was created except for creating water exchange openings in the container. The water was changed at a rate of 10% per week. Both tests were carried in natural seawater under room temperature, and polarised to a potential of -1050 mV vs. Ag|AgCl.

3.2 Materials

The material to be used will be standard structural steel 52 (St52) which equivalent to the S355. St52 is a low carbon manganese steel. It is known for its weldability properties and high ductility. The chemical composition and mechanical properties of the St52 are displayed in Table 3.1 and Table 3.2, respectively.

Table 3.1: *Chemical composition of the St52/S355 and St37 [wt%] [80].*

Element	Fe	C	Mn	Si	P	S	Cu	N
St 52	Balance	≤ 0.22	≤ 1.60	≤ 0.05	≤ 0.025	≤ 0.025	≤ 0.55	≤ 0.012
St 37	Balance	≤ 0.22	≤ 1.60	≤ 0.05	≤ 0.05	≤ 0.05	-	-

Table 3.2: *Mechanical properties of the St52 and St37[80].*

Property	Yield Strength [MPa]	Ultimate Tensile Strength [MPa]	Young's modulus [GPa]	Elongation [%]	Brinell hardness [HB]
St 52	355	450-600	190-210	22	146-187
St 37	235	360-510	190-210	22-26	100-154

3.3 Specimens Preparation

Cathodic Potentiostatic Polarisation

The specimen preparation of for the cathodic polarisation is quite straight forward. 12 cylindrical samples of thickness 4 mm were cut from an St52 and St37 bolts. Thereafter, threads were bored on the side of the specimens where a threaded rod (3mm in diameter) is inserted. The dimensions of the test sample are displayed in Figure 3.1. Thereafter, the samples have been grinded with SiC paper P80 & P500 to finish, cleaned in water and ethanol followed by drying, and were stored in a desiccator until test start.

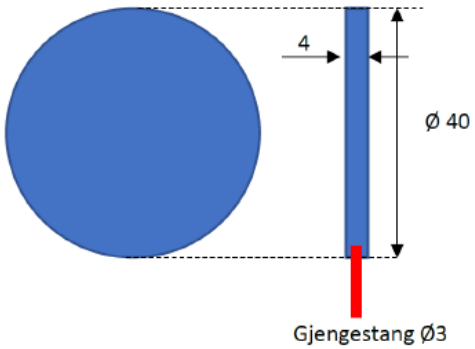

Figure 3.1: *Dimensions of the test sample.*

3.4 Test Electrolyte

3.4.1 Volume to Area Ratio

The acidification of the seawater occurs due to the production and dissolution of chlorine. Hence, the dissolution of chlorine highly depends on the volume. An important aspect of the test electrolyte is the volume to area ratio as the test set-up should be similar to the reality. This is easily done by calculating the area/volume ratio for both the set-up and the monopile foundation. Let's assume a monopile foundation with 5 meter in diameter and take a 1 meter unit for height. The calculation shows that for a 14-15 liter container 6 samples would give very similar relations (3% difference) such as that of a 5 meter in diameter monopile.

$$V_{experiment} = 0.015 m^3$$
$$V_{monopile} = \pi \cdot \frac{5^2}{4} = 19.625$$
$$A_{experiment} = 12 \cdot (\pi \cdot \frac{0.04^2}{4}) + 6 \cdot (\pi \cdot 0.04 \cdot 0.004) = 0.0181$$
$$A_{monopile} = \pi \cdot 5 \cdot 1 = 15.7$$
$$R_{monopile} = V_{monopile} / A_{monopile} = 1.25$$
$$R_{experiment} = V_{experiment} / A_{experiment} = 1.21$$

3.4.2 Ventilation and Water Evaporation

The ICCP on the samples will be performed in small 14-20 liters containers to keep the area to volume ratio similar to reality. However, a challenge arises as the CP system has to be ventilated to let the gasses out but this comes with the cost of the water evaporating as it will be exposed to room temperature for approximately 3-4 months. This was avoided by wrapping the top of the tubs with saran wrap and creating holes to let the gasses escape. Moreover, 1% of the volume was added each 2-3 weeks to make up for the evaporated water but at the same time not affecting the pH of the tubs significantly.

3.4.3 Water Renewal System

As mentioned earlier, there will be 2 test set ups; 1) Completely closed system with no water exchange, 2) Partially open system with controlled water exchange. The second experiment was achieved by using the pressure differences. The test setup can be seen in Figure 3.2.

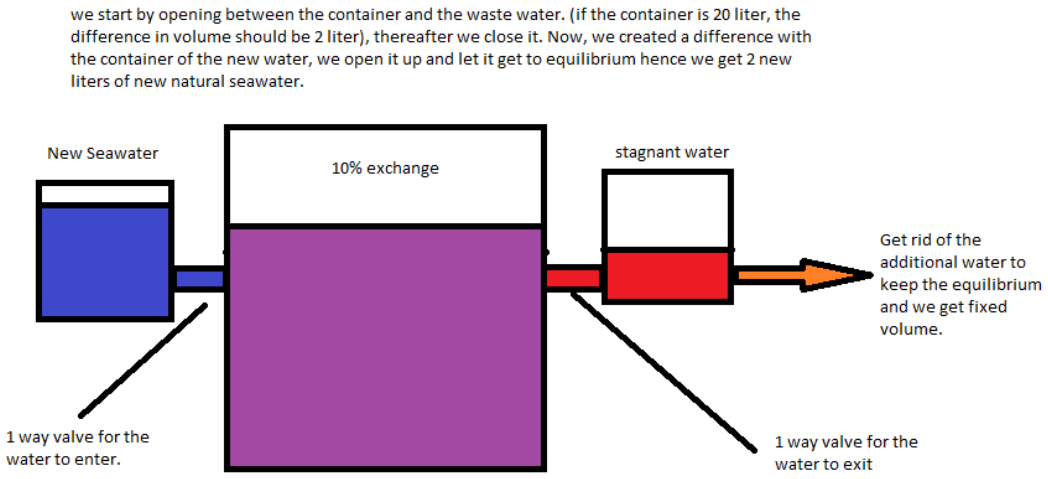

Figure 3.2: *Water replenishment system for the partially open ICCP.*

3.5 Test Matrix

During this work, 2 cathodic protection systems were tested. One of which was completely closed with no water exchange while the other was partially open with 10% water exchange per week. Half of the specimens were pre-corroded for 3 days in 3.5% NaCl solution under 40 $^{\circ}C$, while the other samples were grinded to a P500 surface roughness. The test matrix of the experiment is displayed in more detail in Table 3.3.

3.5.1 ICCP Systems

Table 3.3: *Test matrix of the Cathodic Protection Systems*

	Closed ICCP system		Partially open ICCP system	
	Grinded Samples	Pre-corroded Samples	Grinded Samples	Pre-corroded Samples
Potential (vs. Ag|AgCl)	-1050 mV	-1050 mV	-1050 mV	-1050 mV
Polarisation Time	3 months	3 months	3 months	3 months
No. of Samples	6	6	3	3
Volume	22 Liters	14 Liters	15 Liters	15 Liters
Material	St 52 cylinders	St 52 cylinders	St 37 cylinders	St 37 cylinders
Area to Volume ratio	0.82	1.29	1.20	1.20
Total Anode Area (m^2)	0.01808	0.01808	0.01808	0.01808

3.5.2 Repolarisation under Low pH

As previously mentioned in the theory, the ICCP systems are prone to failure. Therefore, they require continuous maintenance. However, it is crucial to understand the state of the structure when the system is offline. As the use of ICCP system is known to cause acidification due to the production of chlorine, it is of interest to study the OCP and repolarisation current requirements under low pH. To make the experiment as realistic as possible, the test was taken of an ICCP system when the period in which the pH is low. The experiment is displayed in more detail in Table 3.4.

Table 3.4: *Repolarisation experiment under low pH.*

Potential	pH	Polarisation Duration	No. Samples	Volume [l]	Material	Area to Volume ratio
-1050 mV vs. Ag|AgCl	4-4.5	3 weeks	5	12.5	St 37	1,25

3.5.3 Potentiodynamic Cathodic Polarisation

The potentiodynamic cathodic polarisation was conducted to clarify the potential at which the CER starts. This was done on 2 different types of inert anodes, namely, platinum and MMO (Mixed Metal Oxides). The samples were polarised from -710 mV (OCP) to -2000 mV vs. Ag|AgCl, with a rate of 50 mV/hour. This was done while

keeping the cathode to anode area ratio (R = 2.8) similar in both experiments. The electrolyte used during this experiment was natural seawater.

3.6 Logging and Measurements

During this report, different cathodic protection systems were performed as described in the previous section. The logging and measurements of the parameters are described and displayed in Table 3.5.

Table 3.5: *List of the performed logging and measurements.*

Measurements	Purpose	Method	Frequency
Cathodic Current	Cathodic current demand	Potential drop over 1Ω resistor	Every 5 minutes
Electrochemical Potential	Counter electrode potential	Ag|AgCl reference electrode	Every 5 minutes
pH	pH in the electrolyte	pH-meter	Once per week
Polarisation Curves	Effect of the calcareous deposit on the cathodic reaction	Polarised from -500 mV to -1100 mV Ag|AgCl ; 600 mV/h)	Once per 6 weeks
Mg and Ca Concentrations	The presence of buffers for the calcareous deposit formation	Inductively Coupled Plasma analysis (ICP)	Once per 6 weeks

3.7 Post-Test Investigation of the Samples

During the period under cathodic protection, the specimens were extracted and investigated with SEM microscope. This was conducted to study the structure and composition of the calcareous deposits. The following analysis was conducted with a Hitachi S-3400N scanning electron microscope. Moreover, energy dispersive X-ray spectroscopy (EDS) was utilized to investigate the chemical composition of the calcareous deposit formed on the steel samples. Finally, polarisation curves were taken of the specimens were also measured to observed the electrochemical/corrosion behavior of the specimens and how it was affected by the calcareous deposit.

Chapter 4

Results

4.1 Potentiostatic Cathodic polarisation

During this thesis, 5 cathodic protection systems were set up with different parameters. All of the systems were polarised to -1050 mV vs. Ag|AgCl for 12 weeks. The systems were as follows:

1. Polarisation of precorroded samples in a closed system.
2. Polarisation of grinded samples in a closed system.
3. Polarisation of precorroded samples in a partially open system (with 10% water exchange weekly).
4. Polarisation of grinded samples in a partially open system (with 10% water exchange weekly).
5. Short term (3-4 weeks) polarisation of precorroded samples in a closed system.

Precorroded Samples

Figure 4.1 displays the average current density of 6 precorroded steel samples polarised to -1050 mV vs. Ag|AgCl. The current density curves of the samples are displayed in chapter 7. The samples were precorroded for 3 days in a 3.5% NaCl solution at 40 °C. The initial current density is approximately 750 $\frac{mA}{m^2}$. This current density remains unchanged for the first 7-9 days. During this period, it can be seen that acidification had occurred and the potential had dropped to pH 4.5. Thereafter, the current density starts to decrease continuously from week 2 to week 3 where it stabilises again. During this period, it was noticed that the solution maintained a low pH until the end of the 3rd week. Again, the current density seems to have hit a plateau and stabilises at 480 $\frac{mA}{m^2}$ until the beginning of week 6. It can be noticed that during this period, the pH seems to be increasing and stabilises at around pH 7-8. This is when the current density starts to decrease again. However, this time it can be noticed that the decrease in current density is much slower. Finally, after 12 weeks of continuous polarisation the average current density was measured to be 170 mA/m^2.

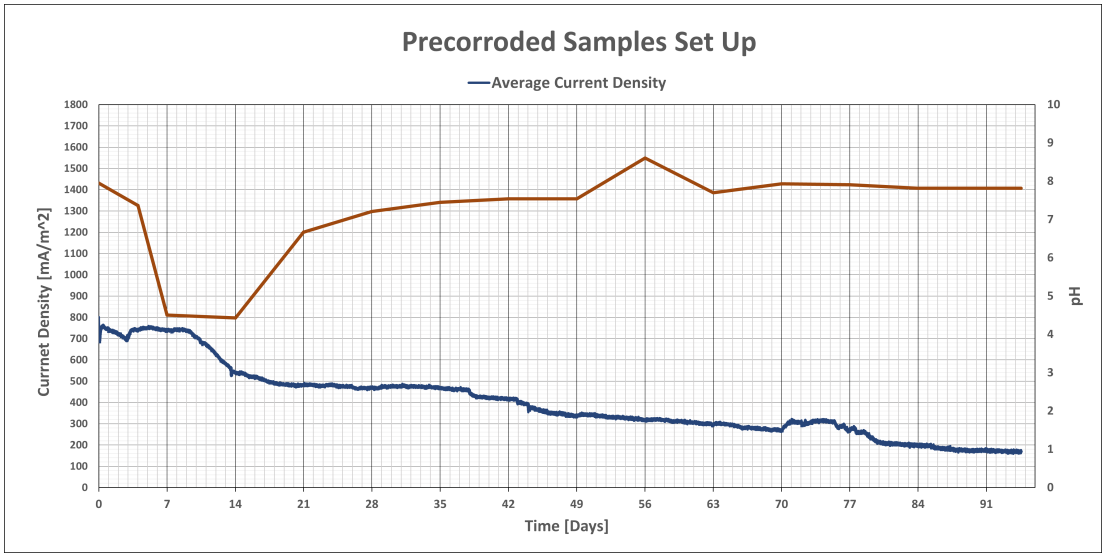

Figure 4.1: *pH and average protection current density on the precorroded samples polarised to -1050 mV Vs Ag|AgCl for 12 weeks in seawater.*

4.1.1 Grinded Samples

Figure 4.2 displays the average current density of 6 steel samples polarised to -1050 mV vs. Ag|AgCl. The current density curves of the samples are displayed in Figure 7. The samples were grinded to P500 surface roughness and were cleaned with ethanol and acetone. The initial current density in this set up was measured to be around 1500-1600 $\frac{mA}{m^2}$. However, these values were not very precise as there was found some bad contacts in the wiring between the samples and the potentiostat which may have increased the resistance in the system, hence, higher unstable current densities were observed. Nevertheless, this problem was fixed was fixed from day 9 where the current density was measured to be at 850 $\frac{mA}{m^2}$. From the 9th day and forward, the current density seems to be decreasing continuously but this was happening slower and slower with time until approximately week 6 where the current density stabilised at 260-290 $\frac{mA}{m^2}$. Similar to the precorroded samples set up, acidification occurred quite fast as the pH reached a pH 4.5 after 1 week. However, unlike the precorroded samples, acidification lasted much longer (double as long) and the increase of pH to a neutral pH didn't occur until approximately week 7-8. Moreover, it seems that the largest increase in pH occurred after 6 weeks when the current density had stabilised. The final current density after 12 weeks of continuous polarisation was measured to be 190 mA/m^2.

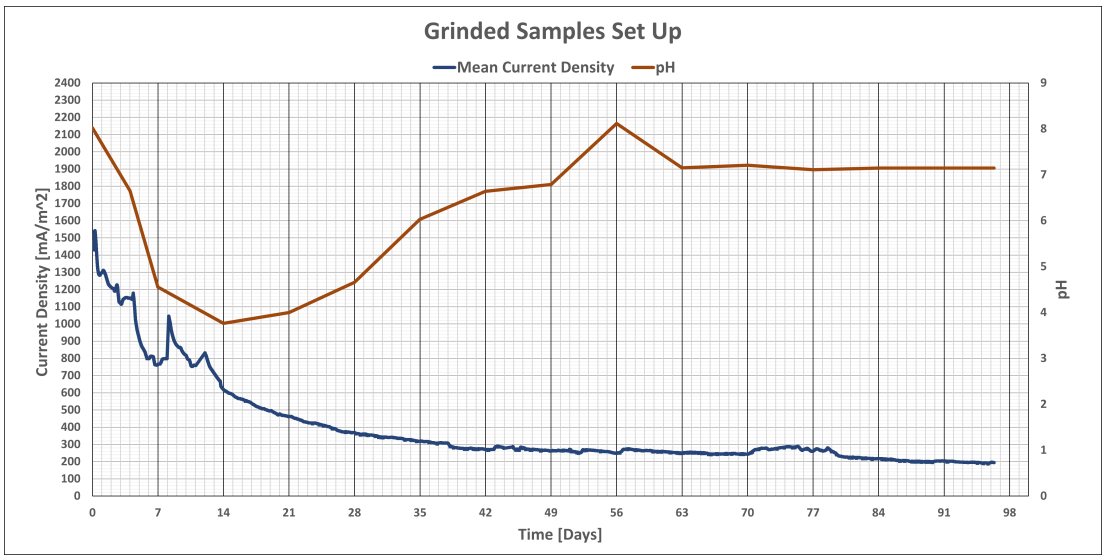

Figure 4.2: *PH and average protection current density on the grinded samples polarised to -1050 mV vs. Ag|AgCl for 12 weeks in seawater.*

4.1.2 Partially Open System

Figure 4.3 displays the average current density curve of the grinded and precorroded samples under polarisation to -1050 mV vs. Ag|AgCl. The initial current density was measured to be approximately 1300-1400 mA/m^2. The highest drop decrease in current density occurred during the first week, where it was measured to be almost half that of the initial current density. From this point on, the current density decreased continuously but a much lower rate up until week 6 where it seemed to have hit a plateau at 400 mA/m^2. The final current density was measured to be 290 mA/m^2 after 12 weeks of continuous polarisation. There were some trouble with the following experiment as the potentiostat used was not stable and lead to various peaks where the polarisation potential decreased below -1100 mV vs. Ag|AgCl. This may have lead to damaging the calcareous deposit or changed the composition of the deposit. Hence, the final value is not optimal and new tests should be conducted to verify this information. Nevertheless, the unstable potentiostat was the only available equipment in the laboratory and no new tests could be conducted to verify these numbers. Nevertheless, the potentiostat was changed after week 10 when a new potentiostat was available. The curve displayed is the average of both the grinded and the precorroded samples. The reason being is the tracking of samples was lost during the experiment, moreover, the values from the different samples did not deviate by a lot to differentiate the precorroded from the grinded samples. In addition, all the samples followed the same data trend which suggests that the fact that the samples were precorroded or grinded did not induce a significant difference in a long term experiment.

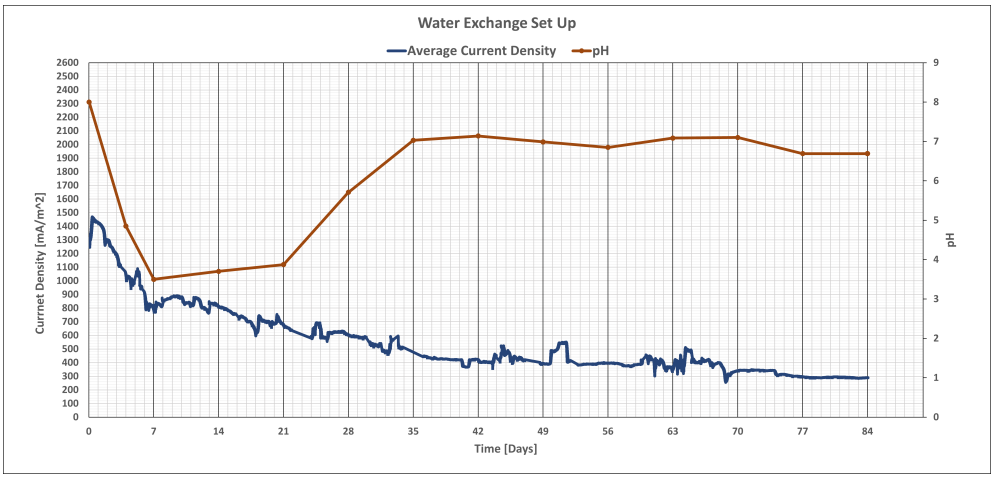

Figure 4.3: *PH and average protection current density on the Water Renewal samples polarised to -1050 mV vs. Ag|AgCl for 12 weeks in seawater.*

4.2 Evolution of the Cathodic Polarisation Curves

Various polarisation curves were taken at different points of time of a precorroded sample and a grinded sample. The following was done exhibit the effect of the calcareous deposit formation on the cathodic reaction. Figure 4.4 displays the cathodic polarisation curves of the precorroded and grinded samples. The polarisation curves were taken before the polarisation (week 0), after 6 weeks and after 11.5 weeks of continuous polarisation. As it is displayed the calcareous deposit did indeed affect the cathodic polarisation curve as the current density required to polarise the samples decreased. The decrease of the required current density between week 0 and week 6 was larger on the precorroded samples. However between week 6 and week 11.5, the decrease was larger on the grinded samples.

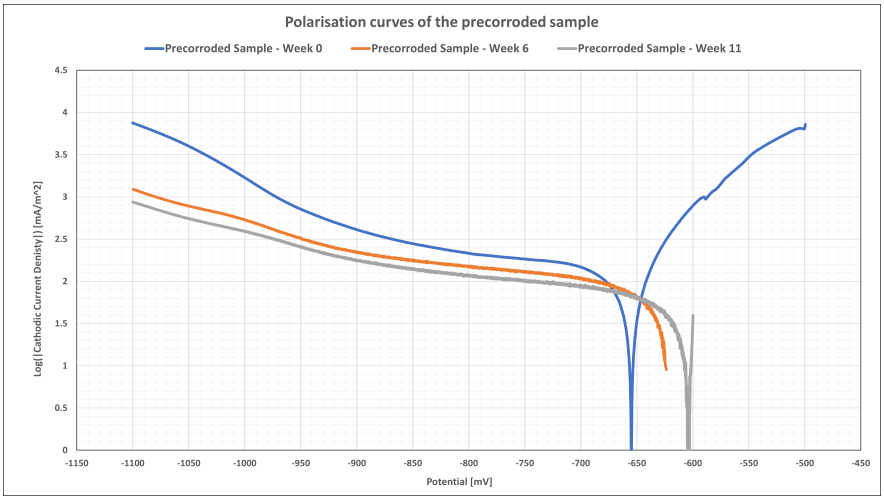

(a) Precorroded sample.

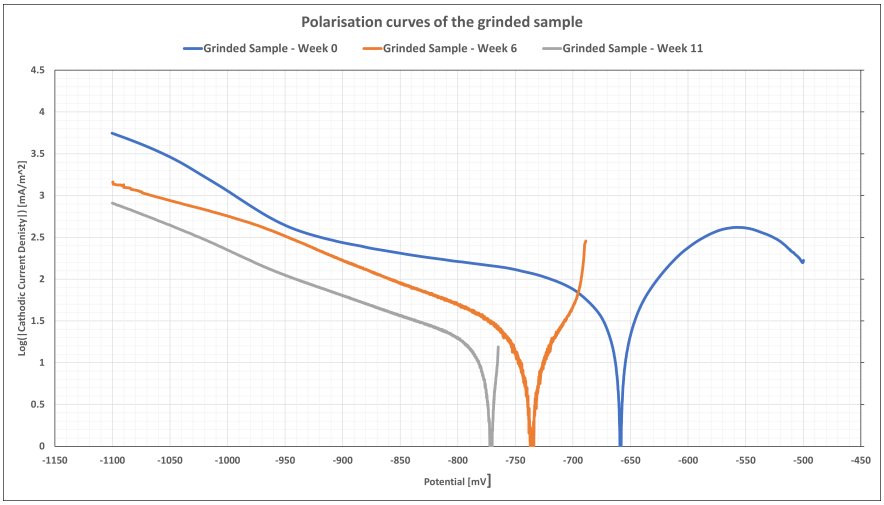

(b) Grinded sample.

Figure 4.4: *Polarisation curves of the precorroded and grinded samples.*

4.3 SEM & EDS Analyses

This section contains the results from the SEM and EDS analyses of the calcareous deposits formed under continuous potentiostatic polarisation. Figures of the different microstructures were taken with SEM to define the microstructures. This was followed up by an EDS mapping analysis and a point analysis to confirm the by investigating their chemical compositions.

4.3.1 Precorroded Samples After 4 weeks of Polarisation

4.3.1.1 SEM Analysis

After approximately 4 weeks of continuous polarisation, one sample was extracted for SEM analysis. The microstructure of the formed calcareous deposit is displayed in Figure 4.5. From Figure 4.5a and Figure 4.5b, it can be seen that the formed microstructure is mostly brucite ($Mg(OH)_2$) with some aragonite ($CaCO_3$) islands. Figure 4.5c displays a magnified region that is highlighted in Figure 4.5b. The magnification shows 3 types of microstructures. The highlighted region is thought to be brucite due to its needle-like microstructure as shown in Figure 4.5d. The flower-like or leaf-like microstructure seems is thought to be aragonite. Judging by the size of the aragonite flowers, it seems that they are in the initial phase of nucleation. The third microstructure, have a sphere-like shape. However, the light on this microstructure was very bright and the SEM machine wasn't able to provide a closer picture. However, these particles are thought to be also another form for aragonite. This microstructure was much more defined in the SEM pictures of the samples that were polarised for 12 weeks which will be presented in the next section.

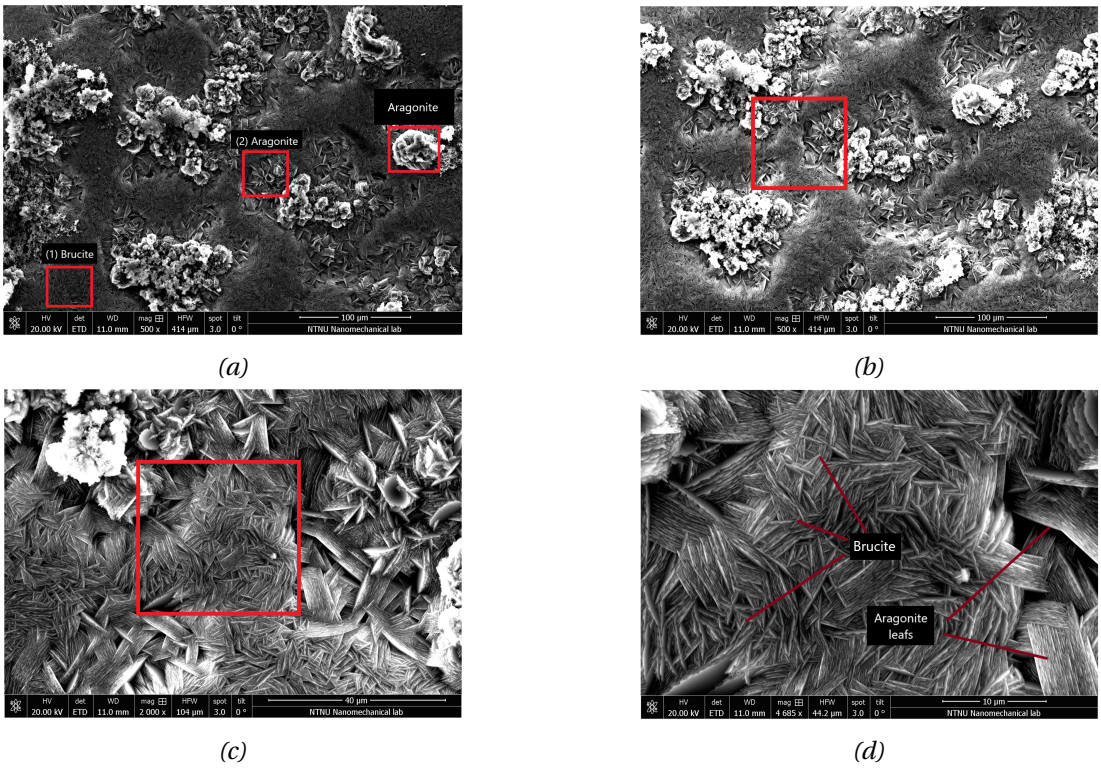

(a) *(b)*

(c) *(d)*

Figure 4.5: *SEM pictures of the calcareous deposit formed under potentiostatic polarisation to -1050 mV vs. Ag|AgCl in seawater for 4 weeks of the precorroded samples.*

4.3.1.2 EDS Analysis

Figure 4.6a displays an SEM picture of the analysed area. The results of the mapping analysis is displayed in Figure 4.6b. 3 elements were found from this analysis, namely, oxygen, magnesium and calcium. The distributions shows that most of the microstructure is made of magnesium hydroxide, brucite. However, there is also some overlap between the calcium, magnesium and oxygen, as shown in Figure 4.6e, Figure 4.6d and Figure 4.6c. Hence, there could also be some magnesium carbonate as well but this could not be confirmed. However, the carbon was not spotted which could be due to the limitations from the SEM machines or that more time was required to identify this element. Moreover, the microstructure was very small to analyse. Nevertheless, from the SEM analysis combined with the EDS analysis, there must be some carbon even though it was not detected during this analysis. This was proven in the next subsection, as the calcium carbonate crystalls increased in size after 12 weeks of polarisation. The EDS map sum spectrum of cross section of calcareous deposits is displayed in Figure 4.7.

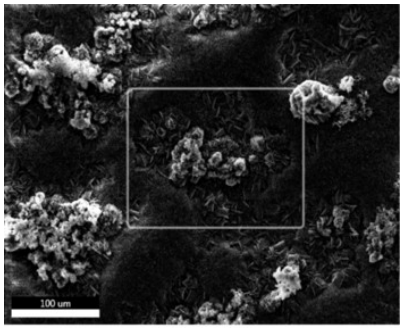

(a) SEM picture of the analysed area.

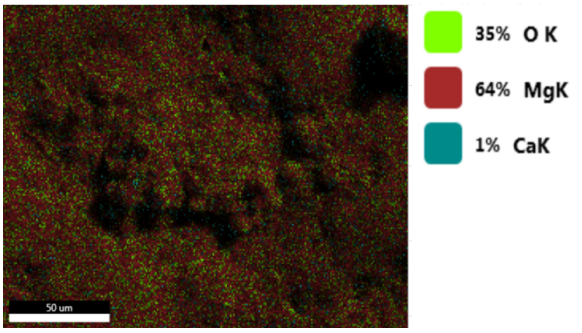

(b) Element Overlay of the calcareous deposit.

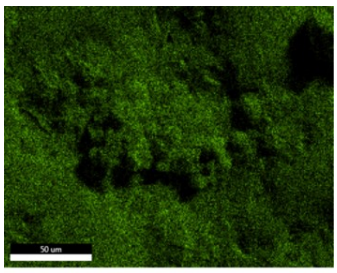

(c) Oxygen distribution.

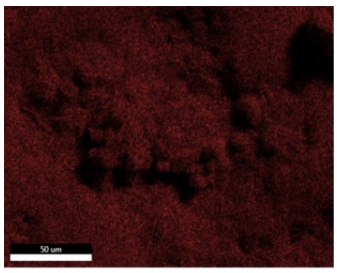

(d) Magnesium distribution.

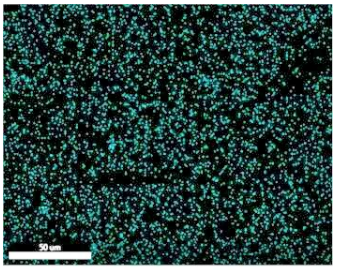

(e) Calcium distribution (this picture was edited to enhance its quality/clarity).

Figure 4.6: *EDS Analysis of the calcareous deposit formed under potentiostatic polarisation to -1050 mV vs. Ag|AgCl in seawater for 4 weeks of the precorroded samples.*

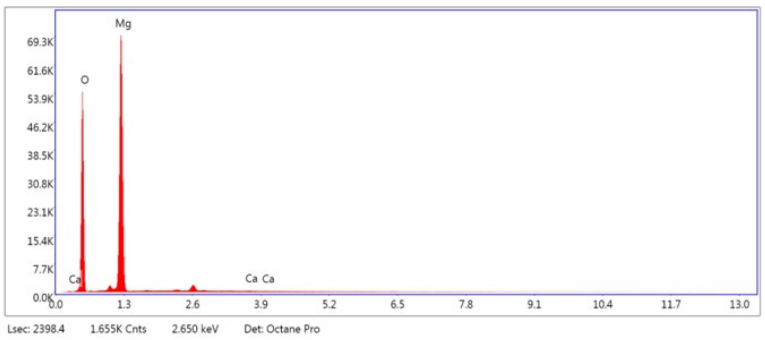

Figure 4.7: *Sum Spectrum of the analysed area.*

4.3.2 Precorroded Samples After 12 weeks of Polarisation

4.3.2.1 SEM Analysis

After approximately 12 weeks of continuous polarisation, 1 sample was extracted for SEM and EDS analysis. Figure 4.8a and Figure 4.12 displays an overview of the different microstructures found on the calcareous deposit, namely: brucite and aragonite. The microstructure of brucite is shown closer in Figure 4.8b. The microstructure seems a little different compared to the one observed after only 4 weeks of polarisation. The brucite layer seems to be much denser and more uni-

form after 12 weeks of polarisation. The microstructure of aragonite is displayed in Figure 4.11b. Aragonite seems to have formed non-uniformly over the brucite layer. Finally, the last microstructure is also thought to be another form for aragonite. From Figure 4.10a it can be seen that this calcium carbonate microstructure formed in a sphere-like shape. However, from a closer look in Figure 4.10b, it can be seen that this particle is actually constructed by many small needle and cubic particles of calcium carbonate.

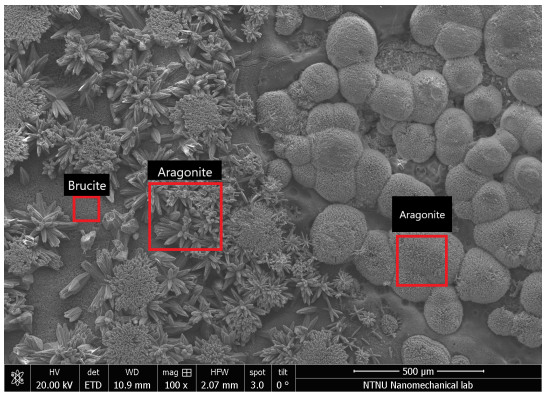

(a) Magnification: 500 µm

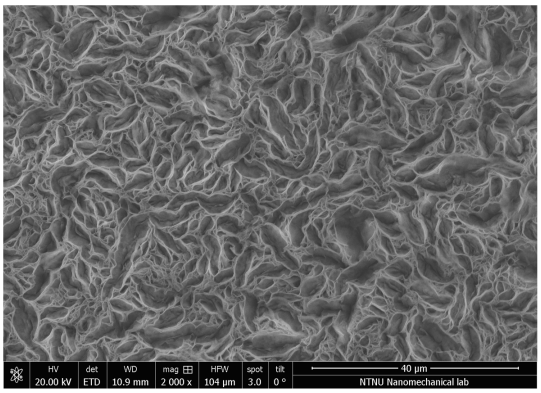

(b) Magnification: 40 µm | Close up of the microstructure of Brucite.

Figure 4.8: *SEM pictures of the calcareous deposit formed under potentiostatic polarisation to -1050 mV vs. Ag|AgCl in seawater for 12 weeks of the precorroded samples.*

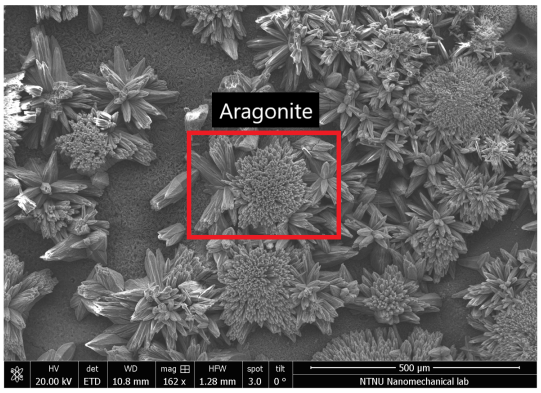

(a) Magnification: 500 µm

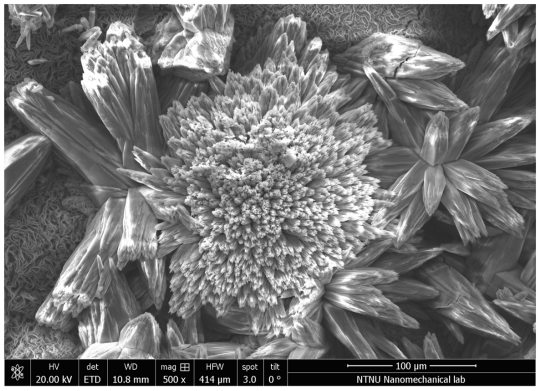

(b) Magnification: 100 µm | Close up of the microstructure of Aragonite.

Figure 4.9: *SEM pictures of the calcareous deposit formed under potentiostatic polarisation to -1050 mV Ag|AgCl in seawater for 12 weeks of the precorroded samples.*

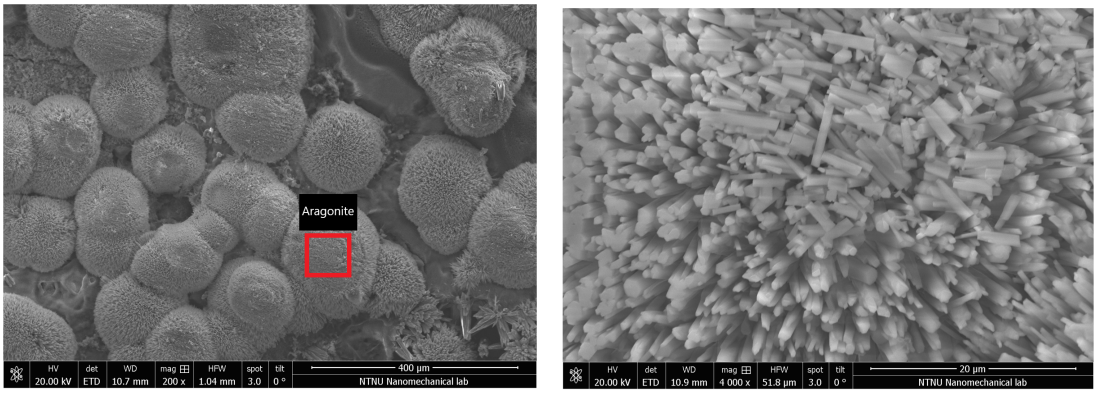

(a) Magnification: 400 µm *(b) Magnification: 20 µm*

Figure 4.10: *SEM pictures of the calcareous deposit formed under potentiostatic polarisation to -1050 mV vs. Ag|AgCl in seawater for 12 weeks of the precorroded samples.*

4.3.2.2 EDS Analysis

Figure 4.11a displays an SEM picture of the analysed area. The results of the mapping analysis are displayed in Figure 4.11b. Four elements were detected from this analysis, namely, carbon, oxygen, magnesium and calcium. Based on the distribution and the overlap of the elements, it can be seen that there are 2 types of calcareous deposit compounds. The first is magnesium hydroxide (brucite) which can be seen from the overlap of the oxygen and magnesium. The second microstructure made of calcium carbonate which can be seen from the overlap of the oxygen, calcium and carbon. This compound came in form of aragonite as shown earlier from the SEM analysis. However, from the SEM analysis it was speculated the microstructure shown in Figure 4.10 is calcium carbonate.

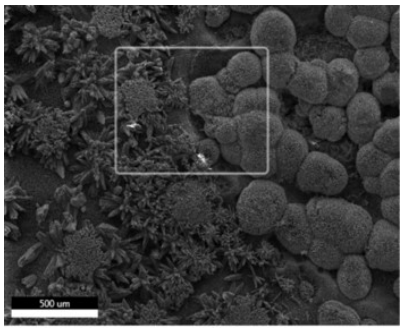

(a) SEM picture of the analysed area.

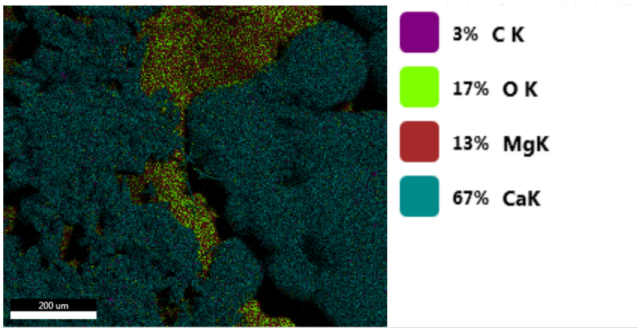

(b) Element Overlay of the calcareous deposit.

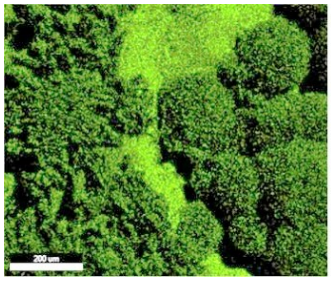

(c) Oxygen distribution.

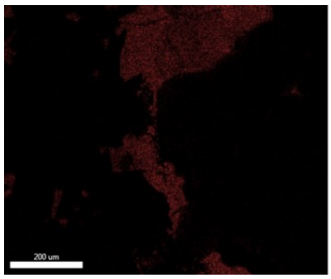

(d) Magnesium distribution.

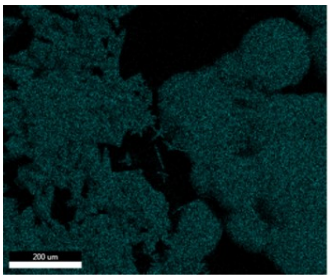

(e) Calcium distribution.

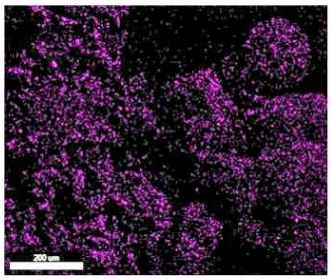

(f) Carbon distribution (this picture was edited to enhance its quality/clarity).

Figure 4.11: *EDS Analysis of the samples.*

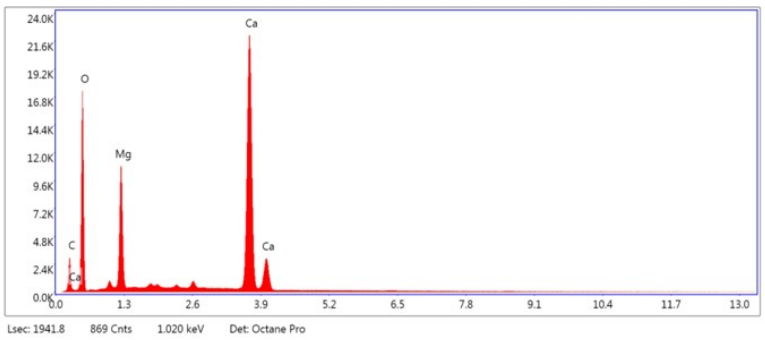

Figure 4.12: *Sum Spectrum of the analysed area.*

4.3.3 Grinded Samples After 12 weeks of Polarisation

4.3.3.1 SEM Analysis

After approximately 12 weeks of continuous polarisation, 1 sample was extracted for SEM and EDS analysis. Figure 4.13 displays an overview of the different microstructures found on the calcareous deposit, namely: Brucite and Aragonite. The microstructure seems to be mostly brucite with some aragonite islands that are non-uniformly laid on the brucite layer. Compared to the precorroded samples, the calcium carbonate compounds are much smaller and seem to be made of two forms of aragonite. Furthermore, the microstructure of the magnesium hydroxide seems to be much larger. Hence, it can be speculated that the brucite layer formed on these samples are much denser and thicker compared to the precorroded samples.

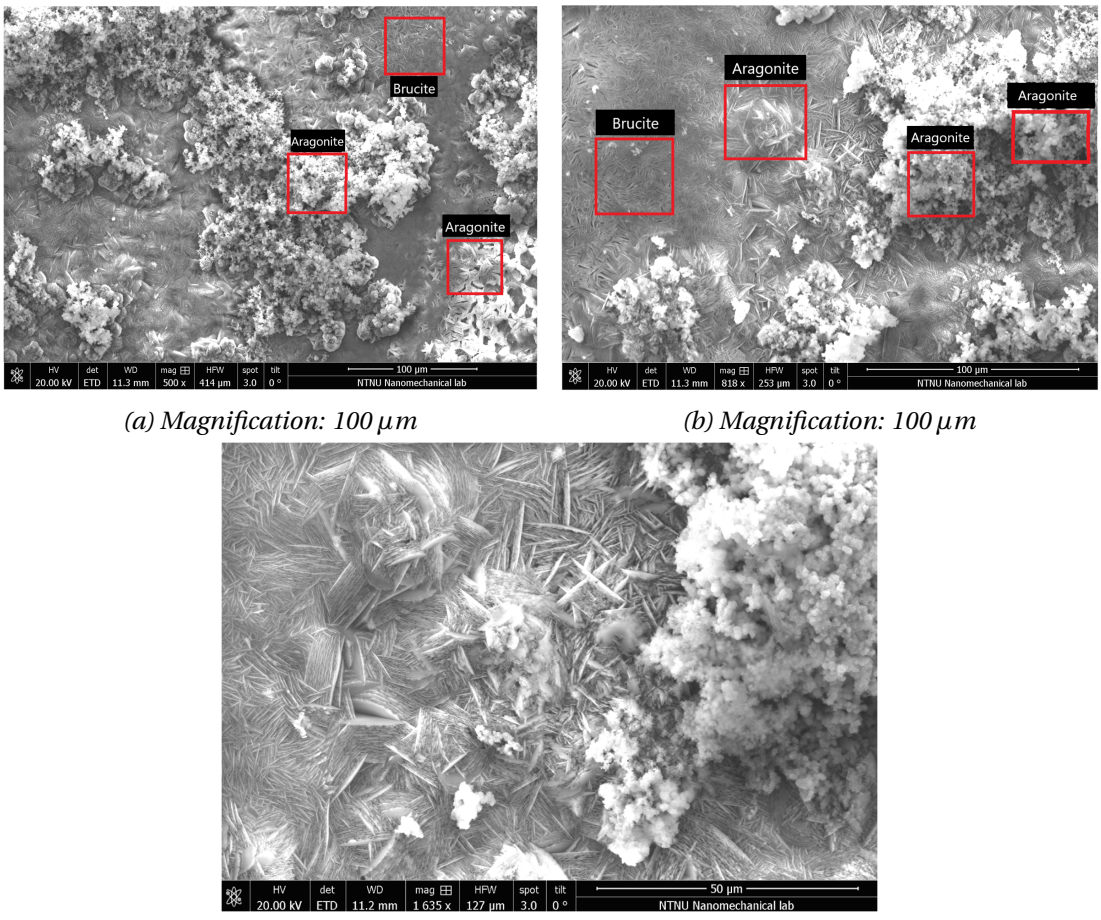

(a) Magnification: 100 µm

(b) Magnification: 100 µm

(c) Magnification: 50 µm

Figure 4.13: *SEM pictures of the calcareous deposit formed under potentiostatic polarisation to -1050 mV vs. Ag|AgCl in seawater for 12 weeks of the grinded samples.*

4.3.3.2 EDS Analysis

Figure 4.14a displays an SEM picture of the analysed area. The element overlay of the calcareous deposit found from the mapping is shown in Figure 4.14b. As it is shown in Figure 4.15, there were 5 elements that were identified, namely, Carbon, oxygen, magnesium, calcium and iron. The distribution of the individual elements is displayed in Figure 4.14. Based on the overlap between these elements, the main calcareous compound is magnesium hydroxide (Brucite) with some calcium carbonate (Aragonite).

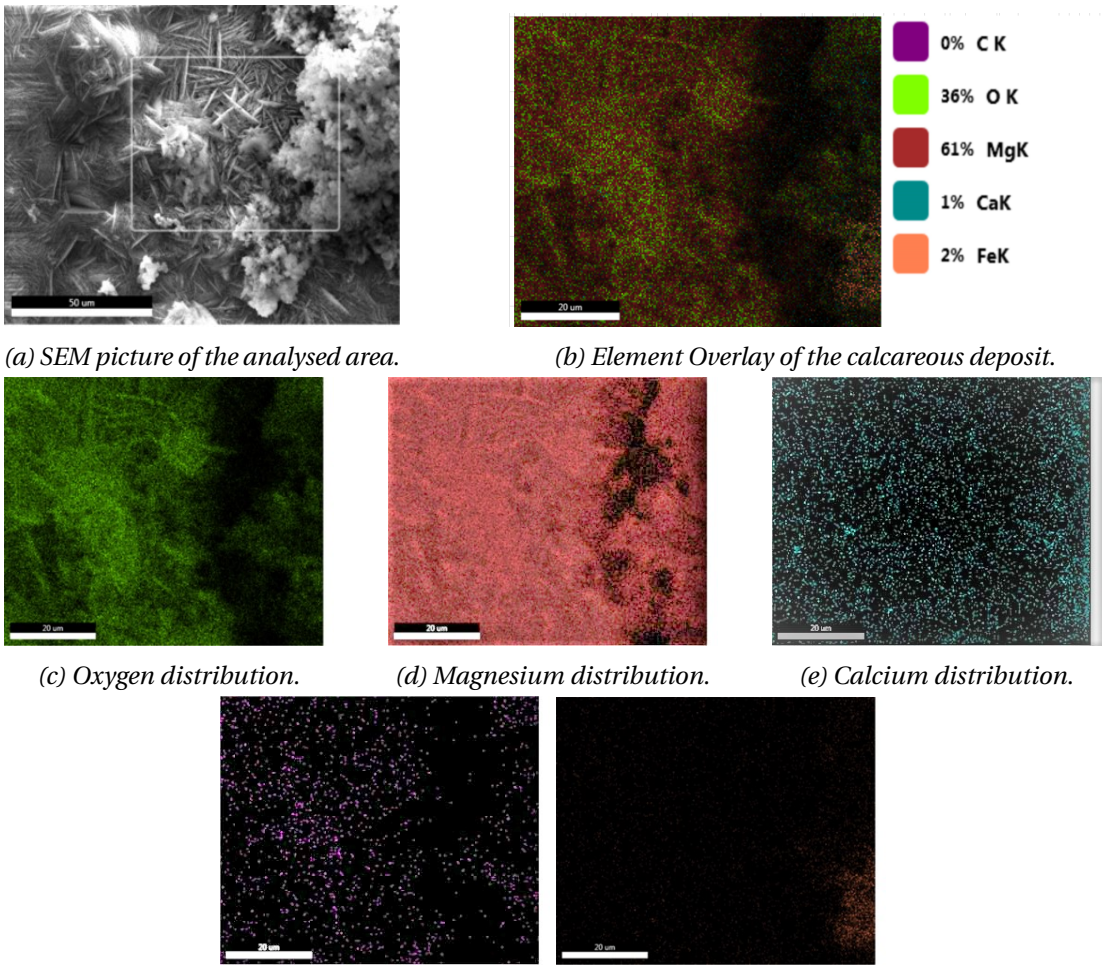

(a) SEM picture of the analysed area. *(b) Element Overlay of the calcareous deposit.*

(c) Oxygen distribution. *(d) Magnesium distribution.* *(e) Calcium distribution.*

(f) Carbon distribution. *(g) Iron distribution.*

Figure 4.14: *EDX Analysis of the samples.*

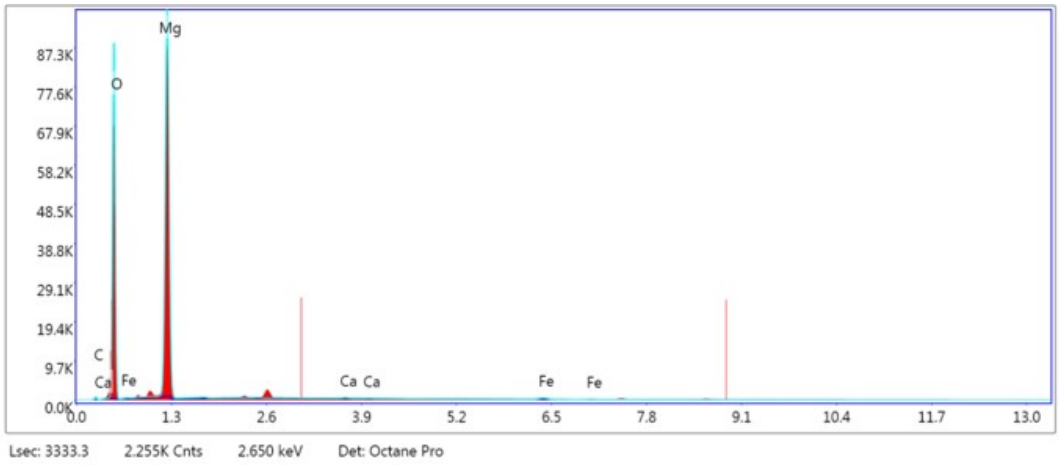

Figure 4.15: *Sum Spectrum of the analysed area.*

4.4 ICP Analysis

As shown in the previous section, the calcareous deposit came in different forms, namely, calcium carbonate and magnesium hydroxide. To investigate the amount of elements precipitated on the surface in the different experiments, an ICP analysis was taken after 6 weeks of continuous polarisation. The analysis reports the change of magnesium and calcium concentrations from which their precipitated amounts was calculated as the volume is constant. The control sample was lost during this experiment and no new analysis was conducted due to the time limitations. Nevertheless, as the chemical composition of the seawater is constant, the control values were extracted from an ICP analysis of the same seawater which was conducted by Jevremovic and Øystein Knudsen [81]. From the following analysis, the calcium and magnesium concentrations were measured to be 422 mg/l and 1299 mg/l, respectively. Table 4.1 displays the change of concentrations and the corresponding calculated amounts of calcium and magnesium consumed to form the calcareous deposit.

As it is shown in Figure 4.16a the amount of magnesium precipitated on the grinded samples is much higher than the ones on the precorroded samples. In fact it is approximately 3.5 times higher. On the other hand, the amounts of calcium precipitated on the surface is relatively similar as shown in Figure 4.16b.

Table 4.1: *ICP analysis results of magnesium and calcium in the different electrolytes, after 6 weeks of continuous polarisation polarisation.*

Sample Name	Comment	Mg^{2+} Conc. [mg/L]	Ca^{2+} Conc. [mg/L]	Volume [L]	Mg^{2+} Consumed [mg]	Ca^{2+} Consumed [mg]
Sample 1	Electrolyte of the grinded samples experiment	1170	398	22.0	2840	533
Sample 2	Electrolyte of the precorroded samples experiment	1243	392	15.0	833	451
Sample 3	Electrolyte of the water renewal experiment	1103	370	14.0	2749	730

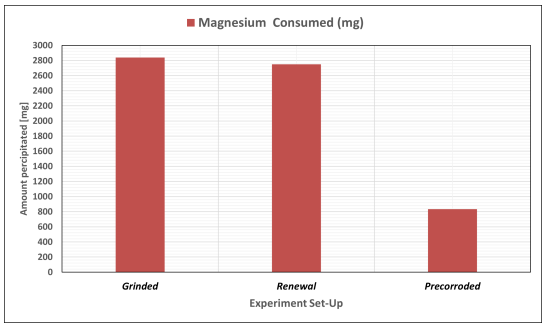

(a) Amount of magnesium, Mg^{2+}, consumed.

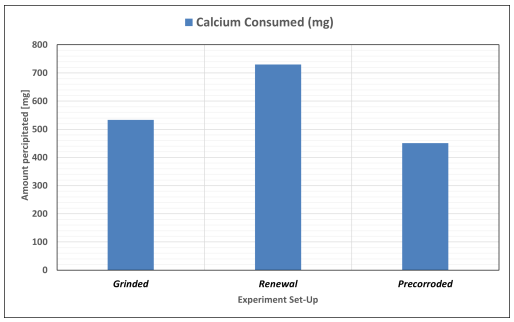

(b) Amount of calcium, Ca^{2+}, consumed.

Figure 4.16: *Amounts of calcium and magnesium that precipitated as calcareous deposits.*

4.5 pH & Counter Electrode Potential

The pH and the counter electrode potential in the potentiostatic polarisation experiments were recorded for 12 weeks. The pH was measured weekly, while, the counter electrode potential was measured every 5 minutes. Figure 4.17 displays the weekly pH measurements of the 3 experiments. As it is shown, there is a trend in the behaviour of the pH. The pH decreases during the first 2-3 weeks and increases again with time until it stabilises at pH 7-8. However, the main difference in this behaviour is how fast acidification occurs and how fast the pH stabilises again. All of the set ups showed acidification after approximately 1 week. However, acidification seems to have lasted the longest for the grinded samples set up (largest volume, 22 liters). While, the pH neutralised the fastest in the precorroded samples experiment (least volume, 15 liters). On the other hand, the water renewal experiment exhibited a trend between the two experiments. It should be noted that by week 6, there was 3 water exchanges of 10% each time. Hence, a total of 30% water was renewed by the point the pH had neutralised.

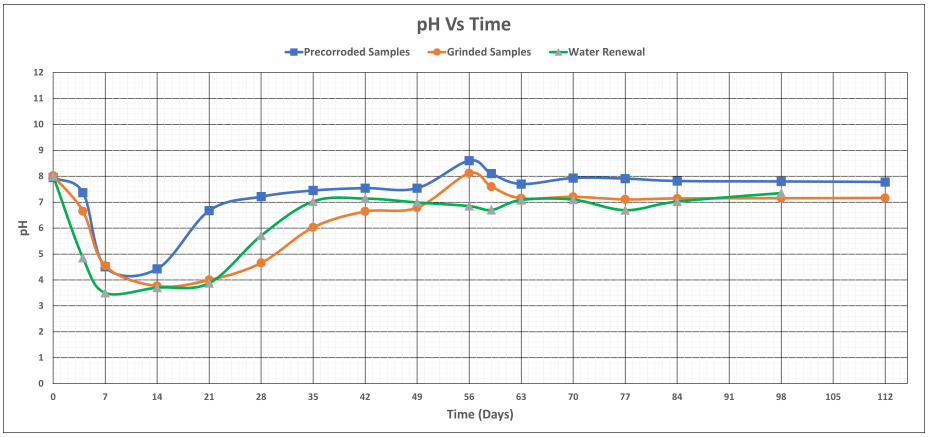

Figure 4.17: *Weekly pH measurements of the 3 cathodic protection set ups.*

Figure 4.18 displays the counter electrode potentials during the polarisation. Both the precorroded samples and the water renewal experiments exhibited potentials on the counter electrode higher than the CER limit (1200 mV vs. Ag|AgCl). Meanwhile, the grinded samples experiment exhibited lower counter electrode potentials which was below the CER limit. For the latter two experiments, the acidification during the first week could be justified by the counter electrode potentials, but this is not the case for the grinded samples experiment. As one could still observe very aggressive acidification during the intial phase even though the counter electrode potential was below the CER limit, which begs the question of what else could be inducing acidification. Moreover, the counter electrode potential on the precorroded samples experiment was around the CER limit but the pH was unchanged and had stabilsed at pH 7.5-8. Thus, there is another driving factor that could be causing acidification which will be discussed further in the next chapter.

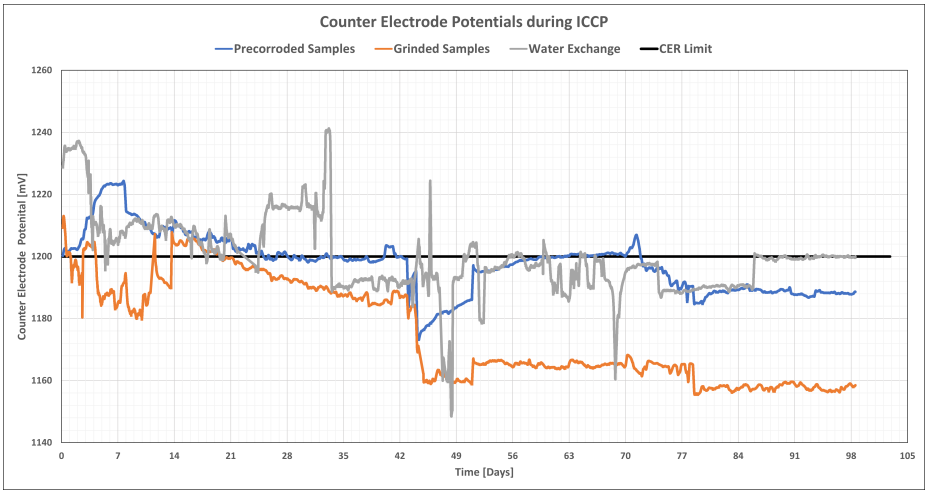

Figure 4.18: *Counter electrode potentials during polarisation to -1050 mV vs. Ag|AgCl for 12 weeks. Potential is given in [mV vs. Ag|AgCl].*

4.6 Chlorine Evolution on MMO Vs Platinum Anodes

The difference of the counter electrode potential during polarisation on MMO and Platinum anodes was investigated. This was done by conducting potentiodynamic polarisation on steel samples with similar anode and cathode areas (similar anode to cathode area ratio). The experiments were conducted separately in two different containers but all the parameters were kept the same for both. The open circuit potential of the steel samples was measured as well to ensure similar polarisation behaviour as it is displayed in Figure 4.20. The OCP was measured at approximately -710 mV and -720 mV vs. Ag|AgCl for the steel samples used with the MMO and platinum anodes, respectively. The polarisation curves of the steel samples and anodes are displayed in Figure 4.19. As it is displayed, it is clear from the anodic branch of the platinum anode that the chlorine evolution reaction occurs between 1160-1200 mV vs. Ag|AgCl. However, the CER potential on the platinum anodes was not as clear. As it is shown from the anodic branch, there are two sudden increases in the current density. The first increase occurred at 1160-1200 mV vs. Ag|AgCl, whereas the second sudden increase occurred at 1400 mV vs. Ag|AgCl. It was earlier reported by Hesjevik [78], that the CER potential on the platinum branch occurs at around 1200 mV vs. Ag|AgCl. Therefore, the first point is most likely the point at which the chlorine evolution starts. Hence, the chlorine evolution potential occurred at the same potential (1160-1200 mV vs. Ag|AgCl) for both the MMO and platinum anodes.

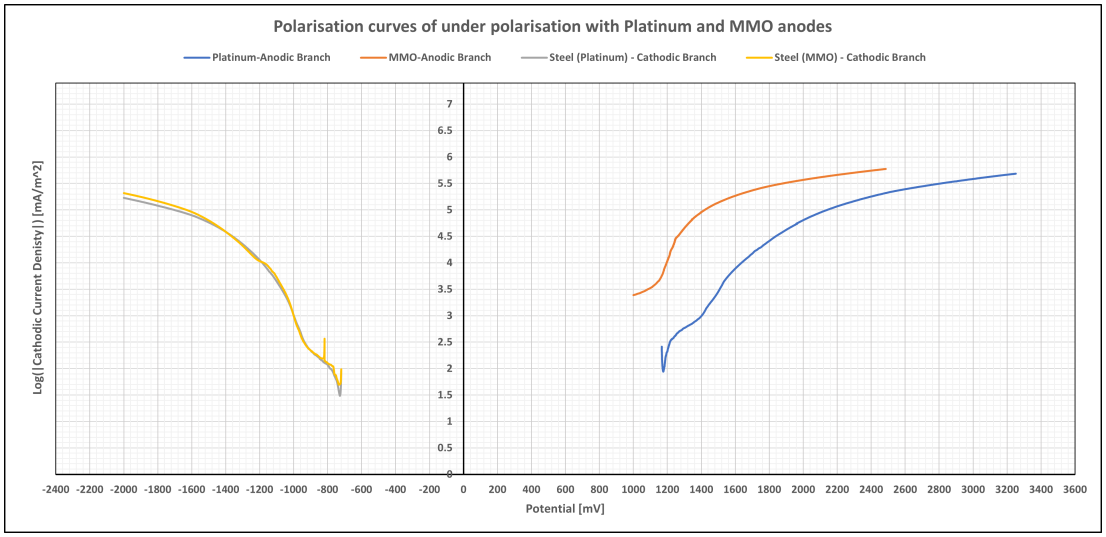

Figure 4.19: *Polarisation curves of samples using a platinum anode and an MMO anode (Steel samples polarised from -720 mV to -2000 mV vs. Ag|AgCl with a speed of 50 mV/hour).*

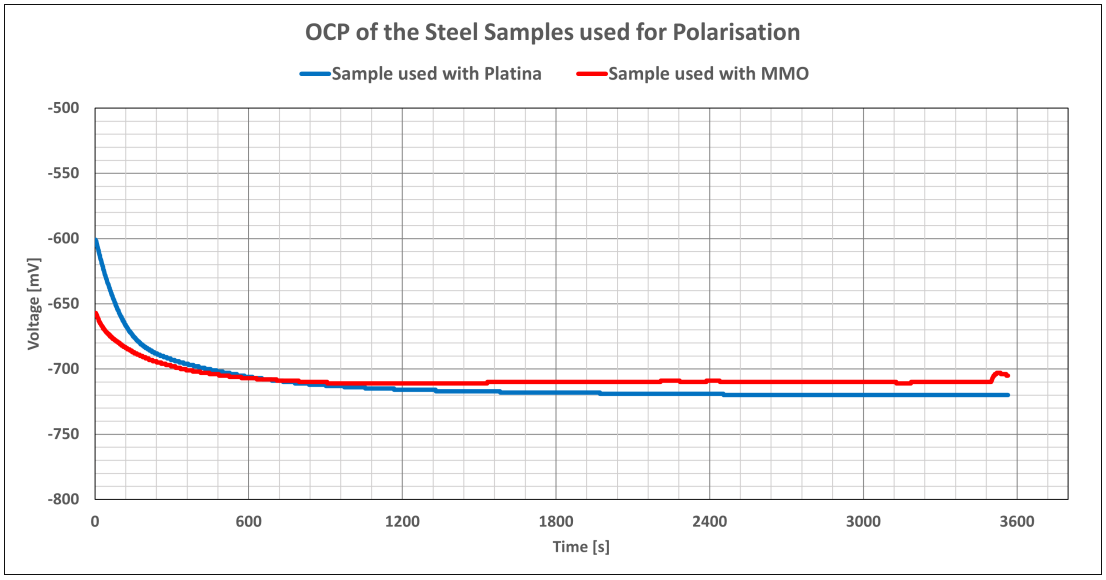

Figure 4.20: *Open Circuit Potential of the steel samples used in the polarisation with MMO and Platinum Anodes.*

4.7 OCP & Repolarisation

After approximately 6 weeks of continuous polarisation, 1 sample in each experiment samples were disconnected for 1 week to measure the open circuit potential. Thereafter, cathodic protection was reapplied on the samples and the required repolarisation current density was measured. The following was performed on the grinded and precorroded samples under neutral pH initially. Thereafter, a precorroded sample was polarised for approximately 10 days before it was repolarised. However, the repolarisation occurred under low pH this time to study whether the repolarisation current density depends on the pH.

4.7.1 Precorroded Samples Under Neutral pH

Figure 4.21 displays the OCP of the precorroded sample. As it is shown, the OCP stabilised at -590 mV vs. Ag|AgCl. Thereafter, the samples was repolarised as it is shown in Figure 4.22. The pH was stable at approximately pH 7.4 both under the free corroding and the repolarisation. The repolarisation current was measured at approximately 1450 mA/m^2, and took approximately 5 days to stabilize back to the current density of the continuously polarised samples. It should be noted, that the repolarisation current density was significantly higher than the initial current density. However, this current density occurred very fast, and the actual/stable repolarisation current density was measured to be 600 $\frac{mA}{m^2}$.

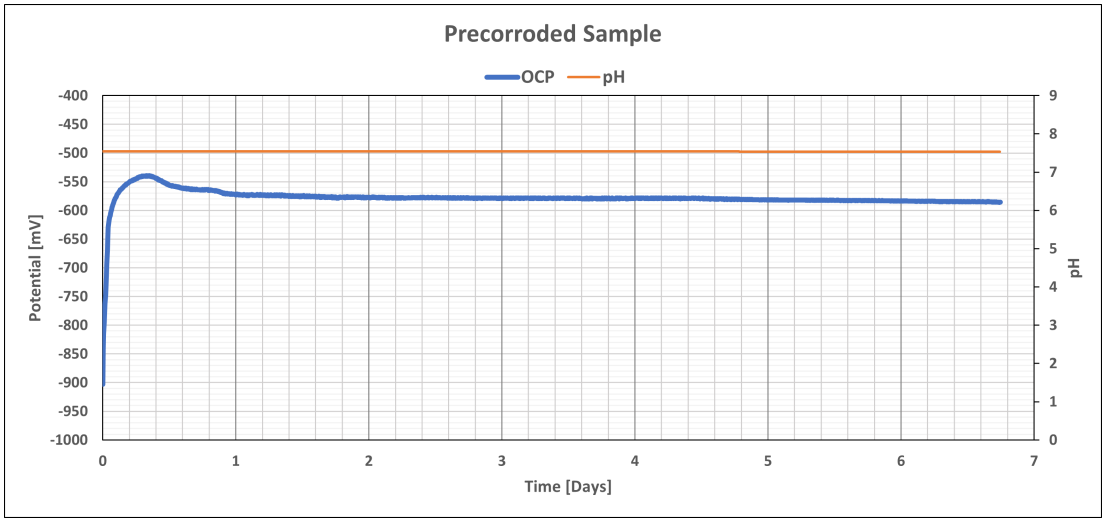

Figure 4.21: *Open circuit potential after continuous polarisation to -1050 mV Vs Ag|AgCl for 7 weeks of the precorroded samples.*

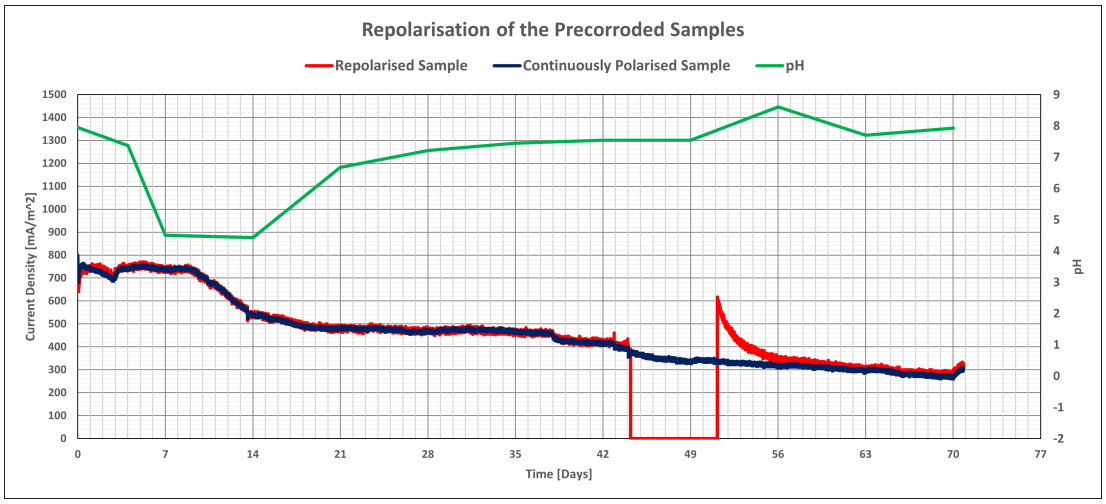

Figure 4.22: *Current density curve after continuous polarisation for 6 weeks and freely corroding for 1 week. And the average current density curve of the continuously polarised samples.*

4.7.2 Precorroded Samples Under Low pH

After approximately 5 days of polarisation, 1 sample were disconnected to observe the OCP under low pH. Figure 4.23 displays the OCP under pH 4. As it is exhibited, the OCP stabilised at a potential of -635 mV vs. Ag|AgCl. The repolarisation occurred at a pH 4-4.5 as it is shown in Figure 4.24. The required repolarisation current density was measured at approximately 1700 mA/m^2 which is not a lot larger than the sample polarised under neutral pH. Moreover, similar to the previous experiment, the current density stabilised after approximately 5 days. Hence, the difference between repolarisation under the aforementioned pH is not of large

significance.

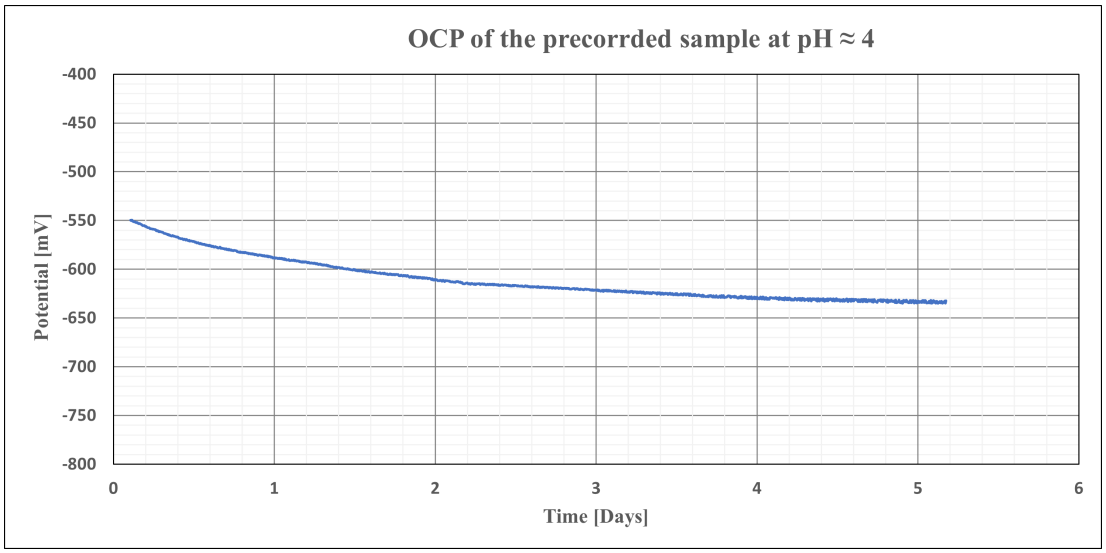

Figure 4.23: *Open circuit potential under low pH after continuous polarisation to -1050 mV vs. Ag|AgCl for 1 week of the precorroded samples.*

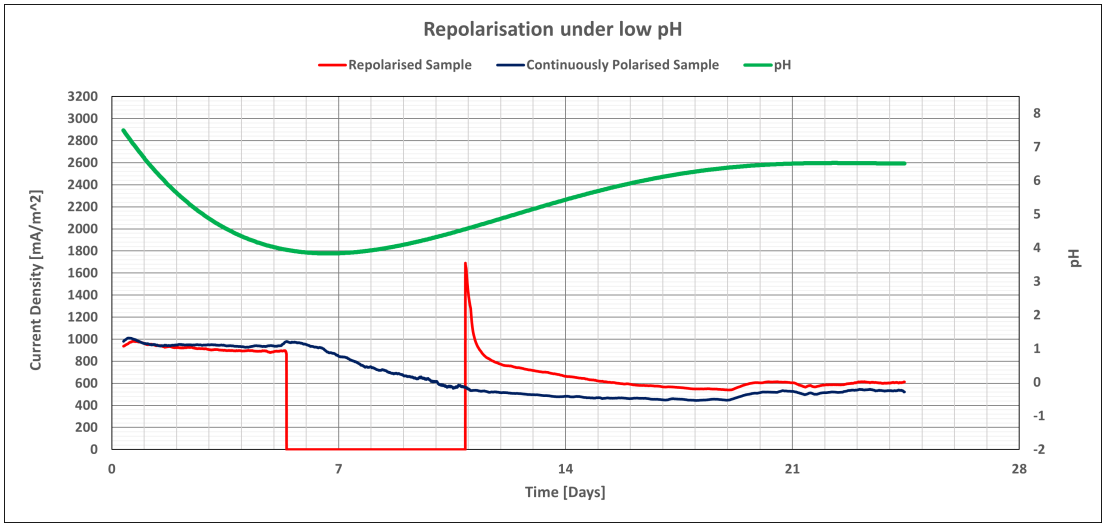

Figure 4.24: *Repolarisation current density requirement under low pH of the precorroded samples after freely corroding for 6 days.*

4.7.3 Grinded Samples

Again, the grinded samples were also polarised for approximately 44 days before disconnecting 1 sample from the CP system. The OCP is displayed in Figure 4.25 and was measured at -610 mV vs. Ag|AgCl, after 1 week of freely corroding. Unlike the precorroded samples, the required repolarisation current density was lower than the initial current density and was measured at approximately 1310 mA/m^2.

The following is shown in Figure 4.26. The repolarisation of the samples occurred under a 6.8 pH which quite neutral.

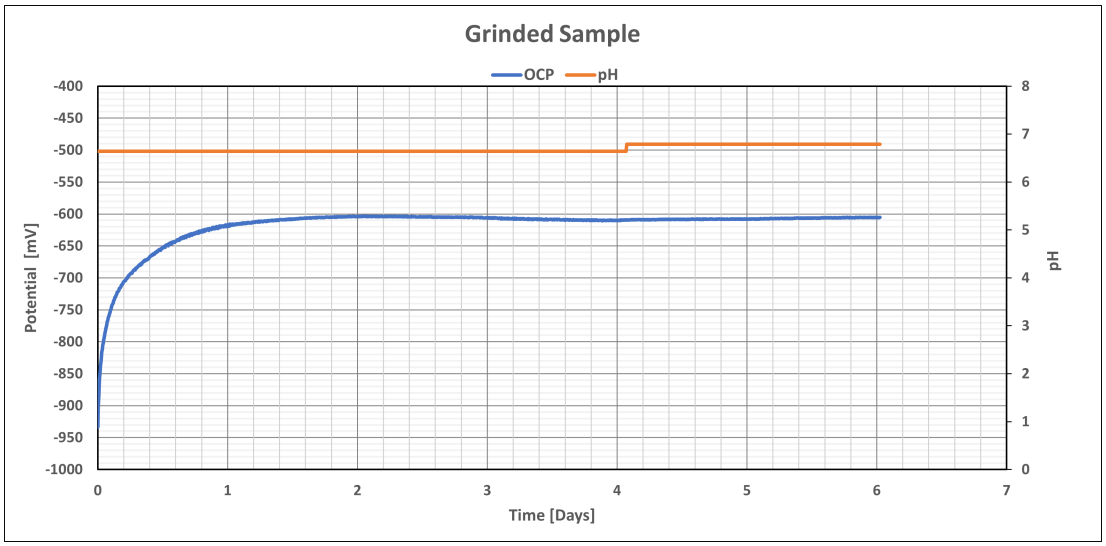

Figure 4.25: *Open circuit potential after continuous polarisation to -1050 mV vs. Ag|AgCl for 7 weeks of the grinded samples.*

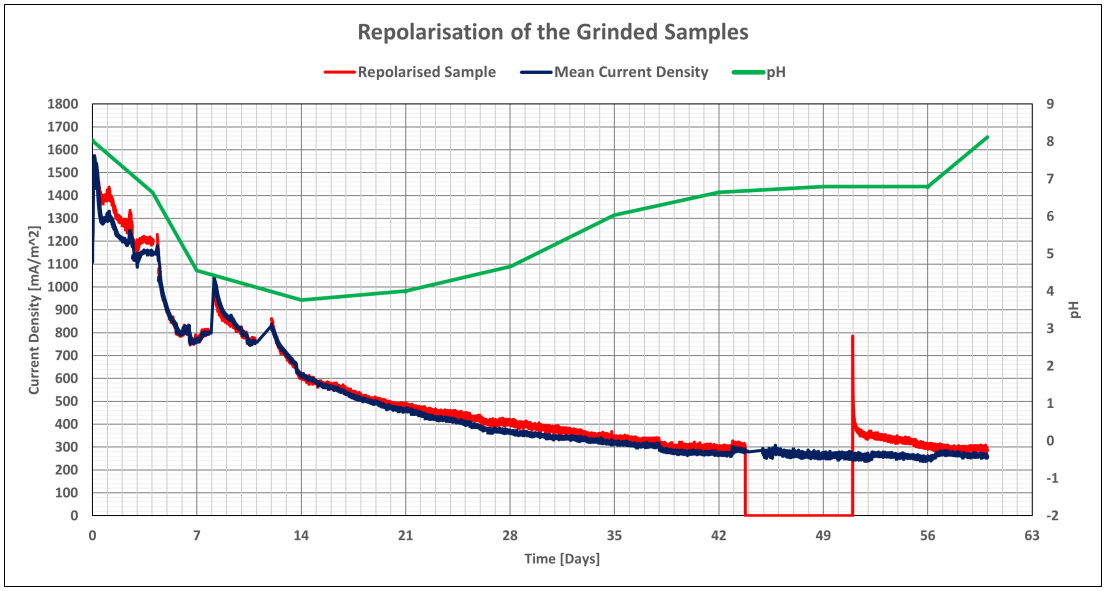

Figure 4.26: *Repolarisation current density requirement of the precorroded samples after freely corroding for 1 week.*

Chapter 5

Discussion

In this chapter, a deep discussion of the results will be conducted. The first part of the discussion contains an analysis of the cathodic current density curves obtained from the experiments. From the following analysis, various questions regarding the behaviour observed from the current density curves will be discussed and answered. The first step was to analyse the dependency of the counter electrode potential and the pH. Thereafter, the calcareous deposit quality was studied and investigated. As a result of these analyses, a hypothesis was developed to describe the trend observed on the potentiostatic curve of the precorroded samples. From there, the repolarisation behaviour of the samples under low and neutral pH was investigated to clarify the dependency of the required current density from the pH. Finally, the inert anode design, as well as, the state of the system (closed Vs partially open) were both studied to find ways to optimise the ICCP system.

5.1 ICCP in Seawater

During this report, 6 grinded and 6 precorroded samples were continuously polarised to -1050 mV vs. Ag|AgCl. During this period, temporary acidification was observed which is normal as the use of ICCP leads to the chlorine generation. However, after some time the pH neutralized again. The initial current density on the precorroded samples was measured at 750 mA/m^2. While, the initial current density on the grinded samples was measured at 1300-1500 mA/m^2. After approximately 96 days of continuous polarisation, the average current density value of the precorroded samples was found to be 170 mA/m^2 and 195 mA/m^2 for the grinded samples. Based on the following results, it seems that the calcareous layer formed on the precorroded samples is of slightly higher quality as it required lower cathodic current to maintain polarisation. The cathodic current density curves are displayed in Figure 5.1. However, The current density did continue to decrease and was measured at 150 mA/m^2 and 170 mA/m^2 on the precorroded and grinded samples, respectively after continuous polarisation of 108 days.

The measured current densities seemed to be quite high compared to cathodic protection with sacrificial anodes. Jevremovic and Øystein Knudsen [81] tested the use of aluminum and zinc anodes in stagnant brackish water. From which it was found that the polarisation current density after just 6 weeks was 120 mA/m^2 and 28 mA/m^2 under the use of aluminum and zinc anodes, respectively. However, it should be mentioned that the open circuit potential (OCP) value of the zinc anodes was measured at -1000 mV vs. Ag|AgCl, while the OCP of the aluminum anodes was approximately -1080 mV vs. Ag|AgCl. Hence, the steel was polarised to a more negative potential under the use of aluminum anodes combined with the acidification effect which could explain the relatively high current density observed. On the other hand, the low OCP of the zinc anodes suggests that the steel was polarised to a more positive potential which explains the lower current density observed. Hence, it might be wise to polarise the samples to a more positive potential under the use of ICCP in confined compartments, to achieve a lower current density.

As it can be seen, there seems to be 2 different behaviours of the evolution of the cathodic current density. As the current density on the grinded samples seems to decrease continuously, before hitting a plateau after approximately 6 weeks where the current density decrease extremely slowly. This suggests that most of the calcareous deposit formation occurred during the intial phase. Meanwhile, the precorroded samples exhibited a step-wise decrease in the cathodic current density. The following suggests the formation of calcareous deposit in different regions of the curve or at different times. The second main difference, is the acidification

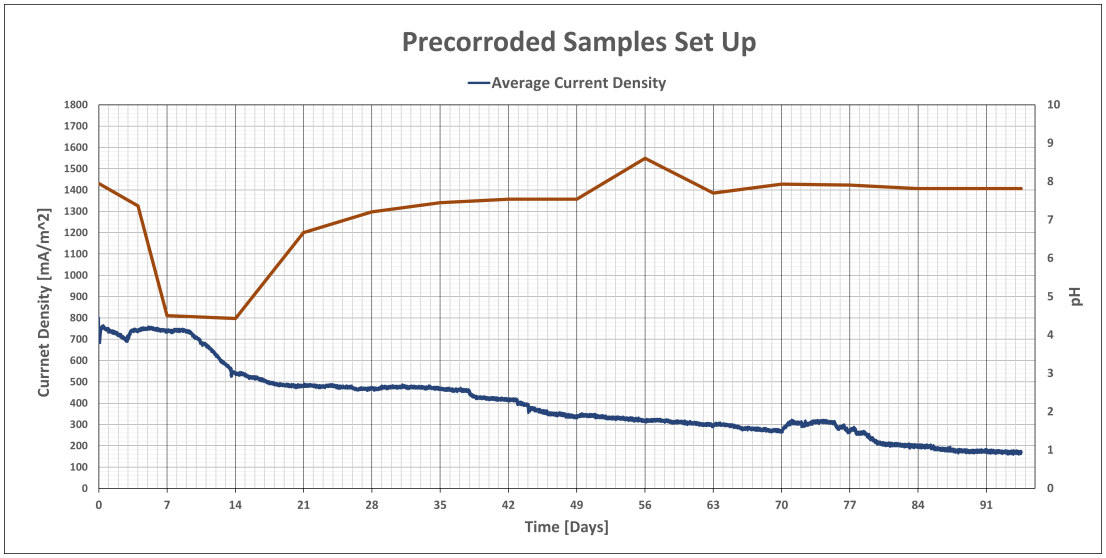

(a) Precorroded Samples Experiment.

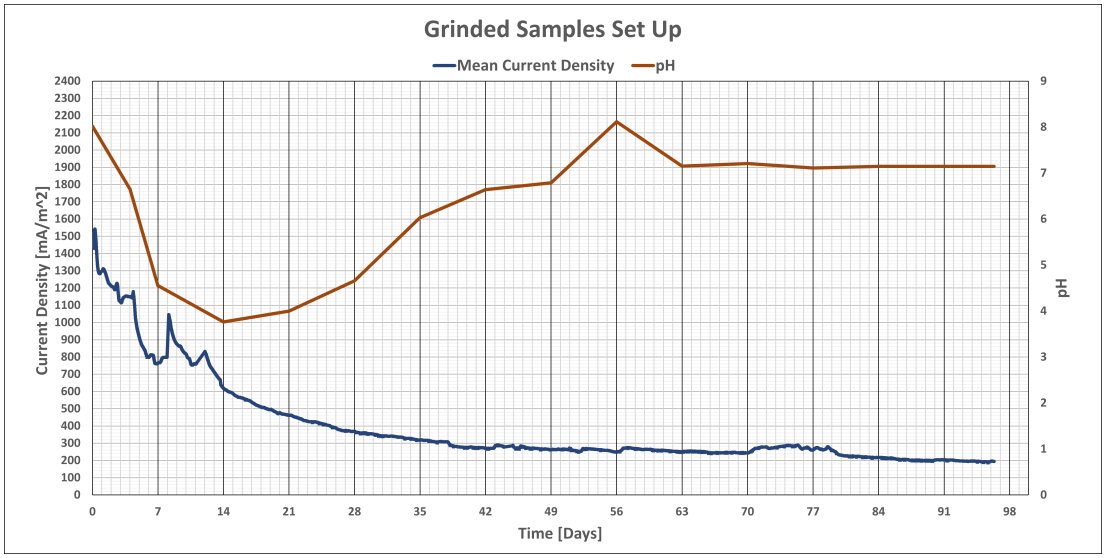

(b) Grinded Samples Experiment.

Figure 5.1: *Cathodic Current density, pH and counter electrode potential measurements after 3 months of potentiostatic polarisation to -1050 mV vs. Ag|AgCl in confined compartments.*

behaviour. It seemed that the acidification lasted twice as long for the grinded samples compared to the precorroded samples. This behaviour was quite odd as one would think that the reason for this difference is the potential on the counter electrode. However, the potential on the counter electrode of the grinded samples was lower than that of the precorroded samples which contradicts the logic. Hence, another factor is affecting this behaviour.

To explain the above observation, the pH, the counter electrode potential and the cathodic current density were investigated. The dependency of the pH on the counter electrode potential is studied in section 5.2, where it is explained in

detail how the pH is not necessarily dependent on the counter electrode potential. Finally, a hypothesis was developed with respect to explain the behaviour exhibited in the precorroded samples experiment. This hypothesis is explained in detail in section 5.4.

Figure 5.2 displays the average cathodic current density curve of the water exchange experiment under potentiostatic polarisation to -1050 mV vs. Ag|AgCl. After 12 weeks of continuous polarisation, the current density was measured to be 290 mA/m^2. The following value seemed to be much higher compared to the other two experiments for the same period of time. However, it should be noted that this experiment was the most unstable as the potentiostat delivered very low potential which lead to the production of hydrogen and probably had damaged the calcareous deposit formed on the surface. Hence, the quality of the deposit is most likely not optimal. The following was observed by Xu et al. [82] where AISI 4135 was polarised to -1100 and -1200 mV vs. Ag|AgCl, from which the calcareous deposit seemed to have cracked and looked very porous which is a result to the bubbles produced from the hydrogen evolution on the steel surface. Xu et al. [82] reported that the brucite formed at these potentials had a honeycomb structure and was of low quality as a result. Thus, a relatively a high final current density was recorded.

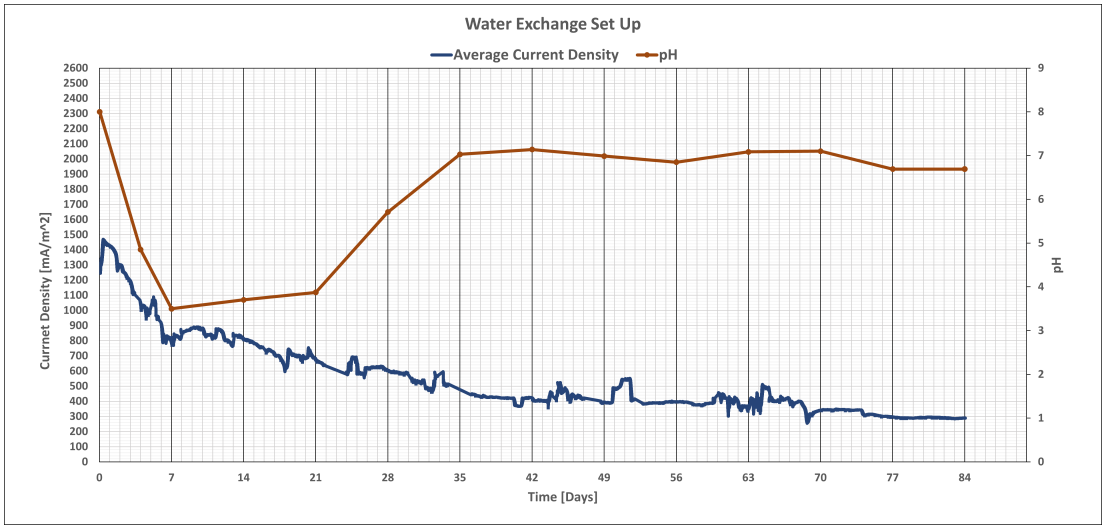

Figure 5.2: *Average cathodic current density curve of the samples polarised to -1050 mV vs. Ag|AgCl and pH measurement of the water exchange experiment.*

5.2 Counter Electrode Potential and pH Dependency

During the potentiostatic polarisation of the samples, the counter electrode potential was measured each 5 minutes, while, the pH was measured weekly. The measurements are displayed in Figure 5.3. The first observation to be taken is that the acidification lasted 2 times as longer in the grinded samples set up than the precorroded samples set up. The following observation is a little bizarre as the counter electrode potential on the grinded samples was slightly lower than that on the precorroded samples. Hence, the acidification can't directly be justified by the chlorine evolution on the counter electrode. **Thus, the pH is not significantly affected by the potential on the counter electrode for this case.**

This statement can be further proved by analysing each of the experiments individually. Figure 5.3a shows the measurements of the precorroded samples. In the intial period, the counter electrode potential was measured to be around 1200-1220 mV vs. Ag|AgCl. Which was the highest potential seen throughout the whole duration. This could probably explain the intial acidification as the potential on the counter electrode is more positive than the CER potential limit (1160-1200 mV vs. Ag|AgCl from section 4.6) which decreases the pH as a result of the chlorine evolution on the counter electrode. Thereafter, the potential on the counter electrode was stable at potentials 1200-1210 mV vs. Ag|AgCl which are potentials that should be high enough to continue causing the acidification based on what was seen. However, this was not the case as the pH increased back to a neutral pH under the same potential. This behaviour shows that there is a weak link between the counter electrode potential and the pH. As if there was a direct link, the acidification should have lasted throughout the duration. One may justify this behaviour by domination of the OER which leads to the production of the OH^- anions. Nevertheless, this would not make sense as it is well known that the kinetics of the CER leads to a faster production of H^+ than the production of OH^-anions from the OER as proven by Bennett [70]. In other words, if the CER is active, then, the pH will decrease as it is controlled by the production of $H+$ anions. Hence, the chlorine and oxygen evolution reactions can't explain directly this change of pH.

The previous analysis can be further supported by observing the relation between the counter electrode potential and pH in the grinded samples set up as shown in Figure 5.3b. During the first 3 weeks, the potential on the counter electrode was recorded to be 1180-1200 mV vs. Ag|AgCl. Acidification was observed during this period. Based on this information, it will make sense that the chlorine evolution is present under this potential which leads to the observed acidification. However, this would not make sense as the pH increased again under higher

counter electrode potential which contradicts the basis of the acidification by the chlorine evolution. Again, the pH seems to not be dependent on the counter electrode potential and another hidden factor seems to be controlling the pH.

Similarly, the pH and the counter electrode potential in the water exchange system set up seemed to be independent from each other as displayed in Figure 5.3c. In the initial phase the potential was quite high which could explain the sudden drop in pH. However, it quickly decreased and stabilised at a a lower potential but one could still see acidification. Thereafter, the counter electrode potential slightly increased and the pH seemed to increase as well which again contradicts the reasoning that the CER is what is causing acidification. **The second observation is that the acidification lasted longer on the precorroded samples set up but shorter than on the grinded samples set up.**

The following observation led to studying the differences between the 3 experiments. The main difference is the seawater volume of the experiments. The grinded samples experiment had the largest volume with 22 liter, while, the other experiments had a volume of 14-15 liter. Nevertheless, it should not be forgotten that the water renewal set up, had 4 water exchanges of 1.5 liters during the first 6 weeks. Hence, a total of 6 liters (40% compared to the intial volume) was renewed. **Thus, one explanation could be that the concentrations of the chemical elements in the seawater have affected the pH.** The second parameter to look at is the current density during the changes of pH. One specific trend was observed especially for the precorroded samples set-up. As it seemed that the pH was low when the current density was decreasing, and increased when the current density was stable at a specific value. But how can the concentration of the waters chemical composition and the current be related. Well, the main difference is the concentration of the calcareous deposit buffers. The current density's decrease suggests the formation of the calcareous deposit which is directly related to the pH and the consumption of the OH^-. With the previous information, the observed trend can be seen as that the pH decreased during the formation of the calcareous deposit. In other words, the drop in pH is an indicator for the large formation of the calcareous deposit.

It is well known that the calcareous deposit formation depends on the concentration of the magnesium and calcium in water. As the water volume is larger for the grinded samples and water exchange set ups, the concentrations of these elements will stay higher for longer period of time even if similar amounts is consumed. As the concentration of Mg^{2+} and Ca^{2+} remains higher for a longer period, the calcareous deposit formation also lasts longer. Hence, the consumption of OH^- lasts longer and the acidification is caused by this mechanism. This was proven with the ICP analysis were it was shown that almost twice as much magnesium was

deposited on the surface of the grinded samples than the precorroded samples. Which again proves that the calcareous deposition lasted longer in the grinded samples experiment where the acidification was observed for a much longer time under a lower counter electrode potential, compared to the precorroded samples set up. Therefore, it was hypothesised that **the acidification was caused by the formation of the calcareous deposit formation**. This hypothesis is further discussed in subsection 5.4.2.

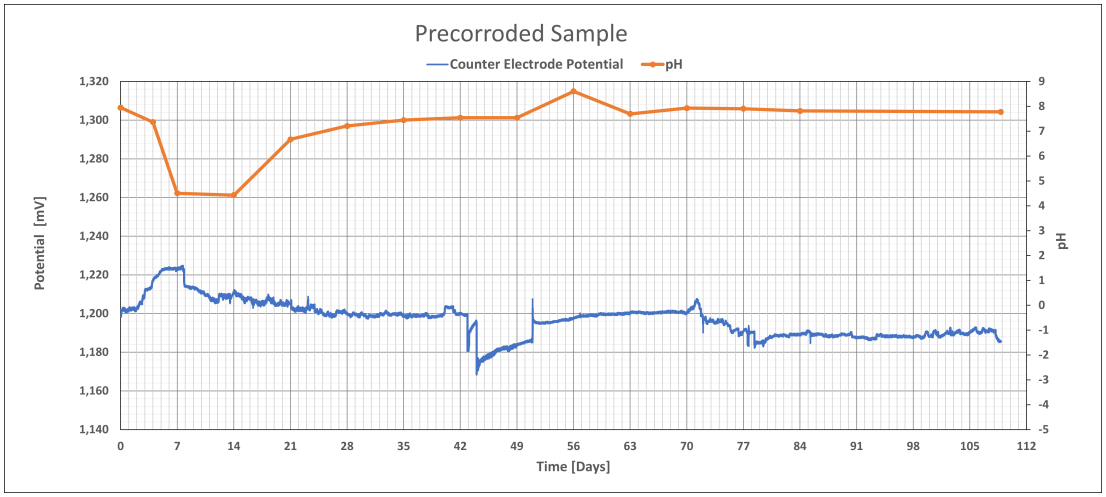

(a) Precorroded Samples Experiment.

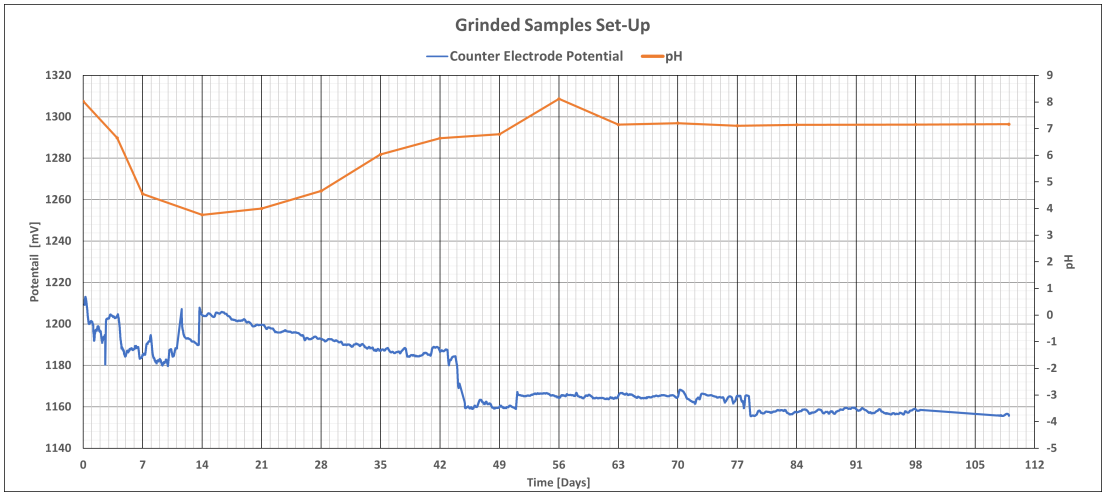

(b) Grinded Samples Experiment.

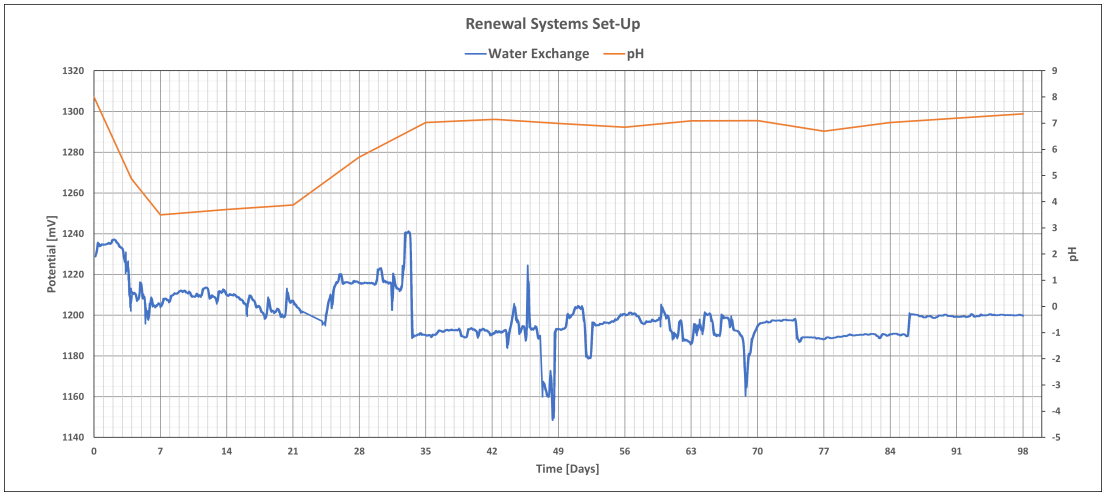

(c) Water Renewal System Experiment.

Figure 5.3: *Counter Electrodes Voltages and pH measurements of the experiments. Potential is given in [mV vs. Ag|AgCl].*

5.3 Calcareous Deposit Quality

Calcareous deposits are solid products that promote a physical barrier against oxygen diffusion which protects the steel surface and decreases the current density required to maintain polarisation. This physical barrier comes in different forms, mainly, $CaCO_3$ (aragonite) and $Mg(OH)_2$ (Brucite). From the results shown in subsection 4.3.1, the calcareous deposit formed during the first 4 weeks of polarisation of the precorroded samples was mainly made of brucite with some aragonite. This was confirmed with an EDS analysis where the main elements were magnesium, oxygen and a little calcium. This was further confirmed with an ICP analysis of the seawater, where it was found that large amounts of magnesium and smaller amounts of calcium precipitated on the surface.

The calcium/magnesium ratio was found to be 3 times higher in the precorroded samples set up compared to the grinded samples set up as it is shown in Table 4.1. This means that the calcareous deposit formed on the grinded samples set-up is of lower quality than the one made on the precorroded samples. The reason being is that the magnesium based compounds are very porous and tends to have lower isolating properties than the calcium based compounds [49, 82]. The following observation was explained in more detail in subsubsection 2.3.3.1. The difference in the calcareous deposit quality is the acidification effect. At very low pH, the brucite formation seems to dominate the calcareous deposit formation as observed from the SEM results in section 4.3. Since the acidification lasted twice as long in the grinded samples experiment, then it is reasonable to think that the calcium carbonate didn't have time to form. Furthermore, the initial current density was much higher on the grinded samples which may have led to the precipitation of higher amounts of magnesium. As mentioned the protectiveness index of on the precorroded samples calcareous deposit is better than the one formed on the grinded samples. This can be seen from the current density on the samples, as the grinded samples had 3 times more magnesium precipitated on the surface but still required almost as much current density to keep the samples polarised. Hence, the calcareous deposit formed on the precorroded samples is much more effective.

The microstructure of the calcareous deposit was investigated again after 12 weeks of polarisation of the precorroded samples. From which it was found that the microstructure was made of mainly calcium carbonate (aragonite) with some magnesium hydroxide (brucite). Similar microstructures were obtained by Xu et al. [82], [41] and [55], where similar morphologies of the aragonite were reported. On the other hand, the calcareous deposit on the grinded samples was still made of magnesium hydroxide with some calcium carbonate. Hence, the calcareous de-

posit formed on the precorroded samples is definitely of higher quality as it has a higher protectiveness index. This is due to the longer acidification which prevented the formation of calcium carbonate and left the sample with a relatively thick magnesium hydroxide layer. So why did the precorroded samples have more amounts of calcium carbonate precipitated on the surface than the grinded samples even after the acidification was over?

To answer this question, one should investigate the relation between the calcareous deposit thickness, the current density and the interfacial pH. As it has been established, the rate of calcareous deposition is a function of the applied current density, interfacial pH and exposure period. On the other hand, it was shown from the results that the formation of the calcium carbonate seems to be more dependent on the bulk pH. Hence, there are two questions to answer to develop an explanation. The first is when did the pH neutralize for the experiments. This is important to answer, as this marks the point at which the calcium carbonate starts to form. From the test results, it seemed to be that the pH had neutralized after 3 weeks and 6 weeks for the precorroded samples and the grinded samples, respectively. The second question would be, what is the current current density at the point when the pH had neutralised. The following was found to be 500 mA/m^2 and 300 mA/m^2 for the precorroded samples and the grinded samples, respectively. Thus, the precorroded samples had both longer time and higher current density when the calcium carbonate was formed. Meanwhile, the grinded samples had lower current density which means lower formation rate, in addition to a shorter duration. Using the following information, it completely makes sense that larger amount of calcium carbonate had formed on the precorroded samples compared to the grinded samples.

From the discussed observations, it is clear that the calcareous deposits quality was negatively affected by the acidification. As the decrease in pH, inhibited the formation of calcium carbonate. The negative effect on quality can be seen from the cathodic polarisation curves in Figure 4.4, specially between week 0 and week 6. During this period, the decrease in the cathodic current density was much larger on the precorroded samples compared to the grinded samples. Hence, the calcareous deposit formed on the precorroded samples had better barrier properties or in other words better quality. Meanwhile, it seems that the quality of the calcareous deposit formed on the grinded samples became better. As the decrease in the required cathodic current density was larger on the grinded sample compared to the precorroded sample, between week 6 and week 12. The reason for the larger decrease is the neutralisation of the pH after week 5-6 which enabled the calcium carbonate to precipitate on the surface. Thus, the quality of the calcareous deposit was enhanced and will most likely continue to enhance as the formation rate of

the calcium carbonate takes over the calcareous deposition in the long run [45].

To summarize this section, the quality of the calcareous deposit was indeed affected by the acidification. At lower pH, the magnesium hydroxide seems to be the favorable mineral. While, the calcium carbonate was the dominating mineral at higher pH. The following suggested that the formation of calcium carbonate is more dependent on the bulk pH. Hence, the acidification led to a delay in the formation of the calcium carbonate. Thus, more calcium carbonate was found on the precorroded samples contra the grinded samples. Furthermore, the current density during the acidification was much larger than the current density when the pH had neutralised. This lead to a faster formation rate (larger amounts) of the magnesium hydroxide compared to the calcium carbonate which started forming at a lower current density. However, this only means that the quality of the calcareous deposit is affected during the initial period. Nevertheless in the long run, the calcium carbonate will be the dominating mineral and the quality of the calcareous deposit will improve. But this may take longer time than usual due to the lower current density which leads to a lower formation rate.

5.4 Hypothesis for The Behaviour of the pH and The Cathodic Polarisation Curve

During the potentiostatic polarisation, an odd behaviour of the evolution of the current density was observed on the precorroded samples. The reason being is that it was observed that the acidification did occur as a result of the chlorine evolution reaction for the first few days, however, the potential on the counter electrode did not always explain the observed pH behaviour. During the beginning of the polarisation, the potential on the counter electrode was quite high and we observed acidification after a few days which does make sense. After the first week, the potential on the counter electrode stabilized but we still saw some changes in the pH which could not be explained with the CER. Hence, a hypothesis was established to identify the observed behaviour and identify the mechanisms of the calcareous deposit formation under the application of ICCP in confined compartments. Figure 5.4 demonstrates this behavior which will be discussed in the following section. Figure 5.4 displays the potential drop from which the current density is calculated (proportional relationship), the pH and the counter electrode potential.

To be able to give a clear explanation, 3 parameters were put in focus. The 3 parameters are the current density, the counter electrode potential and the pH. From the hypothesis, it is thought that the evolution of the current density occurs

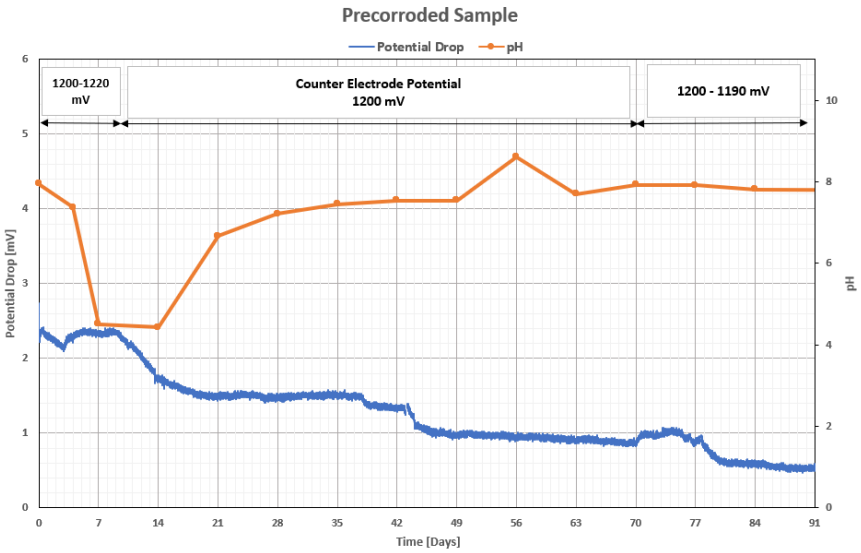

Figure 5.4: *Potential drop and pH measurements of a precorroded sample under potentiostatic polarisation to -1050 mV vs. Ag|AgCl for 90 days.*

in 5 phases as shown in Figure 5.5.

1. pH is controlled by the CER.
2. Acidification is induced by the formation of magnesium hydroxide, $Mg(OH)_2$.
3. Development of the calcareous deposition stops, leading to the increase of pH.
4. The calcareous deposit formation continues as the pH neutralises.
5. No more calcareous deposition as the electrolyte in the closed compartment runs out of buffers.

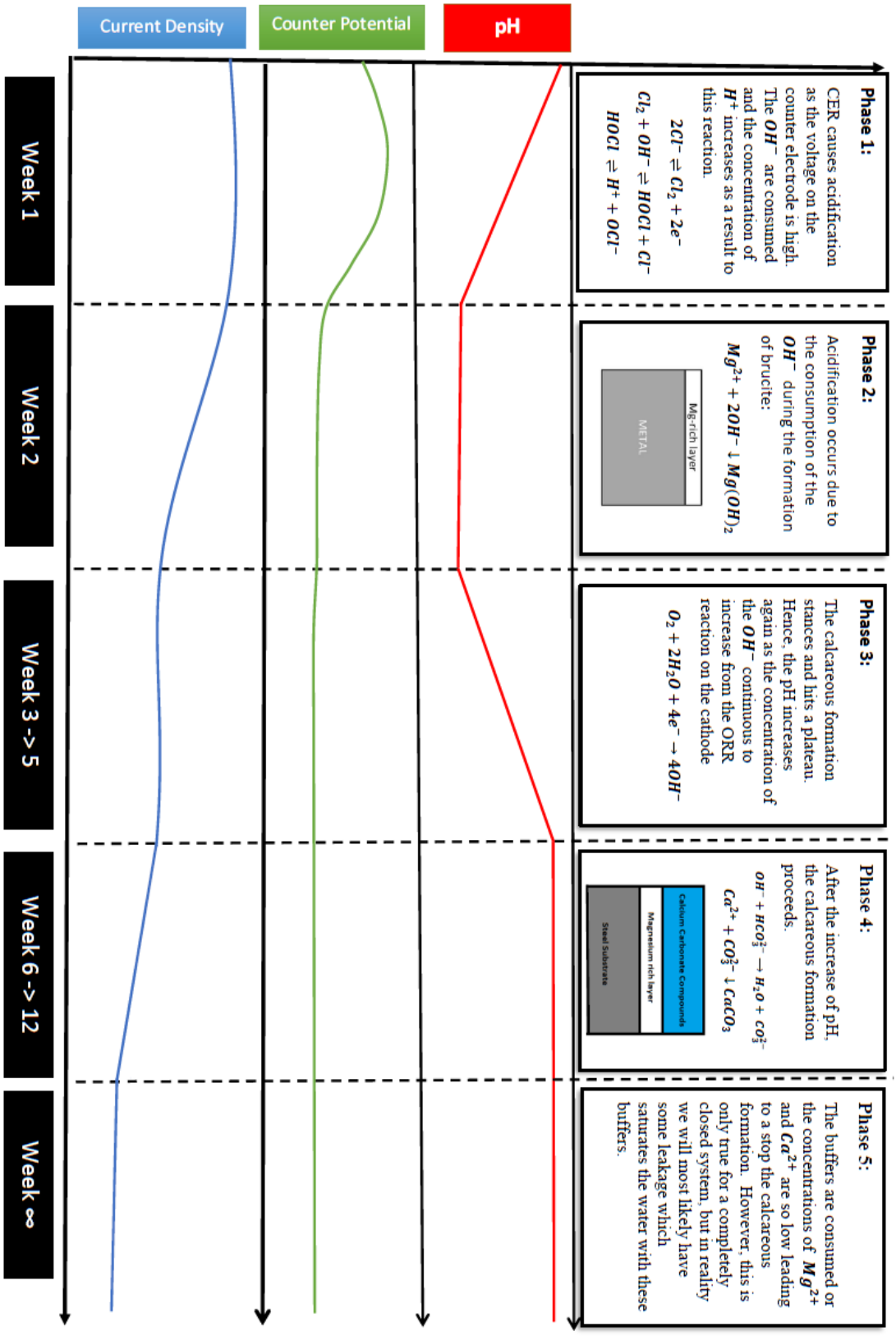

Figure 5.5: *Schematic of the hypothesis explaining the behaviour of the cathodic current density and pH. Potential is given in [mV vs. Ag|AgCl].*

5.4.1 Phase 1: The pH is controlled by the CER

During the first week of polarisation of the precorroded sample, the potential at the counter electrode was at its highest with a value of 1225 mV vs. Ag|AgCl in this specific case. Hence, the potential is over the CER limit and the chlorine evolution is occurring. During this reaction, chlorine is produced and reacts with the hydroxide, OH^- produced from the oxygen reduction reaction (ORR) on the steel surface, resulting in the production of the hypochlorous acid, $HOCl$, as shown in Equation 5.1.

$$Cl_2 + OH^- \rightarrow HOCl + Cl^- \tag{5.1}$$

Thereafter, the hypochlorous acid further reacts and leads to the production of H^+ anions and hypochlorite as displayed in Equation 5.2.

$$HOCl \rightarrow H^+ + OCl^- \tag{5.2}$$

Usually, equal amounts of H^+ and OH^- are produced which keeps the bulk solution at a neutral pH. However, the CER occurs at a faster rate which leads to a higher production of the H^+ anions, thus, the pH decreases. This was further explained in subsection 2.5.2. Nevertheless, the main point is that highly aggressive acidification is observed initially due to the CER. During this phase, the current density remained quite high for approximately 7-8 days before starting to decrease which will be the second phase. After this point on, the CER stabilized at 1200-1210 mV vs. Ag|AgCl as it is shown in Figure 5.6.

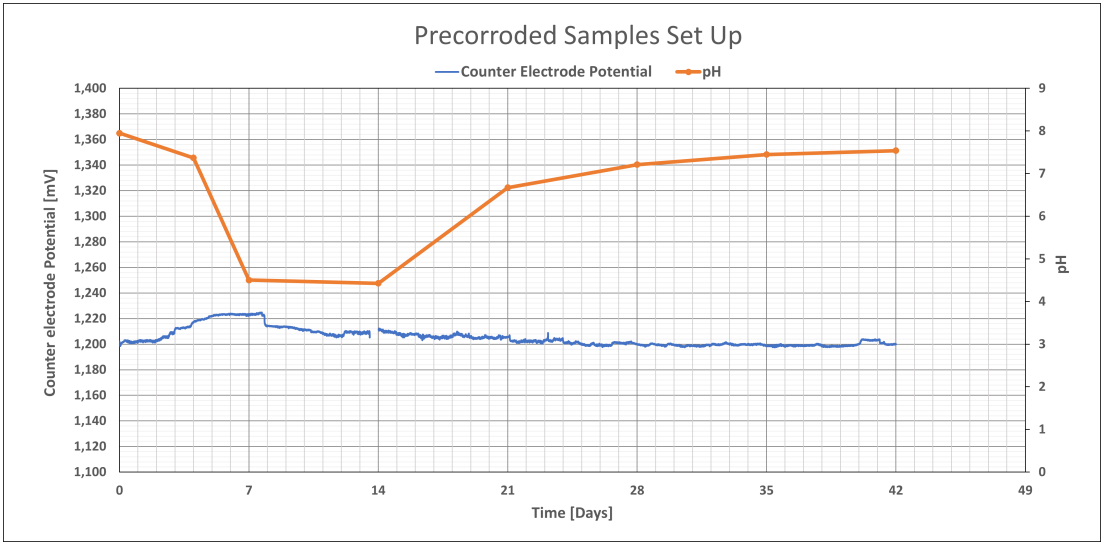

Figure 5.6: *Counter electrode potential and pH of the precorroded samples experiment. Potential is given in [mV vs. Ag|AgCl].*

During this phase, it was noticed that the current density required to polarise the sample were very high. This can be explained with the CER as it lead to an very high increase in the cathodic current. This was specially observed by Abe et al. [61] who measured the cathodic current density in water with increasing NaCl concentrations. As it was clear that the current density required decreased with the decrease of the NaCl concentration as it is displayed in Figure 5.7.

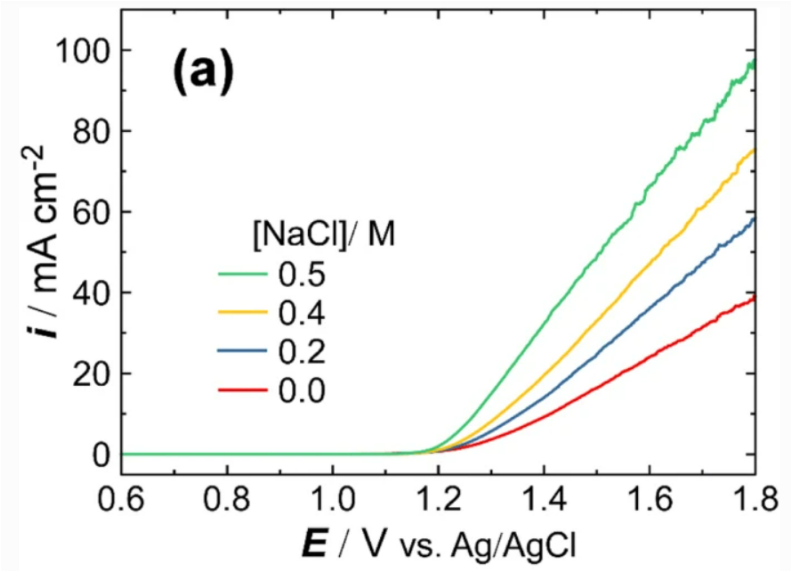

Figure 5.7: *Linear sweep voltammetry (LSVs) for IrO2/Ti electrodes [61].*

5.4.2 Phase 2: Acidification is induced by the formation of Brucite

By the end of the first phase which is during the first week, the potential on the counter electrode had decreased and stabilized but the pH was still low and one could still observe acidification. Hence, one was to wonder why the pH is still low. At the same time, it could be seen that the current density started to decrease gradually. The following trend indicated that there is formation of calcareous deposit on the steel surface. As it was mentioned in various literature, the initial calcareous deposit formed is most likely magnesium hydroxide (Brucite). This was verified with the results from the SEM analysis. As it was found that after 6 weeks the calcareous deposit formed consisted mainly of brucite. One would then ask how is it sure that this calcareous deposit had formed during this period if the SEM was taken 4 weeks later. Simply, the decrease of current density was only observed during week 2 or phase 2, and later between week 6-12. Hence, the calcareous deposit that was observed on the SEM is from this period of time. The realisation of the formation of brucite during this period is crucial, as it can be directly related to the

acidification observed. The formation of brucite highly depends on the presence of OH^-, which in turn is responsible for increasing the pH. The formation of brucite occurs as shown in Equation 5.3.

$$Mg^{2+} + 2OH^- \rightarrow Mg(OH)_2 \tag{5.3}$$

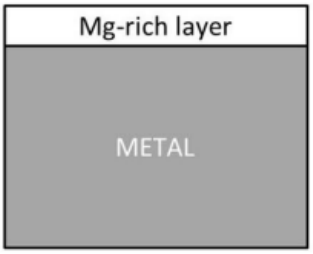

Figure 5.8: *Schematic of the calcareous deposition during phase 2.*

It is clear that the formation of this mineral leads to the consumption of the hydroxides. Hence, one may speculate that the equilibrium between the OH^- and H^+ anions have been interrupted by the formation of the calcareous deposit. Thus, the relative concentration of the hydrogen anions increases and the pH is kept low. Furthermore, the calcareous deposit formed creates a barrier towards the ORR reaction which decreases the production of the OH^- anions. The following theory can be supported with the SEM and ICP analyses conducted on the grinded samples and precorroded samples experiments. The acidification in the grinded samples experiment lasted almost twice as long as it did in the precorroded samples experiment.

Based on the aforementioned hypothesis, if the acidification lasted much longer, then the amount of brucite formed should be much larger (which is the case for the grinded samples experiment). Hence, an ICP analysis was conducted on the electrolytes as shown in Table 4.1. It was found that the amount of magnesium ions consumed as calcareous deposit was 3.5 times larger on the grinded samples where the acidification lasted longer. Furthermore it could be seen from the SEM analysis that the brucite formed on the grinded samples were physically larger and much more visible and defined. This hypothesis could be further proved by looking at the current density and pH in the precorroded samples set-up as shown in Figure 5.10. It is clear that the acidification is observed under the decrease of current density, and as the current density stabilizes, the pH starts to increase again which is when phase 3 starts.

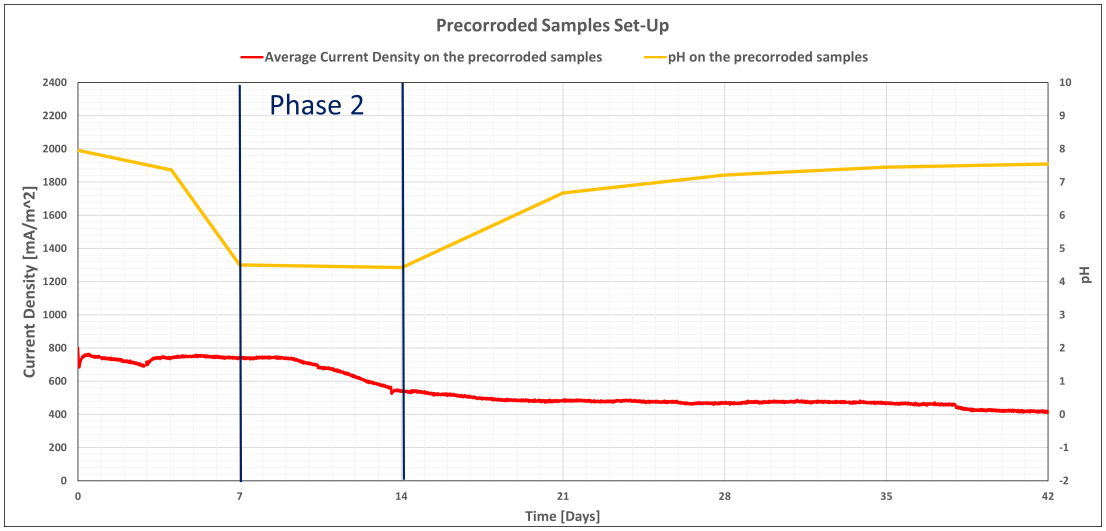

Figure 5.9: *Illustration of phase 2 on the precorroded samples set-up*

Figure 5.10: *Illustration of the relationship between the decrease in current density and the observed acidification.*

5.4.3 Phase 3: Calcareous deposition hits a plateau leading to an increase in pH

By the beginning of phase 3, the current density seized to increase and hit a plateau where it stabilized. At the same time, the pH started to decrease again. This trend of data indicated the interruption of the calcareous deposit formation. Meanwhile the potential on the counter electrode remained unchanged, thus, the acidification effect if there is any from the counter electrode has not changed and the pH increased still. This behaviour further supported the aforementioned hypothesis of that the acidification has been induced by the formation of magnesium hydroxide. Hence, the explanation to this behaviour was that as the magnesium hydroxide seizes to form , the acidification stops. On the other hand, the OER is still occurring and the OH^- anions are still being produced without being consumed as the formation of the calcareous deposit stopped. The OER is displayed in Equation 5.4;

$$O_2 + 2H_2O + 4e^- \rightarrow 4OH^- \tag{5.4}$$

To summarize the explanation, the change in pH occurs due to the absence of the acidification effect from the calcareous deposit formation. And the pH neutralizes as the relation between the production of the H^+ and OH^- ions from the CER and OER are in equilibrium. Hence, a neutralization of the pH was observed.

Usually when the CER is observed, there is always acidification. However in this case, the current density of the CER seems to be not large enough to dominate the cathodic reaction. Therefore, a neutral pH is obtained. A counter argument of the following hypothesis is that the potential had stabilized below the CER and therefore, acidification was not observed. However, this is would not true as aggressive acidification was observed under lower potential such as the grinded samples experiment where the acidification occurred at lower potentials (1180-1205 mV vs. Ag|AgCl). Therefore, the disappearance of the acidification can't be explained with the stop of the CER.

5.4.4 Phase 4: The pH neutralises and the Calcareous Deposition Continues

At the end of phase 3, the pH had stabilized at a neutral pH and the current density resumed to decrease again. This following behaviour was explained with the formation of calcium carbonate as calcareous deposit, which doesn't require as high pH as the magnesium hydroxide. And doesn't affect the pH as much, since, it requires less OH^- anions to precipitate as shown in Equation 5.5 and Equation 5.6.

$$OH^- + HCO_3^- \rightarrow H_2O + CO_3^{2-} \tag{5.5}$$

$$Ca^{2+} + CO_3^{2-} \downarrow CaCO_3 \tag{5.6}$$

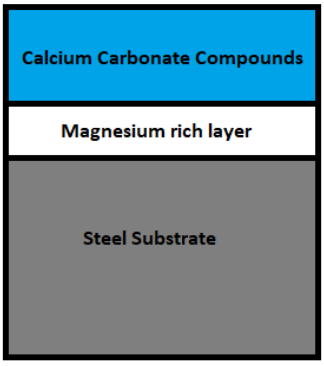

Figure 5.11: *Schematic of the calcareous deposition during phase 2.*

This explanation was proved with the conducted EDS, SEM and ICP analyses on the precorroded samples experiment. After approximately 12 weeks of continuous polarisation, a SEM analysis was conducted on the precorroded and grinded samples. It was clear that the calcareous deposit was mainly made of calcium carbonate. So how can one be sure that the calcium carbonate occurred during this phase. Well, as it's been established that the decrease of the current density is directly correlated with the formation of the calcareous deposit. This decrease in current density was observed in two of the 5 phases of the hypothesis. The first time period was during phase 2, where the SEM and EDS analyses showed in Figure 4.5 and Figure 4.6 that the main mineral formed during this period is mainly magnesium hydroxide. This was further investigated with an ICP analysis which showed that the precipitated calcium was much lower than the precipitated magnesium. In fact, on the precorroded samples the amount of calcium precipitated is half that of the magnesium. Hence, the calcium carbonate occurred during phase 4 where the cathodic current density continued to decrease (after week 6). Therefore, most of the calcium carbonate formed occurred during this phase.

The second question that comes to mind is, why did the calcium carbonate form during this phase and not earlier? To answer this question, one should take a closer look on the precipitation pH of the magnesium hydroxide and calcium carbonate. However, it should be emphasized that the precipitation pH is dependent on the interfacial pH and not the bulk solution pH. The magnesium hydroxide is known to precipitate at an optimal pH of 9.3 at room temperature [51], whereas the optimal pH at which calcium carbonate precipitates at is pH 7.5-8.5 [83]. In the initial phases of the polarisation, the pH on the steel surface is very high (approximately pH 9-10) which favors the precipitation of magnesium hydroxide. This specific behaviour could be observed in the selectivity of the type of calcareous deposit and the polarisation potential. However, as the magnesium hydroxide precipitates and forms a layer, the distance between the reaction location and the interfacial location increases. This was studied by Sun et al. [45], where he described the pH as a function of the distance inside the diffusion layer and time, as displayed in Figure 5.12.

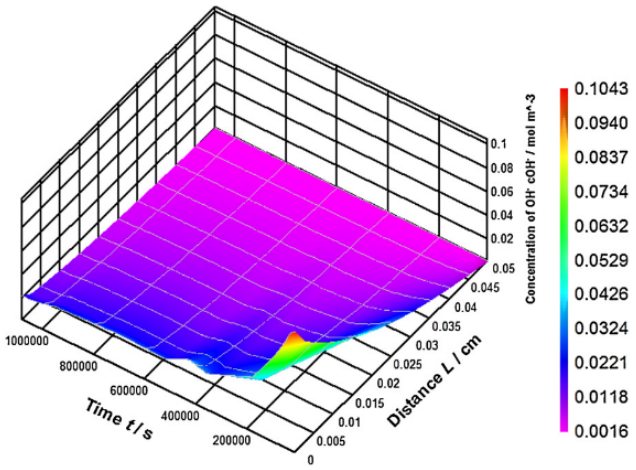

Figure 5.12: *Concentration profile of OH^- ions as a function of the distance and time inside the diffusion layer [45], whereas; RMg(OH)2 is the formation rate of magnesium hydroxide, RCaCO3 is the formation rate of calcium carbonate and $\frac{nCaCO_3}{nMg(OH)_2}$ is the molar ratio of calcium carbonate and magnesium hydroxide [45].*

As the magnesium hydroxide becomes thicker, the reduction of oxygen is further inhibited [45, 82, 84]. Hence, the pH at the calcareous deposition location becomes lower. And At some point the precipitation of magnesium stops and the calcium carbonate precipitation overtakes the calcareous deposition. This behaviour was confirmed by Sun et al. [45] as shown in Figure 5.13 where the calcium carbonate formation rate overtook the magnesium hydroxide formation rate as the calcareous deposit layer became thicker. The overtake of the calcium carbonate formation rate was also justified by the layout of the concentrations of the Mg^{2+}, Ca^{2+} and HCO_3^- ions with respect to time and distance throughout the diffusion layer [45].

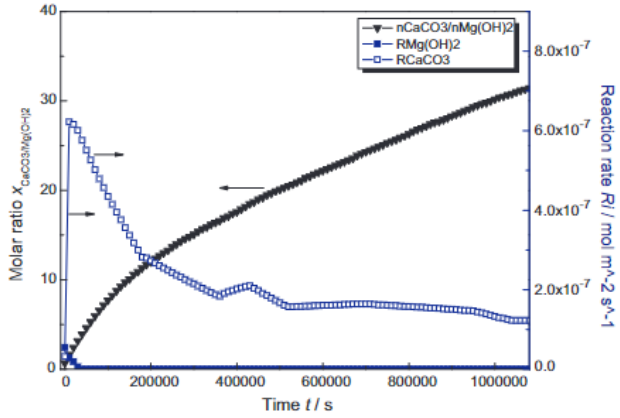

Figure 5.13: *Changes of the reaction rates and mole ration of $CaCO_3$ and $Mg(OH)_2$ of calcareous deposits with time [45].*

5.4.5 Phase 5: No more Calcareous Deposition as the electrolyte runs out of buffers

Finally, the last phase was not observed through the testing, however, it can be reasoned through the facts from this experiment set-up. During the fifth and last phase, it is expected that the buffers that form the calcareous deposit will run out. Hence, the current density will hit a plateau and no more calcareous deposit will form. This behaviour is expected to occur due to the fact that the system is completely closed and no water exchange is observed. Nevertheless, this behaviour is only true in the ideal laboratory conditions. Anyhow in real life conditions, the buffers are expected to never run out as there will definitely be some water exchange through the J-tube valve of the monopile. This is especially true for the leaking monopile foundations where there is a water exchange. As the buffers will continue to stream into the internal part of the monopile and precipitating as a calcareous deposit.

5.5 Repolarisation under Neutral Vs Low pH

ICCP systems are well known for their frequent failures which requires some maintenance. Hence, it is of importance to understand the repolarisation behaviour of the cathodic system in case of malfunction. To do so, one sample from each experiment was disconnected form the ICCP system to freely corrode for 1 week and repolarised again to -1050 mV vs. Ag|AgCl. This was done in low and neutral pH to highlight any significant differences as it is natural to think that the repolarisation current density is controlled by the low pH.

Under neutral pH, both the precorroded and grinded samples showed very similar behaviour as the repolarisation current density was measured to be 1.5 times the current density just before it was disconnected from the CP. For both experiments it took approximately 5 days for the current density to converge back to the continuously polarised samples curve. Meanwhile, the precorroded samples repolarised under low pH (pH 4-4.5), had a repolarisation current density that is 1.9 times the initial current density before disconnection. Moreover, it took approximately 8 days for the current density to converge back to the continuously polarised curve.

However it should be taken onto consideration that the repolarisation under low pH occurred before the development of a calcareous layer, which was the case for the repolarisation under neutral pH. It seemed to be that the calcareous deposit

provides some stability to the sample in terms of the amount of current density required and the time duration to reconvergence. Anyhow, the low pH did not significantly affect the repolarisation current density as the numbers were not unacceptably higher. A summary of the repolarisation current densities and duration are displayed in Table 5.1.

Table 5.1: *Repolarisation current densities and duration under neutral and low pH*

Experiment	pH	Current density before disconnection	Repolarisation Current Density	Time to reach the intial current density	Time to converge back
Neutral pH | Precorroded Samples	7.54	380 mA/m^2	617 mA/m^2	2-3 days	5 days
Neutral pH | Grinded Samples	6.79	290 mA/m^2	452 mA/m^2	2-3 days	5 days
Low pH | Precorroded Samples	4-4.5	870 mA/m^2	1668 mA/m^2	0.5 day	8 days

5.6 Inert Anode Design

As observed from the experiment, the chlorine evolution reaction on the inert anode lead to acidification. The reason being that the potential on the counter electrode exceeded the CER potential. Hence, an optimized inert anode design or material selection should be applied to avoid the acidification effect.

The first approach to do so, is by reducing the potential on the counter electrode to avoid chlorine production. This can be done in two methods. The first would be to regulate the anode-cathode area ratio, in the sense that the area of the inert anode should be increased as much as possible. The logic behind this lays in the basic polarisation principles, as the larger area would mean lower current density. Thus, the counter electrode would be able to supply the same amount of protective current at a lower potential. However, the following is not optimal as the space in the monopile is limited and a significant amount of anodes would be needed to realise the wanted result.

The second method is to polarise the steel structure to a more positive potential (-800 to -900 mV vs. Ag|AgCl). By doing so, a lower amount of current is needed to keep the steel protected, while keeping the potential on the counter electrode lower than the CER limit. The second advantage of this approach is that the number of ICCP inert anodes needs doesn't have to increase. Nevertheless, it is a little unrealistic to polarise the steel to -800 mV vs. Ag|AgCl as there is also resistance

in the seawater, in addition, to the instability from the ICCP system which doesn't guarantee that the steel will actually be polarised to this potential. In fact, the polarisation potential will most likely deviate or decrease below this potential which means that the steel may be exposed to corrosion.

Nevertheless, an alternative approach would be to combine the previous two approaches. The method would be to increase the polarisation potential to for example -900 to -1000 mV vs. Ag|AgCl, while, increasing the number of anodes at the same time. By doing so one is able to reduce the current density on the inert anodes by increasing area, hence, a lower potential on the counter electrode is expected. Moreover, the current needed to polarise the steel structure further decreases as the steel is polarised to a higher potential. The upside of this method is that the structure is safe from the risk brought by the deviation on the polarisation potential. Furthermore, the number of anodes doesn't have to increase significantly which increases the feasibility of the solution, in addition, to avoiding the anodes from interrupting each other. Moreover by polarising the steel from -900 to -1000 mV vs. Ag|AgCl, a high quality calcareous deposit will develop which decreases the required current density in the long run.

Another approach would be to choose an inert anode with a high CER potential limit or an apply a coating on the anode to suppress or at least minimize the production of chlorine. Abe et al. [61] studied the latter solution and found that the application of a thin Film Coating of Mg-intercalated layered MnO_2 suppressed the chlorine evolution at an IrO_2 anode under the application of ICCP. The coating enabled the user to minimize the production of chlorine without prevention of the oxygen evolution reaction (OER). The thin coating is made of a buserite-type layered manganese dioxide. The CER efficiency of the electrode modified with the Mg-buserite layer was as small as 11% at 1700 mV vs. Ag/AgCl. Figure 5.14 displays a schematic of the difference between the bare anodes and the coated anodes.

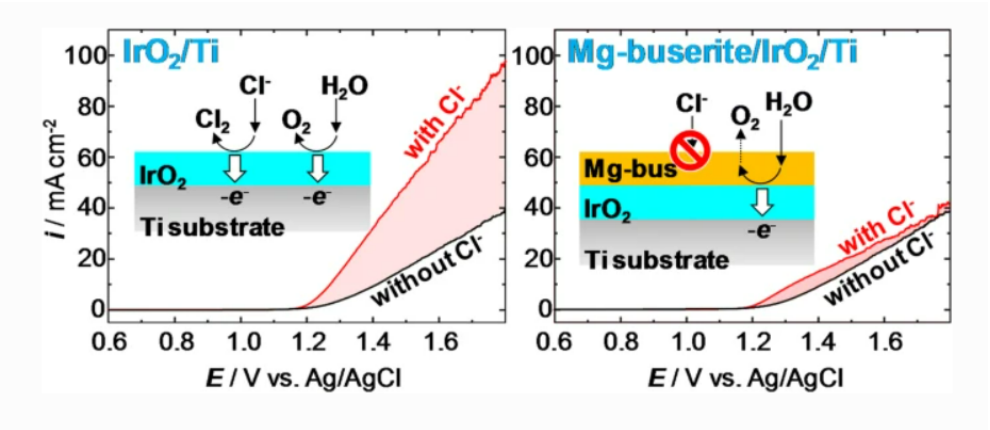

Figure 5.14: *CER on a bare IrO_2Ti anode vs Mg-buserite coated IrO_2Ti anode [61].*

5.7 Closed System Vs Partially Open System

As it has been established earlier, the use of ICCP leads to the production of chlorine which in turn leads to the acidification of the seawater for approximately 3 week before increasing to a more neutral pH (pH $\approx$ 7). Hence, a partially open system with 10% weekly water exchange was set up to investigate the feasibility of avoiding acidification. However, from the results this was not the case as the CER occurs way too fast that the acidification was still observed. Furthermore, it was established earlier that the acidification was also induced with due to the formation of magnesium hydroxide. And as the water renewal keeps the concentration of the magnesium ions relatively high, the acidification turned out to last longer than if the system was closed. The reason being that the formation of magnesium hydroxide took longer time which meant that the acidification lasted longer as well.

As the acidification lasted longer, the quality of the calcareous deposit was most likely affected as well. This could be seen from the current density found on the steel after 12 weeks of polarisation. The final current density of the precorroded samples in the closed system was found to be around 180 mA/m^2. Meanwhile, the current density of the precorroded samples in the partially open system was found to be 280 mA/m^2 after the same duration. Hence, the barrier properties of the calcareous deposit formed in the short term are better in the closed system. However, in the long run the partially open system will sustain high amount of buffers which will promote the formation of more calcareous deposit on the steel surface. This may occur at a lower rate but it will ultimately become better.

The second upside with the partially open system can be seen in case of the loss of protection while the pH is low. As the partially open system will provide some amount of water exchange which will neutralise the pH and avoid excessive corrosion due to the low pH. Meanwhile, the completely closed will maintain the low pH which will lead to a lot of corrosion if protection is not available. Thus, the water exchange led to a longer acidification duration which has affected the calcareous deposit quality and led to a higher current density requirement. However, the negative effect is just a delay in the formation of a high quality calcareous deposit. But as time goes, the quality will enhance specially with the fact that the electrolyte will be saturated with buffers. As it is shown in Figure 5.15, the concentration of the buffers will increase again as their consumption rate decreases and the water exchange makes up for the decreased amount of buffers with the new fresh water which is saturated with buffers. Moreover, the water exchange eliminates the risk of the construction corroding under low pH. Therefore, the partially open system is more sustainable in the long run compared to the completely closed system.

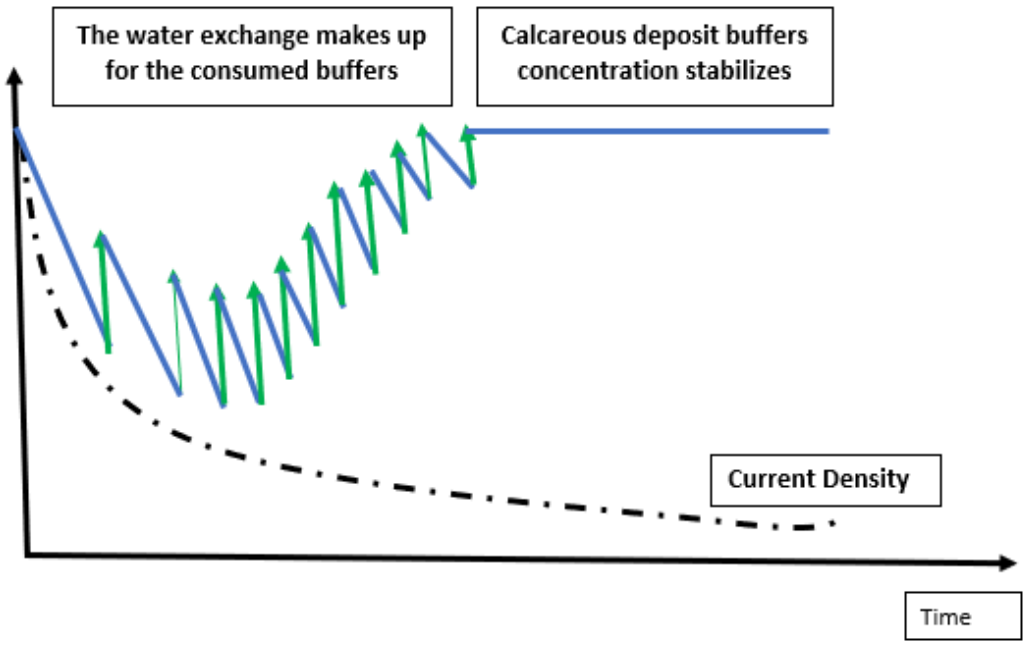

Figure 5.15: *Schematic for the evolution of calcareous deposits buffers in a partially open system*

Chapter 6

Conclusion

During this MSc project, three ICCP systems were tested in simulated confined and partially opened environments. Precorroded and grinded structural steel (St52 and St37) samples were polarised to -1050 mV vs. Ag|AgCl for 3 months. The key results from the ICCP system are displayed in Table 6.1.

Table 6.1: *Key results from the simulated ICCP systems.*

Experiment	Polarisation Duration [Days]	Initial Current Density [$\frac{mA}{m^2}$]	Final Current Density [$\frac{mA}{m^2}$]	Calcareous Deposit Microstructure	Acidification pH	Acidification Duration
Precorroded Samples	94	750	170	Brucite, Aragonite and other form of Calcium Carbonate	4	2 weeks
Grinded Samples	94	1300	190	Brucite and a little Aragonite	3.5-4	4 weeks
Water Exchange System	84	1300	290	NA	3.5-4	3 weeks

In the start of this thesis, five research questions were stated in subsection 1.3.2. These questions were answered from the following conclusions;

1. The water exchange was applied to avoid acidification. However, the acidification occurred too fast and the water exchange was ineffective.
2. The surface conditions did affect the required current density of the polarisation. The initial current density was lower on the precorroded samples compared to the grinded samples. Nevertheless, this effect seemed to only be significant in the initial period but did not affect the current density in the long run. After 12 weeks of polarisation, the calcareous deposit formed on the precorroded and grinded samples was well adhered to both the precorroded and the grinded surfaces.

3. The Precorroded samples had the highest quality calcareous deposit as it was formed larger amounts of calcium carbonate on the surface, while, the calcareous deposit formed on the grinded samples was mainly made of magnesium hydroxide and much less calcium carbonate. This suggests that the acidification does indeed affect the quality of the calcareous deposit, as the lower quality calcareous deposit formed on the samples where the acidification lasted the longest. Nevertheless, the final current densities were not significantly different (8-10% deviation).
4. The chlorine evolution potential on platinum and MMO inert anodes. From which it was found that the CER potential was the same on both anodes and was measured to being between 1160-1200 mV vs. Ag|AgCl.
5. The acidification lasted the longest in the grinded samples experiment. From the observed behaviour it seemed that the acidification highly depends on the volume to area volume as it was speculated in the proposed hypothesis that the acidification is partially induced by the formation of magnesium hydroxide. Hence, the increased amount of magnesium led to larger formation of magnesium hydroxide which could explain the longer acidification duration. This was supported by observing the potential at the counter electrode throughout the polarisation period. As the potential was similar during acidification and at neutral pH. Hence, another factor was affecting the acidification which is the formation of magnesium hydroxide. The pH seemed to initially depend on the CER on the counter electrode. Thereafter, the acidification becomes dominated by the formation of $Mg(OH)_2$. As the formation of $Mg(OH)_2$ ceases, the pH increases again to a neutral pH and the calcium carbonate starts to precipitate on the surface.

Chapter 7

Recommendations and Future Work

Based on the findings from this MSc project, the application of ICCP in confined environment caused temporary acidification. It was also found that the acidification did affect the quality of the calcareous deposit negatively. Furthermore, the final current density was relatively high (170 $\frac{mA}{m^2}$ after 12 weeks of polarisation to -1050 mV vs. Ag|AgCl). Hence, other solutions are needed to decrease the required current density and avoid acidification if possible.

The following is possible by optimising the ICCP system's design. The most suitable approach would be to find an optimal combination between the polarisation potential and the anode to cathode area ratio. Thus, variations between the polarisation potentials and anode to cathode area ratio should be tested in ICCP systems in confined compartments for longer duration (6 months).

Bibliography

[1] Antonio Colmenar-Santos, Javier Perera-Perez, David Borge-Diez, and Carlos dePalacio Rodríguez. Offshore wind energy: A review of the current status, challenges and future development in spain. *Renewable and Sustainable Energy Reviews*, 64:1–18, 2016.

[2] M Vieira, Brian Snyder, Elsa Henriques, and Luis Reis. European offshore wind capital cost trends up to 2020. *Energy policy*, 129:1364–1371, 2019.

[3] U IEA. Global energy review 2020. *Ukraine.[Online] https://www. iea. org/countries/ukraine [Accessed: 2020-09-10]*, 2020.

[4] Vicente Negro, José-Santos López-Gutiérrez, M Dolores Esteban, Pablo Alberdi, Mario Imaz, and José-María Serraclara. Monopiles in offshore wind: Preliminary estimate of main dimensions. *Ocean Engineering*, 133:253–261, 2017.

[5] Clara Matutano, Vicente Negro, Jose-Santos López-Gutiérrez, and M Dolores Esteban. Scour prediction and scour protections in offshore wind farms. *Renewable energy*, 57:358–365, 2013.

[6] Chris Horgan. Using energy payback time to optimise onshore and offshore wind turbine foundations. *Renewable energy*, 53:287–298, 2013.

[7] Brad James and Alexander Hudgins. Failure analysis of oil and gas transmission pipelines. In *Handbook of materials failure analysis with case studies from the oil and gas industry*, pages 1–38. Elsevier, 2016.

[8] Francesco Miceli. Offshore wind turbines foundation types. `https://www.windfarmbop.com/offshore-wind-turbines-foundation-types/`, 2012. Online; accessed 03 September 2021.

[9] Orlando Barbosa Leite. Review of design procedures for monopile offshore wind structures. 2015.

[10] Offshore Standard. Dnvgl-rp-0416: Corrosion protection for wind turbines. *Det Norske Veritas*, 2016.

[11] Offshore Standard. Design of offshore wind turbine structures. *Det Norske Veritas*, 581, 2007.

[12] Giulia Masi, Francesco Matteucci, Jeroen Tacq, and A Balbo. State of the art study on materials and solutions against corrosion in offshore structures. *North Sea Solutions for Innovation in Corrosion for Energy*, 2018.

[13] Sabina AGHASIBAYLI and Feargal BRENNAN. Corrosion damage effects on the structural integrity assessment of offshore structures. 2019.

[14] Dr. Conaill Soraghan. Management of hydrogen sulphide gas in wind turbine sub-structures:identifying and managing h_2s. 2016.

[15] Torsten Krebs. Iccp system for internal protection of monopiles for offshore wind farms. In *NACE International Corrosion Conference Proceedings*, pages 1–13. NACE International, 2018.

[16] Sameer Ayyar, Jacob Jansson, and Ruth Sorensen. Cathodic protection design for offshore wind turbine foundations. *Materials Performance*, 53(9):26–29, 2014.

[17] Det Norske Veritas AS. Dnv-os-j101 design of offshore wind turbine structures, 2014.

[18] Isaac Tavares, Petra Ernst, G John, R Jacob, and B Wyatt. Internal cathodic protection of offshore wind turbine monopile foundations. *Corros. Manag. A J. Inst. Corros*, 123:14–17, 2015.

[19] Birit Buhr Jensen. Corrosion protection of offshore wind farms, protecting internal sides of foundations. In *CORROSION 2015*. OnePetro, 2015.

[20] Oyewole Adedipe, Feargal Brennan, and Athanasios Kolios. Review of corrosion fatigue in offshore structures: Present status and challenges in the offshore wind sector. *Renewable and Sustainable Energy Reviews*, 61:141–154, 2016.

[21] Osema Cherif. Impressed current system for internal corrosion protection in monopiles for offshore windmills. Technical report, Norwegian University of Science and Technology, Department of mechanical engineering, 12 2021.

[22] Kenneth A Chandler. *Marine and offshore corrosion*, volume 222. Elsevier, 1985.

[23] Volkan Cicek. *Cathodic protection: Industrial solutions for protecting against corrosion*. John Wiley & Sons, 2013.

[24] Nicoleta Acomi and Ovidiu Acomi. Cathodic protection by sacrificial anodes or impressed current, comparative analysis. *Constanta Maritime University Annals*, 19, 2013.

[25] H El Ghitani and AH Shousha. Microprocessor-based cathodic protection system using photovoltaic energy. *Applied energy*, 52(2-3):299–305, 1995.

[26] S.M. Bashi, N.F. Mailah, and M.A.M. Radzi. Cathodic protection system. In *Proceedings. National Power Engineering Conference, 2003. PECon 2003.*, pages 366–370, 2003. doi: 10.1109/PECON.2003.1437476.

[27] Richard Baxter and Jim Britton. Offshore cathodic protection 101 what it is, and how it works. *WWW page*, 2011.

[28] C Rousseau, Fabienne Baraud, L Leleyter, and O Gil. Cathodic protection by zinc sacrificial anodes: Impact on marine sediment metallic contamination. *Journal of hazardous materials*, 167(1-3):953–958, 2009.

[29] Anna Maria Bell, Marcus von der Au, Julia Regnery, Matthias Schmid, Björn Meermann, Georg Reifferscheid, Thomas Ternes, and Sebastian Buchinger. Does galvanic cathodic protection by aluminum anodes impact marine organisms? *Environmental Sciences Europe*, 32(1):1–11, 2020.

[30] R Winston Revie. *Corrosion and corrosion control: an introduction to corrosion science and engineering*. John Wiley & Sons, 2008.

[31] DP Schmidt, BA Shaw, E Sikora, WW Shaw, and LH Laliberte. Corrosion protection assessment of sacrificial coating systems as a function of exposure time in a marine environment. *Progress in organic coatings*, 57(4):352–364, 2006.

[32] Bassim N Abdul Sada, Ramzy S Ali, and Khearia A Mohammed Ali. Identification and control of impressed current cathodic protection system. *Iraqi Journal for Electrical And Electronic Engineering*, 12(2):214–20, 2016.

[33] Jason S Lee, Richard I Ray, Brenda J Little, Kathleen E Duncan, Deniz F Aktas, Athenia L Oldham, Irene A Davidova, and Joseph M Suflita. Issues for storing plant-based alternative fuels in marine environments. *Bioelectrochemistry*, 97:145–153, 2014.

[34] J-F Yan, Ralph E White, and RB Griffin. Parametric studies of the formation of calcareous deposits on cathodically protected steel in seawater. *Journal of the Electrochemical Society*, 140(5):1275, 1993.

[35] J-F Yan, TV Nguyen, Ralph E White, and RB Griffin. Mathematical modeling of the formation of calcareous deposits on cathodically protected steel in seawater. *Journal of the Electrochemical Society*, 140(3):733, 1993.

[36] Georgii Vasyliev and Svitlana Vasylieva. Anticorrosion behaviour of calcareous deposits formed on steel heat-exchange surfaces. *Advances in Materials Science and Engineering*, 2020, 2020.

[37] Pierre R Roberge. *Handbook of corrosion engineering*. McGraw-Hill Education, 2019.

[38] William H Hartt, Charles H Culberson, and Samuel W Smith. Calcareous deposits on metal surfaces in seawater—a critical review. *Corrosion*, 40(11):609–618, 1984.

[39] Anne Neville and Arnaud P Morizot. Calcareous scales formed by cathodic protection—an assessment of characteristics and kinetics. *Journal of crystal growth*, 243(3-4):490–502, 2002.

[40] Jun-Mu Park, Myeong-Hoon Lee, and Seung-Hyo Lee. Characteristics and crystal structure of calcareous deposit films formed by electrodeposition process in artificial and natural seawater. *Coatings*, 11(3):359, 2021.

[41] Ch Barchiche, C Deslouis, D Festy, O Gil, Ph Refait, Sébastien Touzain, and B Tribollet. Characterization of calcareous deposits in artificial seawater by impedance techniques: 3—deposit of caco3 in the presence of mg (ii). *Electrochimica Acta*, 48(12):1645–1654, 2003.

[42] Nataly Ce and Shiladitya Paul. The effect of temperature and local ph on calcareous deposit formation in damaged thermal spray aluminum (tsa) coatings and its implication on corrosion mitigation of offshore steel structures. *Coatings*, 7(4):52, 2017.

[43] Karl P Fischer, William H Thomason, and Svein Eliassen. Cp in deep water: The importance of calcareous deposits and the environmental conditions. In *CORROSION 96*. OnePetro, 1996.

[44] Charlotte Carré, Alaric Zanibellato, Marc Jeannin, René Sabot, Peggy Gunkel-Grillon, and Arnaud Serres. Electrochemical calcareous deposition in seawater. a review. *Environmental Chemistry Letters*, 18(4):1193–1208, 2020.

[45] Wen Sun, Guichang Liu, Lida Wang, and Yu Li. A mathematical model for modeling the formation of calcareous deposits on cathodically protected steel in seawater. *Electrochimica Acta*, 78:597–608, 2012.

[46] Jari Aromaa, Antero Pehkonen, and Olof Forsén. Cathodic protection of ships in brackish water. *Journal of Solid State Electrochemistry*, 10(9):681–688, 2006.

[47] JR Ambrose, AE Yaniv, and U Rupurt Lee. Nucleation, growth and morphology of calcareous deposits on steel in sea water. *Corrosion83*, page 1983, 1983.

[48] CJ Li and M Du. The growth mechanism of calcareous deposits under various hydrostatic pressures during the cathodic protection of carbon steel in seawater. *RSC advances*, 7(46):28819–28825, 2017.

[49] Claude Deslouis, A Doncescu, D Festy, O Gil, V Maillot, Sébastien Touzain, and Bernard Tribollet. Kinetics and characterisation of calcareous deposits under cathodic protection in natural sea water. In *Materials science forum*, volume 289, pages 1163–1180. Trans Tech Publ, 1998.

[50] Helga Wiig Stangeland. Cathodic protection in cold climate-current density requirements and quality of calcareous deposits. *Institute of materials science and engineering*, page 92, 2008.

[51] C Deslouis, D Festy, O Gil, V Maillot, Sébastien Touzain, and B Tribollet. Characterization of calcareous deposits in artificial sea water by impedances techniques: 2-deposit of mg (oh) 2 without caco3. *Electrochimica Acta*, 45(11): 1837–1845, 2000.

[52] H Möller. The influence of mg2+ on the formation of calcareous deposits on a freely corroding low carbon steel in seawater. *corrosion science*, 49(4): 1992–2001, 2007.

[53] Faten Al-Hazmi, Ahmad Umar, GN Dar, AA Al-Ghamdi, SA Al-Sayari, A Al-Hajry, SH Kim, Reem M Al-Tuwirqi, Fowzia Alnowaiserb, and Farid El-Tantawy. Microwave assisted rapid growth of mg (oh) 2 nanosheet networks for ethanol chemical sensor application. *Journal of Alloys and Compounds*, 519:4–8, 2012.

[54] Per O Gartland, Einar Bardal, Rolf E Andresen, and Roy Johnsen. Effects of flow on the cathodic protection of a steel cylinder in seawater. *Corrosion*, 40 (3):127–133, 1984.

[55] Chems-Eddine Barchiche. *Caractérisation et cinétique de formation des dépôts calcomagnésiens sur acier en eau de mer artificielle*. PhD thesis, La Rochelle, 2004.

[56] Ph Refait, Marc Jeannin, R Sabot, H Antony, and S Pineau. Electrochemical formation and transformation of corrosion products on carbon steel under cathodic protection in seawater. *Corrosion Science*, 71:32–36, 2013.

[57] Ph Refait, Marc Jeannin, R Sabot, H Antony, and S Pineau. Corrosion and cathodic protection of carbon steel in the tidal zone: Products, mechanisms and kinetics. *Corrosion Science*, 90:375–382, 2015.

[58] Yuanfeng Yang. *Calcium and Magnesium Containing Anticorrosion Films on Mild Steel*. PhD thesis, 2010.

[59] Yuanfeng Yang, James David Scantlebury, and Elena Victorovna Koroleva. A study of calcareous deposits on cathodically protected mild steel in artificial seawater. *Metals*, 5(1):439–456, 2015.

[60] FG Liu, SR Wu, and CS Lu. Characterisation of calcareous deposits on freely corroding low carbon steel in artificial sea water. *Corrosion engineering, science and technology*, 46(5):611–617, 2011.

[61] Hikaru Abe, Tamie Kobayakawa, Heishi Maruyama, Toru Wakabayashi, and Masaharu Nakayama. Thin film coating of mg-intercalated layered mno 2 to suppress chlorine evolution at an iro 2 anode in cathodic protection. *Electrocatalysis*, 10(2):195–202, 2019.

[62] M Rudolf, I Rousar, and J Krysa. Cathodic reduction of hypochlorite during reduction of dilute sodium chloride solution. *Journal of applied electrochemistry*, 25(2):155–165, 1995.

[63] Emma Qingnan Zhang, Zareen Abbas, and Luping Tang. Predicting degradation of the anode–concrete interface for impressed current cathodic protection in concrete. *Construction and Building Materials*, 185:57–68, 2018.

[64] Gidon Amikam, Paz Nativ, and Youri Gendel. Chlorine-free alkaline seawater electrolysis for hydrogen production. *international journal of hydrogen energy*, 43(13):6504–6514, 2018.

[65] Muhammad Saleem, Mohammed Harun Chakrabarti, Diya'uddeen Basheer Hasan, Md Islam, Rozita Yusoff, Sayed Ahmad Hajimolana, Mohd Azlan Hussain, Gazi Md Arifuzzaman Khan, Brahim Si Ali, et al. On site electrochemical production of sodium hypochlorite disinfectant for a power plant utilizing seawater. *International Journal of Electrochemical Science*, 7(5):3929–3938, 2012.

[66] Regina G Damalerio, Aileen H Orbecido, Marigold O Uba, Patricio Elvin L Cantiller, and Arnel B Beltran. Storage stability and disinfection performance on escherichia coli of electrolyzed seawater. *Water*, 11(5):980, 2019.

[67] Charles W Spalding. Reaction kinetics in the absorption of chlorine into aqueous media. *AIChE Journal*, 8(5):685–689, 1962.

[68] JG Vos and MTM Koper. Measurement of competition between oxygen evolution and chlorine evolution using rotating ring-disk electrode voltammetry. *Journal of Electroanalytical Chemistry*, 819:260–268, 2018.

[69] F Hine, M Yasuda, T Noda, T Yoshida, and J Okuda. Electrochemical behavior of the oxide-coated metal anodes. *Journal of the Electrochemical Society*, 126 (9):1439, 1979.

[70] JE Bennett. Electrodes for generation of hydrogen and oxygen from seawater. *International Journal of Hydrogen Energy*, 5(4):401–408, 1980.

[71] Standard ISO17475. Corrosion of metals and alloys—electrochemical test methods—guidelines for conducting potentiostatic and potentiodynamic polarization measurements, 2007.

[72] Weilie Zhou, Robert Apkarian, Zhong Lin Wang, and David Joy. Fundamentals of scanning electron microscopy (sem). In *Scanning microscopy for nanotechnology*, pages 1–40. Springer, 2006.

[73] AJ d'Alfonso, B Freitag, D Klenov, and LJ Allen. Atomic-resolution chemical mapping using energy-dispersive x-ray spectroscopy. *Physical Review B*, 81 (10):100101, 2010.

[74] Alex Delwiche and Isaac Tavares. Retrofit strategy using aluminium anodes for the internal sections of windturbine monopiles. In *CORROSION 2017*. OnePetro, 2017.

[75] Alex Delwiche and Patrick Lydon. the water ph and gas evolution risks associated with the use of aluminium and zinc anodes for the internal cathodic protection of offshore monopiles. In *CORROSION 2018*. OnePetro, 2018.

[76] Monica M Maher and Geoff Swain. Corrosion control and ecosystems enhancement for offshore monopiles. *MATERIALS PERFORMANCE*, 58(8):28–33, 2019.

[77] Stein T Briskeby, Linda Børvik, and Sven M Hesjevik. Cathodic protection in closed compartments–ph effect and performance of anode materials. In *CORROSION 2015*. OnePetro, 2015.

[78] Sven Morten Hesjevik. Testing iccp in confined space. Technical report, Equinor, 19 mai 2017. (Confidential Report).

[79] Quang-Tung Tran, Gwenaelle Benoit, Olivier Le Guennec, and Charles Leballeur. Optimization of the corrosion protection for offshore windfarm monopile foundation-engineering design lessons learnt. In *CORROSION 2019*. OnePetro, 2019.

[80] MeadInfo. Material properties of s355 steel - an overview. https://www.meadinfo.org/2015/08/s355-steel-properties.html, 2015. Online; accessed 01 October 2021.

[81] Ivana Jevremovic and Ole Øystein Knudsen. Cathodic protection design parameter study. Technical report, SINTEF, June 2021. (Confidential Report).

[82] Yong Xu, Yanliang Huang, Dan Yang, Hans Joerg Kunte, Roland De Marco, and Xiutong Wang. Investigation of the calcareous deposits formation controlled by interfacial ph and its effect on the hydrogen entry into aisi 4135 steel in seawater. *International Journal of Hydrogen Energy*, 46(7):5824–5841, 2021.

[83] Nelson Saksono, Yuliusman Yuliusman, Setijo Bismo, Roekmijati W Soemantojo, and Azwar Manaf. Effects of ph on calcium carbonate precipitation under magnetic field. *Makara Journal of Technology*, 13(2):5, 2009.

[84] C Deslouis, P Falaras, O Gil, M Jeannin, V Maillot, and B Tribollet. Influence of clay on calcareous deposit in natural and artificial sea water. *Electrochimica Acta*, 51(15):3173–3180, 2006.

Appendices

Appendix A: Potentiostatic Polarisation Curves of the Precorroded Samples

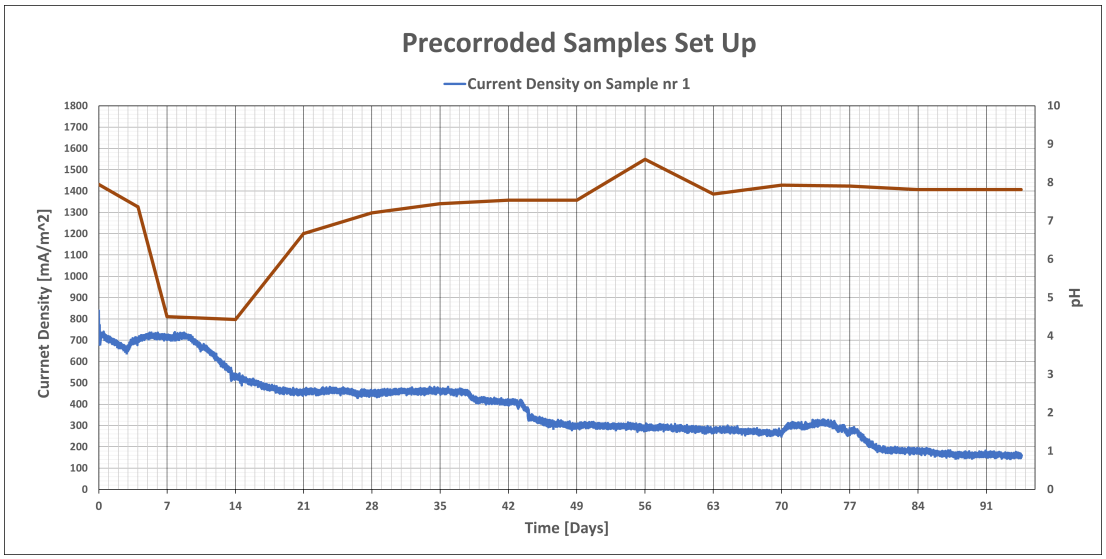

Figure 7.1: *Sample No.1*

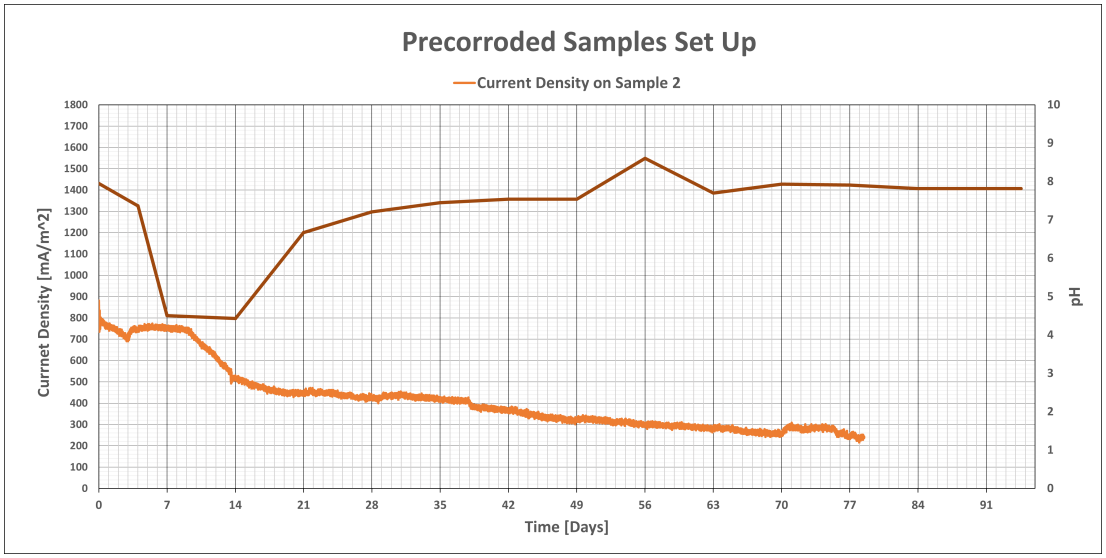

Figure 7.2: *Sample No.2*

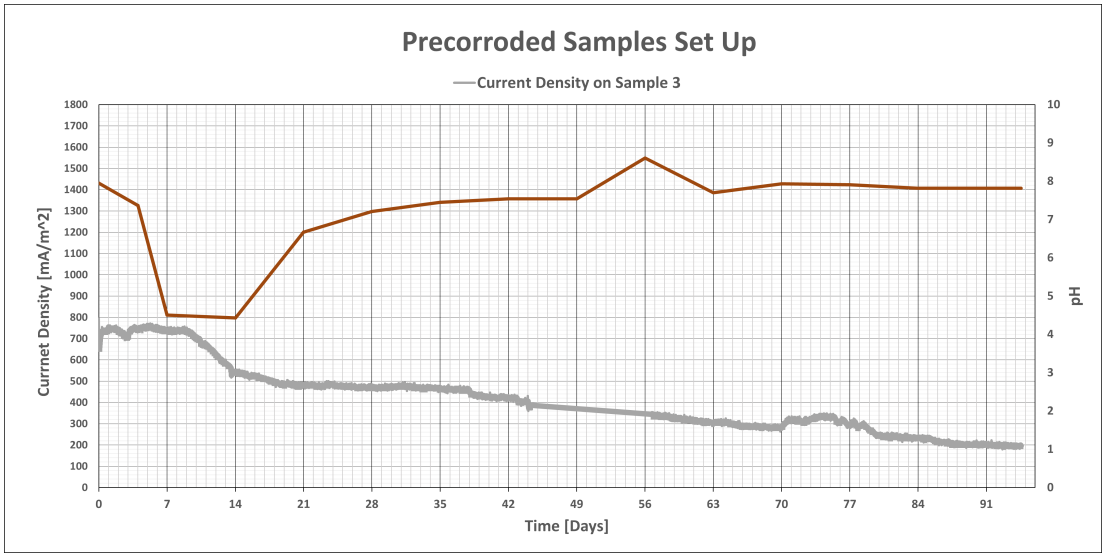

Figure 7.3: *Sample No.3*

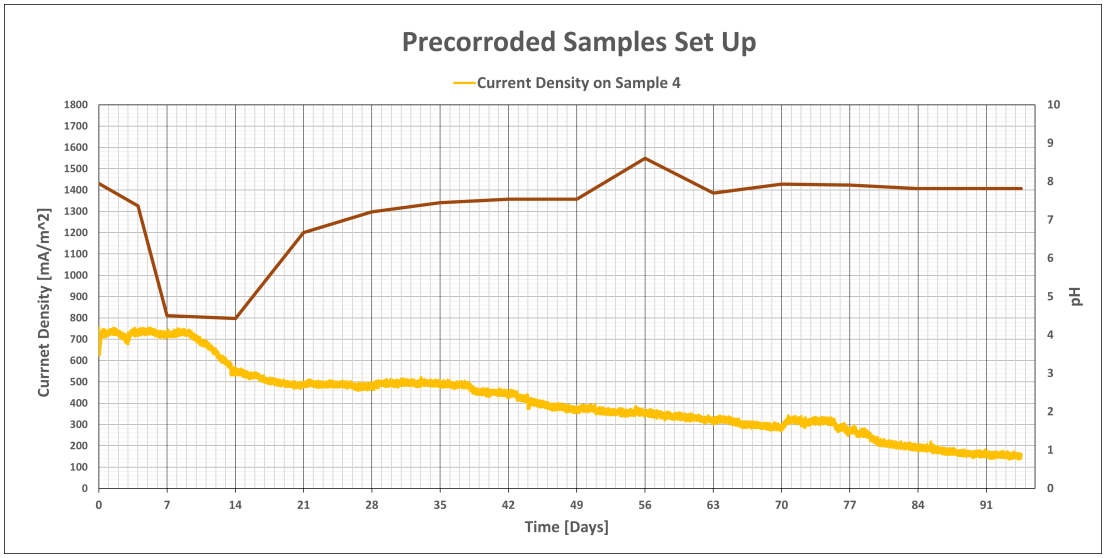

Figure 7.4: *Sample No.4*

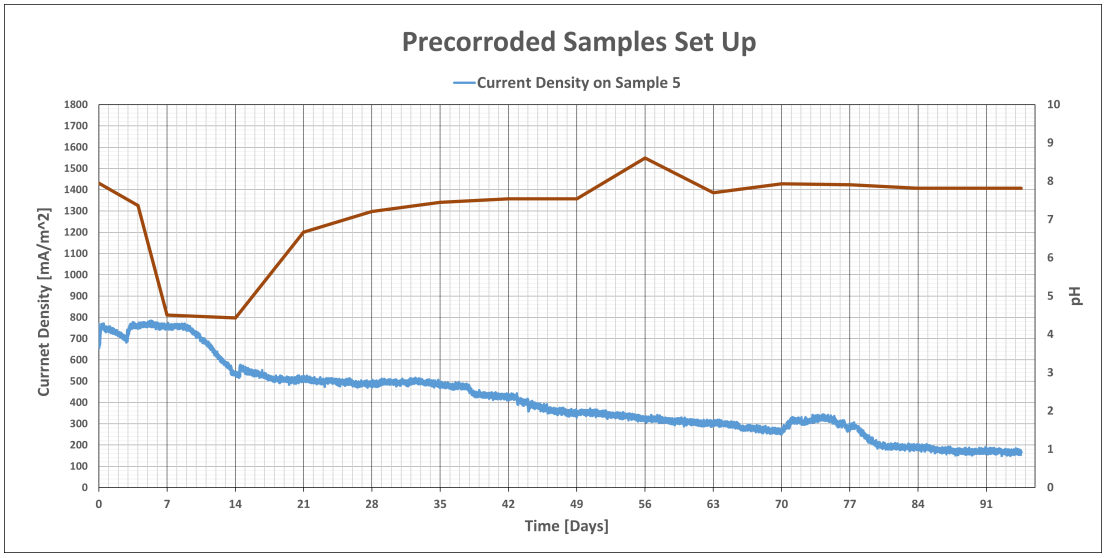

Figure 7.5: *Sample No.5*

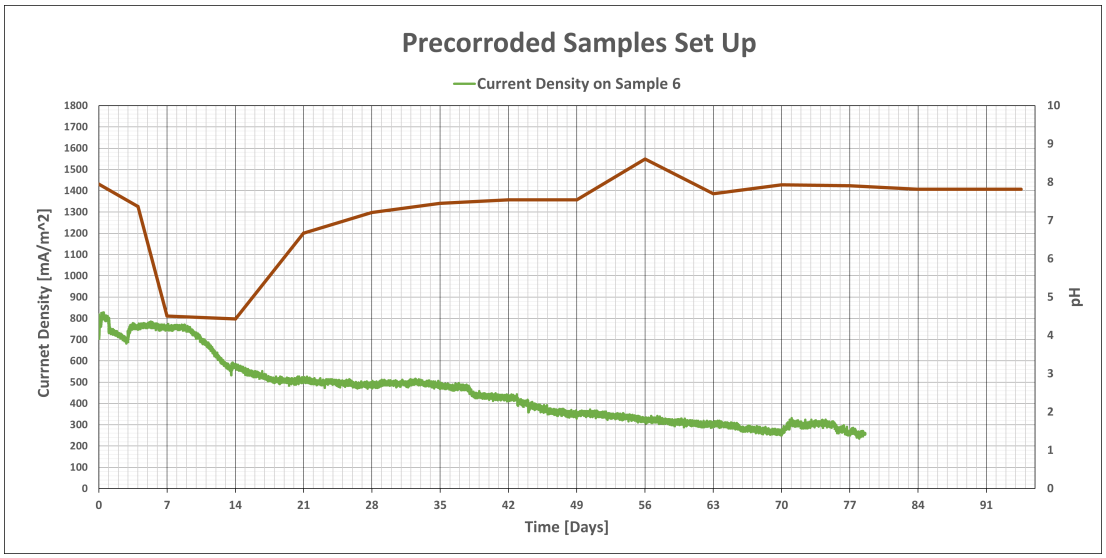

Figure 7.6: *Sample No.6*

Appendix B: Potentiostatic Polarisation Curves of the Grinded Samples

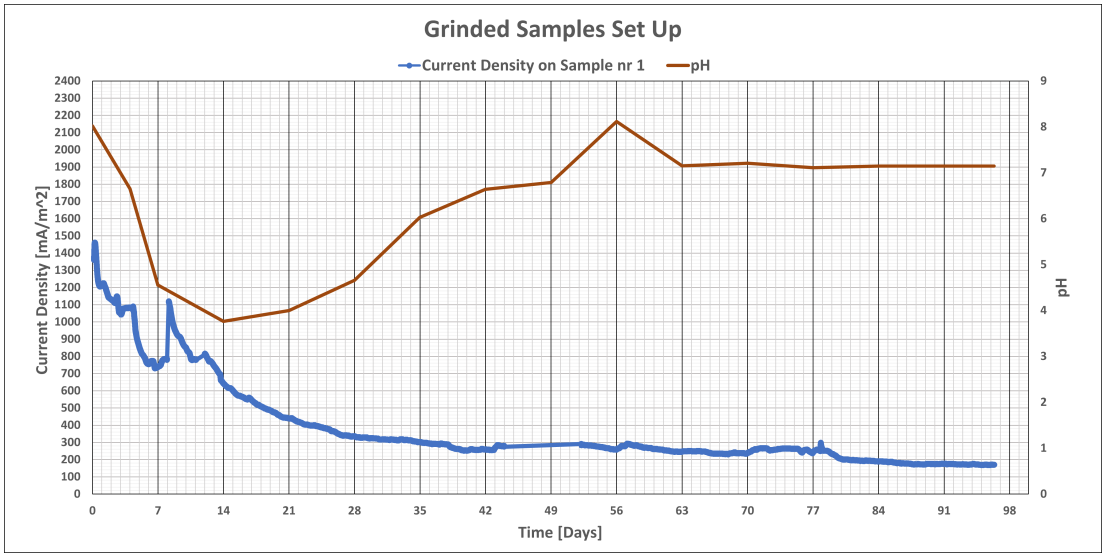

Figure 7.7: *Sample No.1*

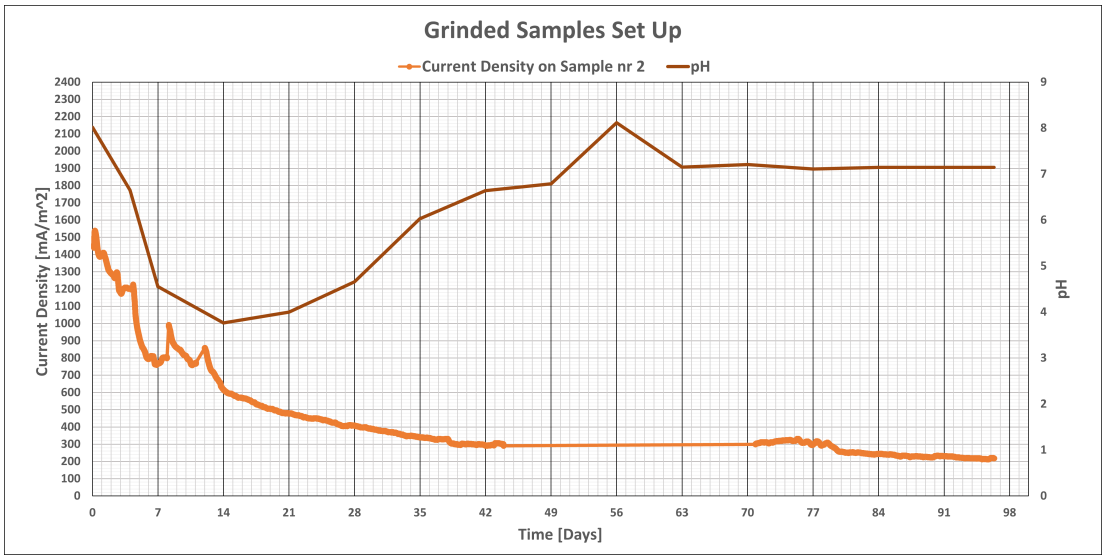

Figure 7.8: *Sample No.2*

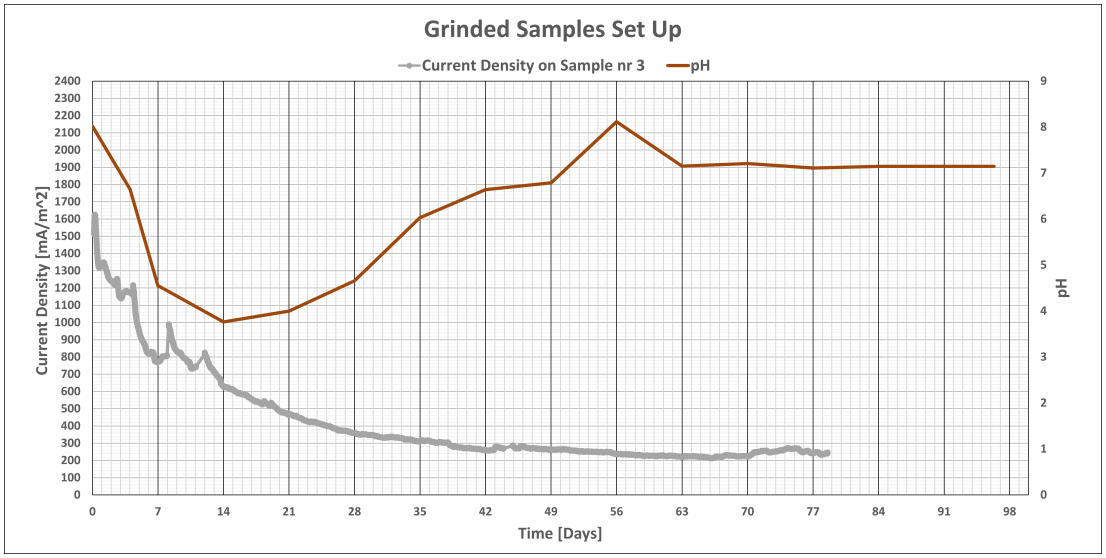

Figure 7.9: *Sample No.3*

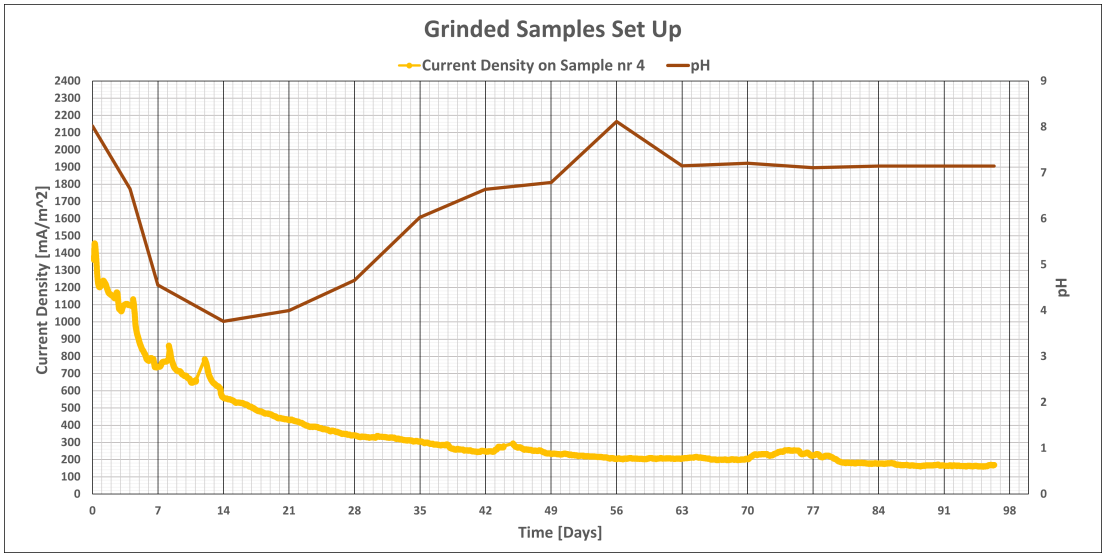

Figure 7.10: *Sample No.4*

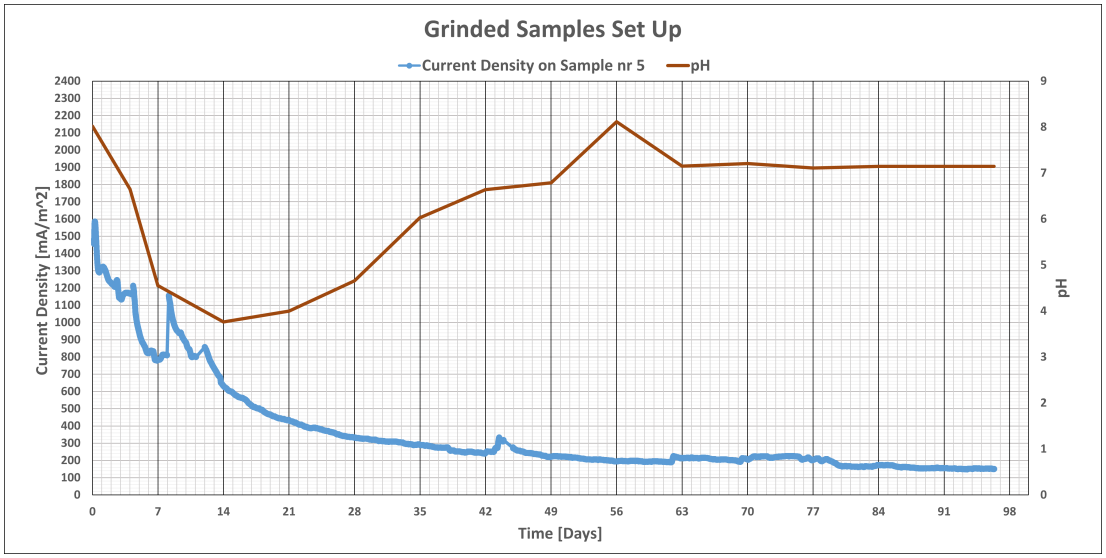

Figure 7.11: *Sample No.5*

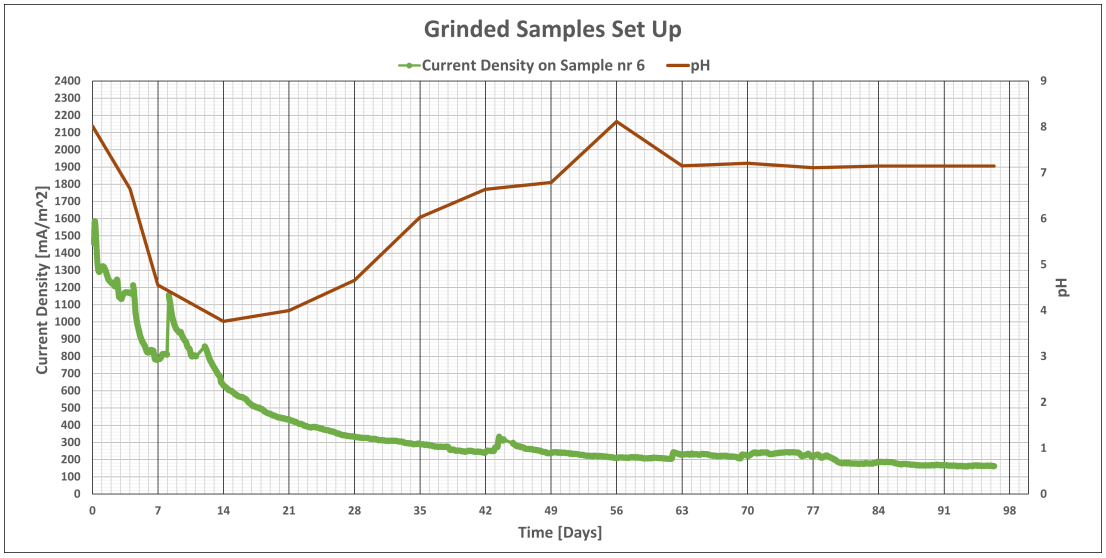

Figure 7.12: *Sample No.6*

Appendix C: Potentiostatic Polarisation Curves of the Precorroded and Grinded Samples in the Partially Open System

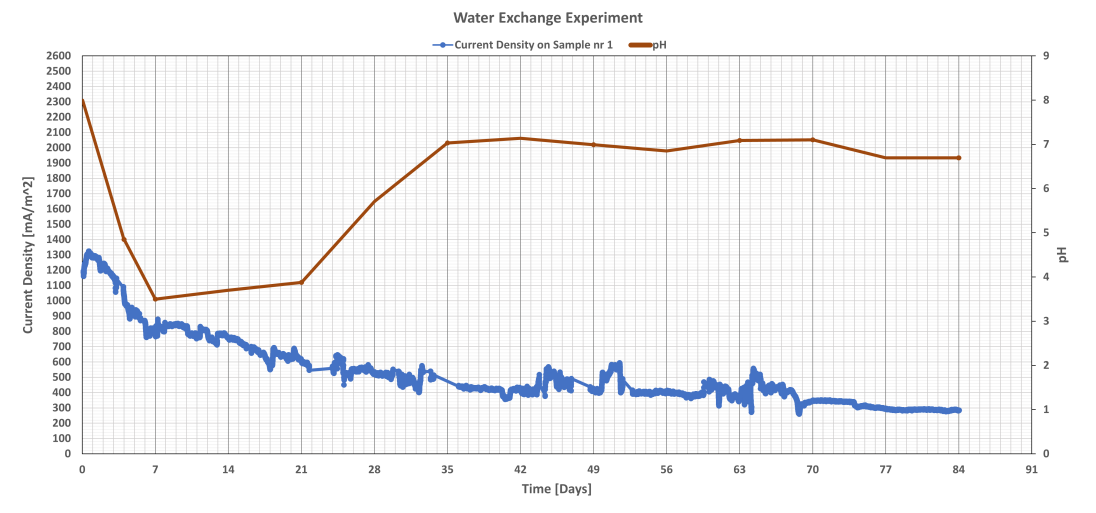

Figure 7.13: *Sample No.1*

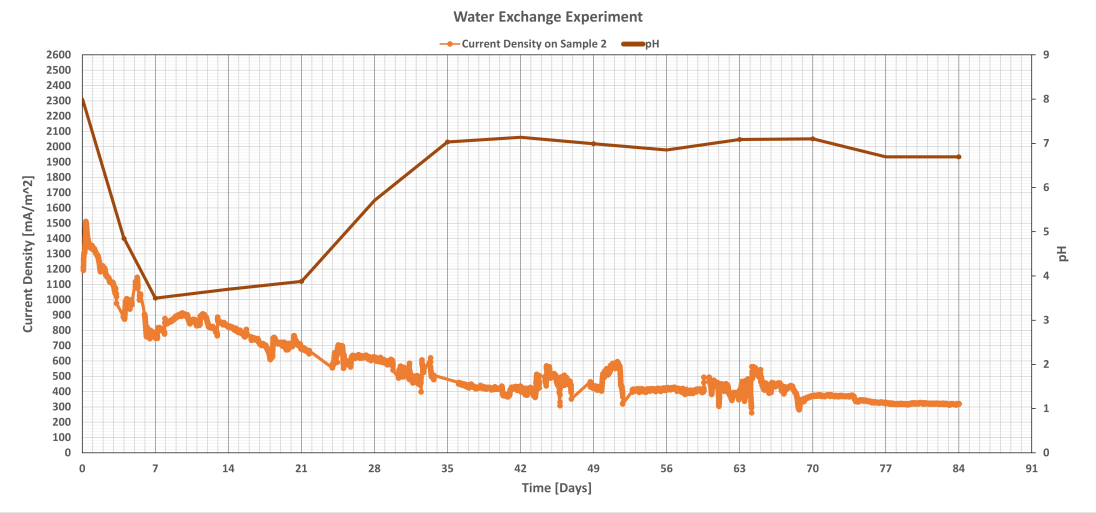

Figure 7.14: *Sample No.2*

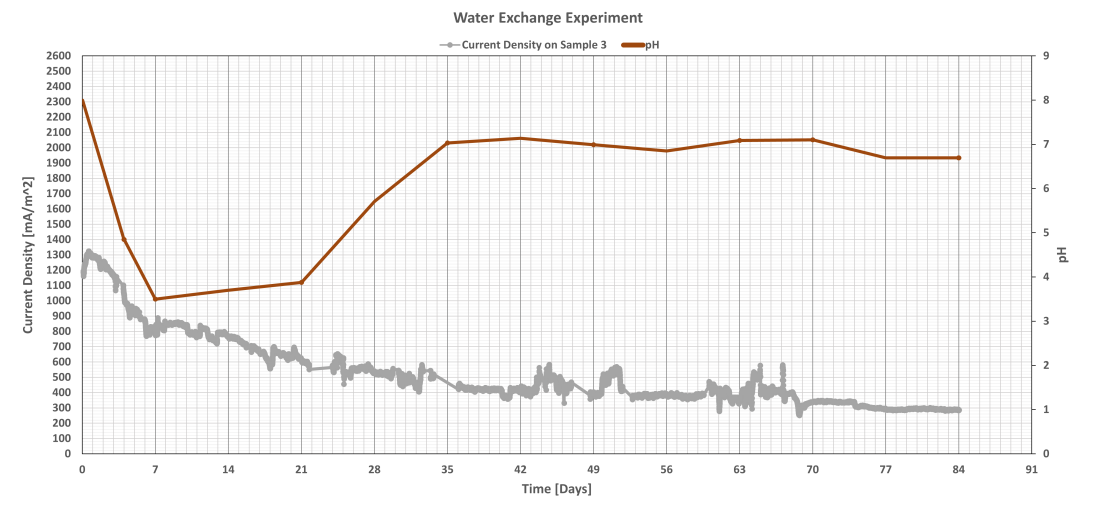

Figure 7.15: *Sample No.3*

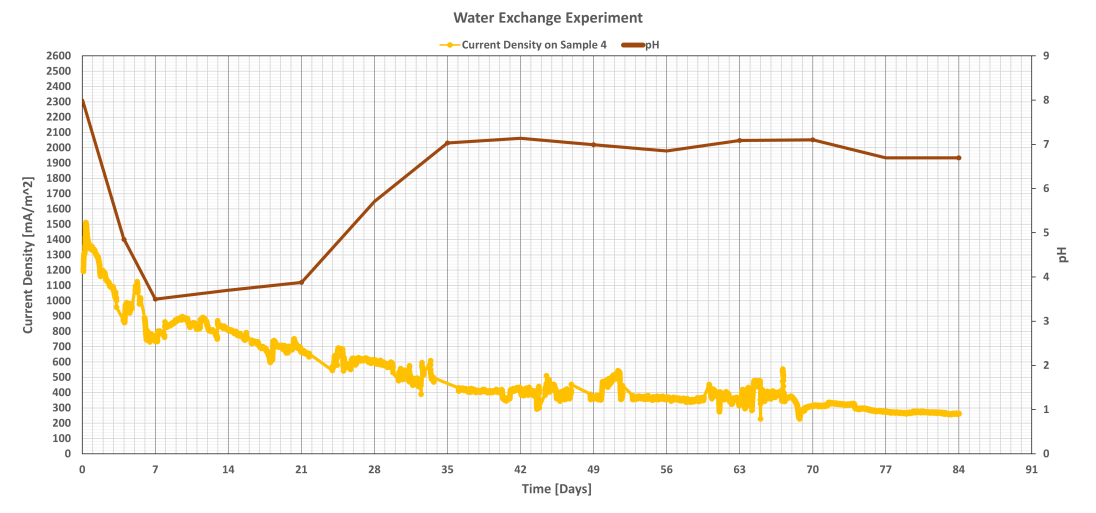

Figure 7.16: *Sample No.4*

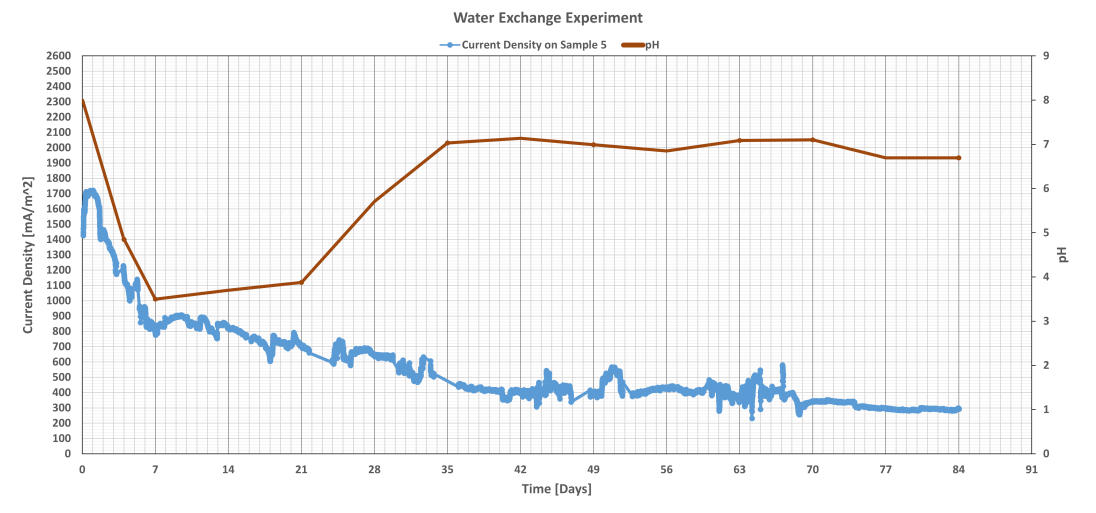

Figure 7.17: *Sample No.5*

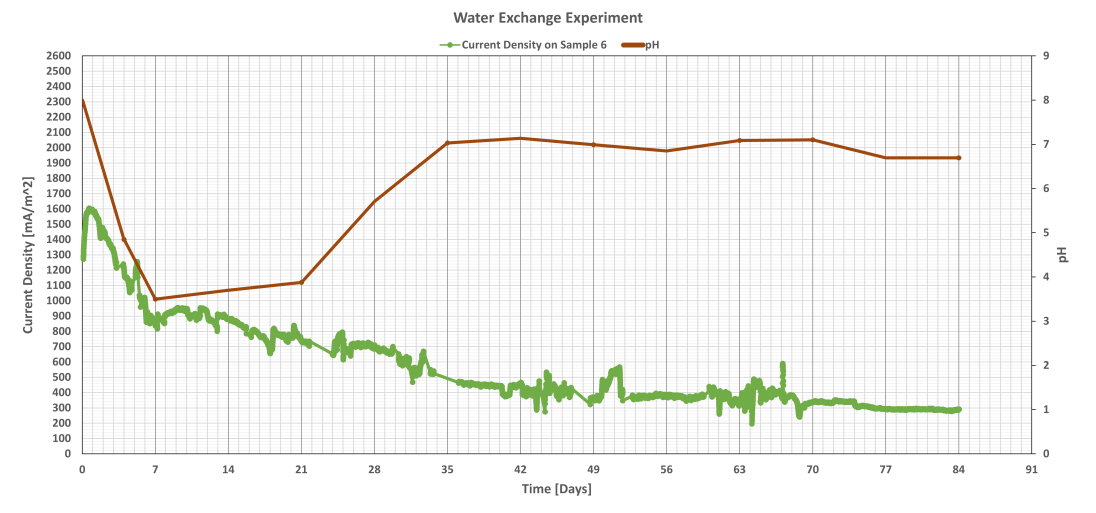

Figure 7.18: *Sample No.6*

Appendix D: Potentiostatic Polarisation Curves of the Precorroded in a closed system for 3-4 weeks

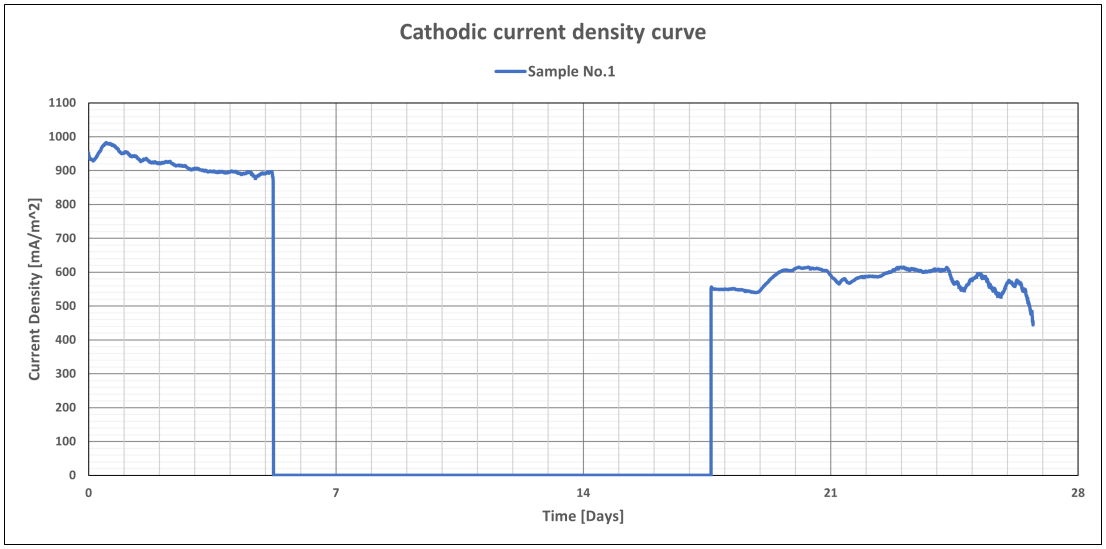

Figure 7.19: *Sample Nr.1*

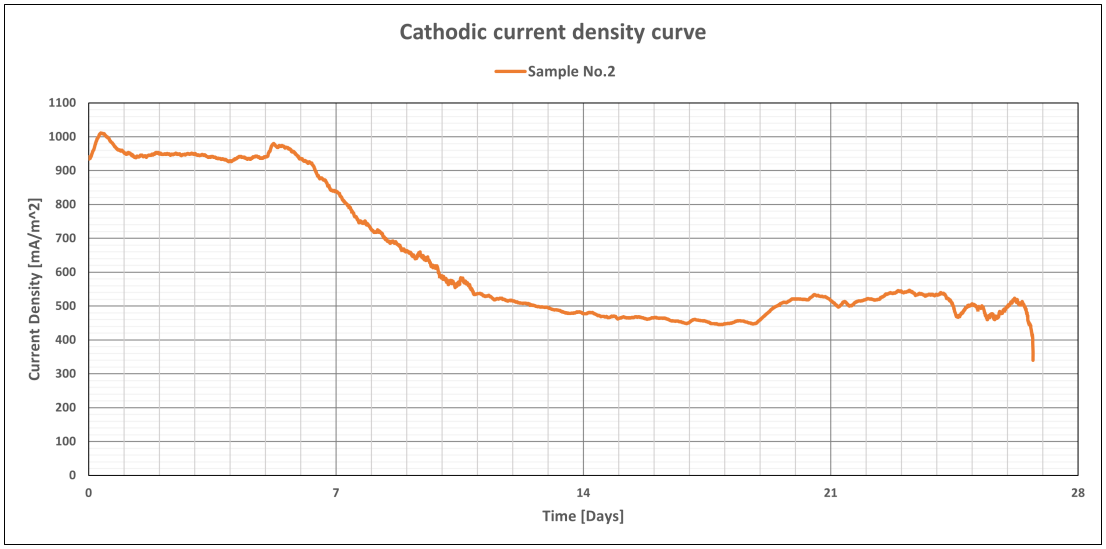

Figure 7.20: *Sample Nr.2*

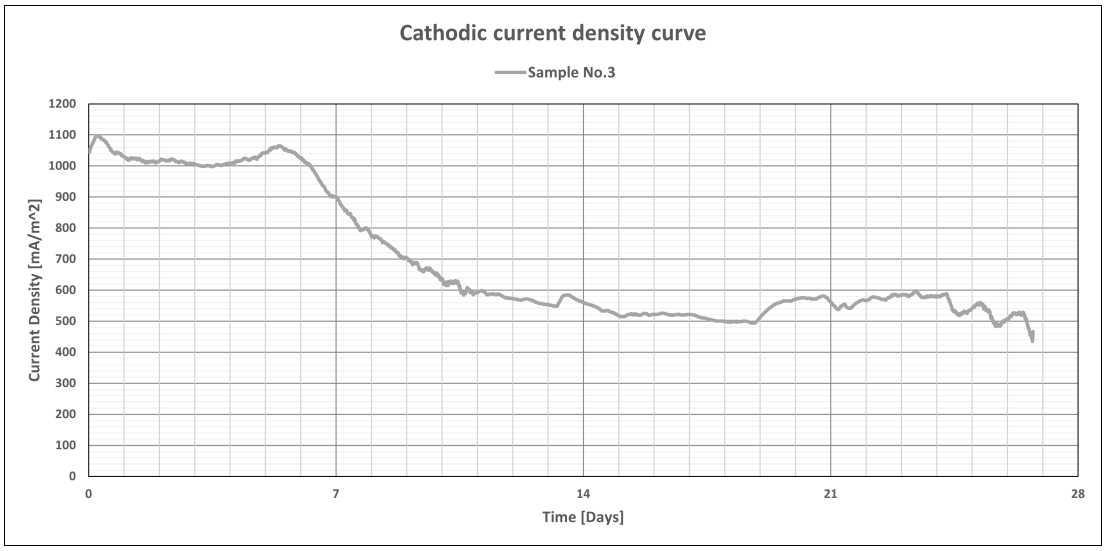

Figure 7.21: *Sample Nr.3*

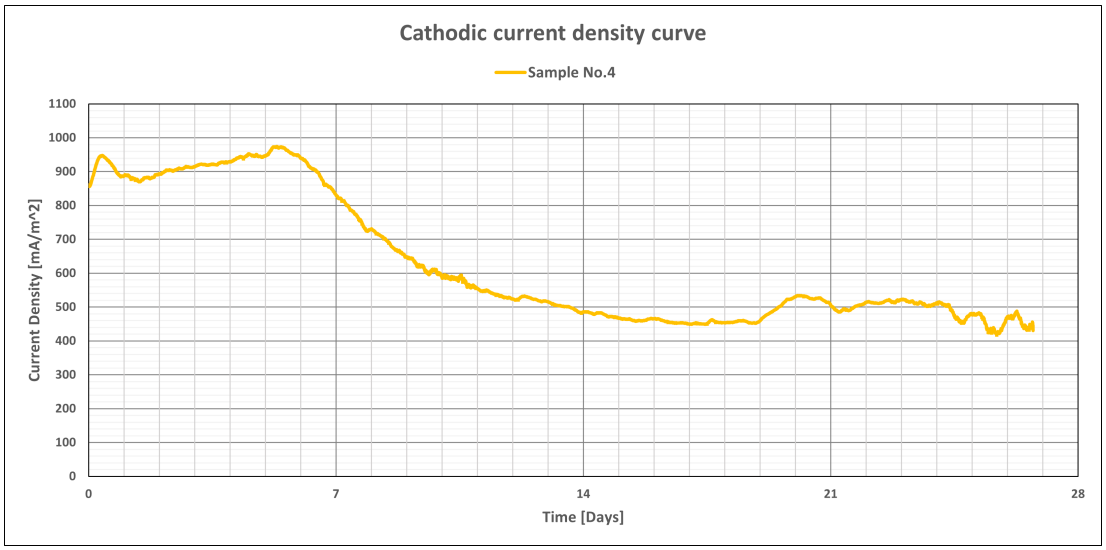

Figure 7.22: *Sample Nr.4*

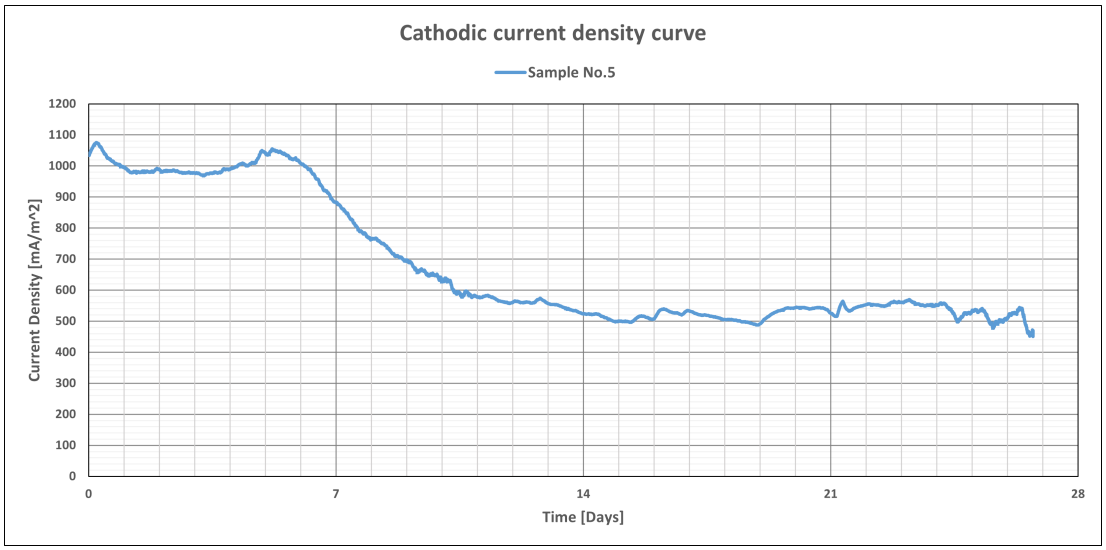

Figure 7.23: *Sample Nr.5*

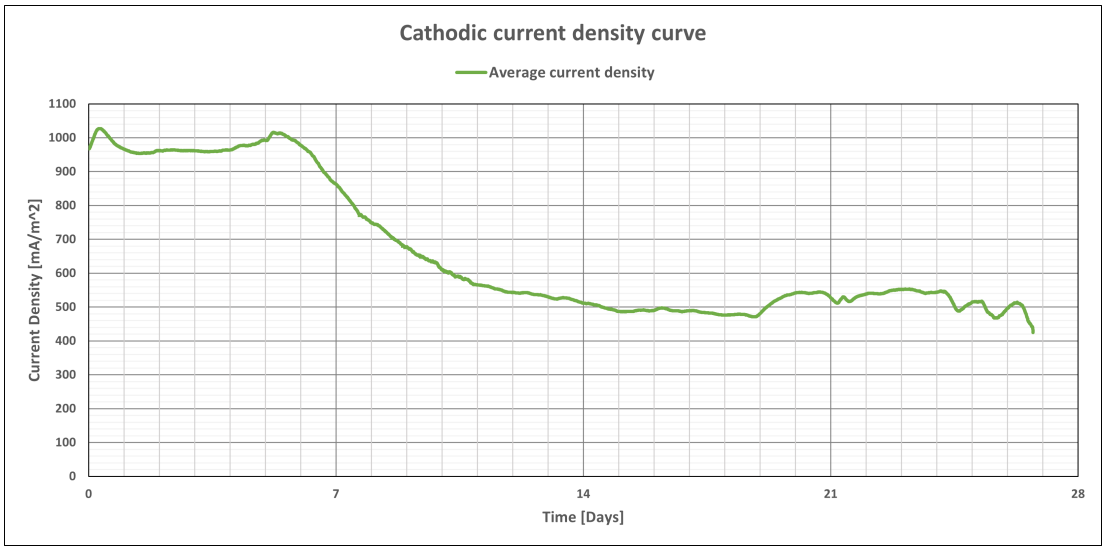

Figure 7.24: *Average Current density on samples Nr.2-5*

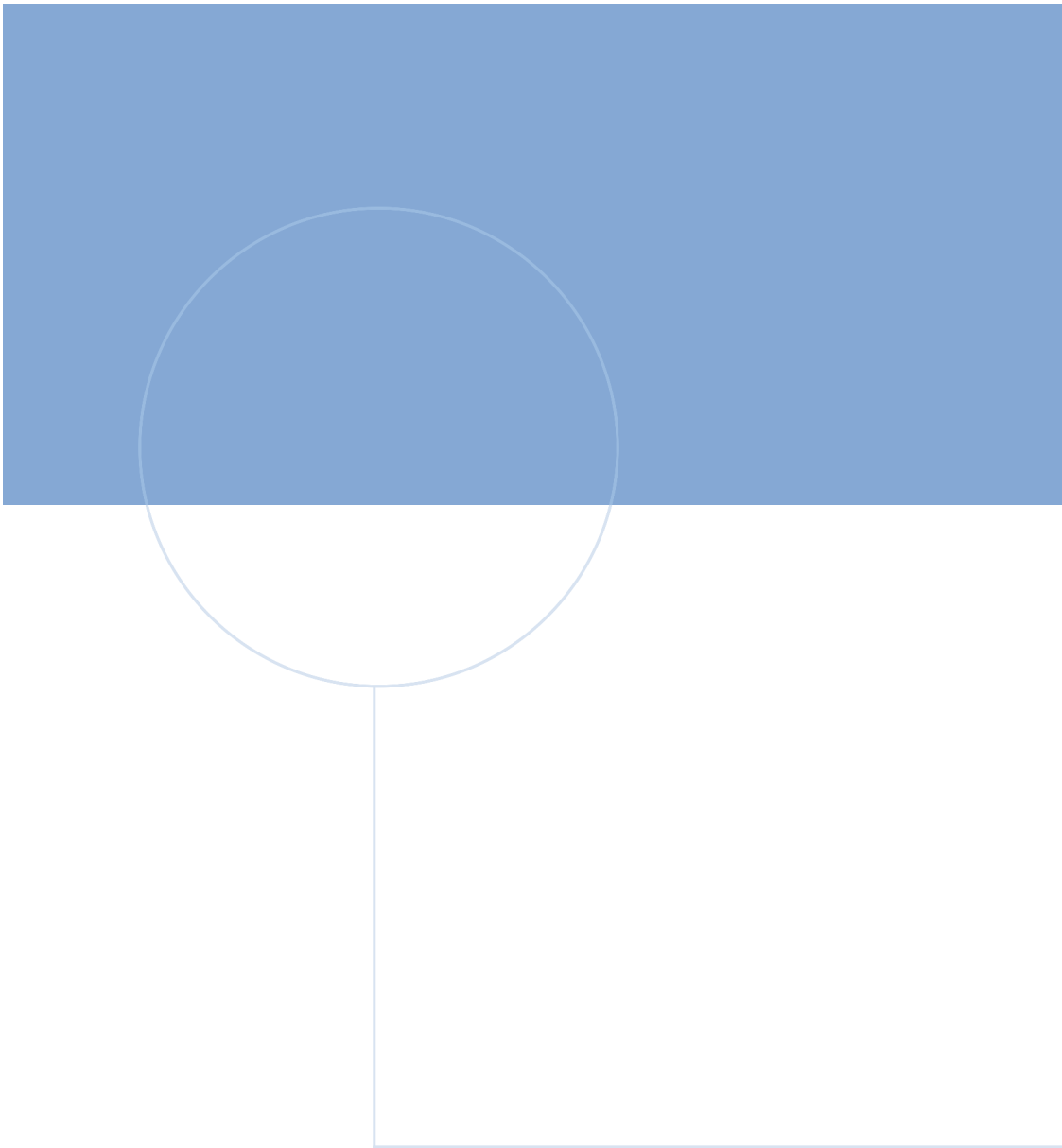

NTNU

Norwegian University of
Science and Technology